

Cellular and Molecular Mechanisms of Retinal Neuron Spatial Patterning

by

Christopher Kozlowski Jr.

Department of Neurobiology
Duke University

Date: _____

Approved:

Jeremy Kay, Supervisor

Debra Silver

Dong Yan

Marc Caron

Dissertation submitted in partial fulfillment of
the requirements for the degree of Doctor
of Philosophy in the Department of
Neurobiology in the Graduate School
of Duke University

2019

ABSTRACT

Cellular and Molecular Mechanisms of Retinal Neuron Spatial Patterning

by

Christopher Kozlowski Jr.

Department of Neurobiology
Duke University

Date: _____

Approved:

Jeremy Kay, Supervisor

Debra Silver

Dong Yan

Marc Caron

An abstract of a dissertation submitted in partial
fulfillment of the requirements for the degree
of Doctor of Philosophy in the Department of
Neurobiology in the Graduate School of
Duke University

2019

Copyright by
Christopher Kozlowski Jr.
2019

Abstract

During development, cell-cell recognition events mediate crucial steps in the formation of organized cellular patterns critical for tissue function. In the nervous system, cell recognition cues guide migrating neurons during development to appropriate terminal locations and sculpt their characteristic sizes, shapes, and circuit connectivity. The retina contains a multitude of neuron types; however, neurons of the same cell type (homotypic) are patterned into evenly spaced arrangements known as “mosaics” across the retina surface. Disrupting mosaic formation impairs visual function, so it is important to understand the precise cellular and molecular mechanisms that allow homotypic neurons to recognize and adjust their proximity to neighbors. To understand this process, we studied two populations of interneurons, the OFF and ON starbursts amacrine cells (SACs), which require the cell-surface receptor MEGF10 to establish their mosaics. We find that SACs in *Megf10* mutants still make lateral movements in the plane of the retina, but fail to recognize their proximity to homotypic neighbors. Using transgenic tools to visualize SACs early in development, we identify a transient developmental phase where SAC dendrite territories are bounded by homotypic somata, a relationship which is lost in SACs lacking MEGF10. Further, we determine that MEGF10 utilizes distinct signal transduction pathways in neurons from those identified in non-neuronal cells. Lastly, we demonstrate that specific amino acids

within the intracellular domain of MEGF10 are required to recapitulate a cellular recognition-like event in a heterologous cell system. These findings support a model whereby MEGF10 signals in SACs by a distinct mechanism to mediate dendrite-soma interactions necessary to pattern the organization of retinal neurons.

Contents

Abstract	iv
List of Tables	ix
List of Figures	x
Acknowledgements	xiii
1. Introduction and Background.....	1
2. Materials and Methods.....	8
2.1 Experimental Mouse Models	8
2.1.1 Animals.....	8
2.1.2 Generation of Megf10-cre mice	9
2.1.3 Generation of Rosa-Megf10 mice	10
2.2 Tissue Processing and Data Collection.....	11
2.2.1 Histology and Immunohistochemistry	11
2.2.3 <i>In situ</i> hybridization	13
2.2.4 Microscopy and image processing.....	14
2.3 Cell Culture	15
2.3.1 HEK293T Cells.....	15
2.3.2 HEK cell plasmid delivery	15
2.3.3 HEK cell immunocytochemistry	16
2.3.5 HEK cell live imaging	17
2.4 Molecular Biology	18

2.4.1 Plasmid cloning	18
2.4.2 Western blot	18
2.4.3 Co-Immunoprecipitation.....	20
2.5 Data Analysis	20
2.5.1 Mosaic Analysis.....	20
2.5.2 Analysis of SAC arbor territories	21
2.5.3 Statistical analysis.....	22
2.6 Key Resources	22
3. Determining cellular mechanism of MEGFG10-mediated mosaic formation in SACs.	25
3.1 Introduction.....	25
3.2 Emergence of OFF SAC regularity requires Megf10 at P0	26
3.3 Tangential dispersion occurs in SACs lacking MEGF10.....	28
3.4 Megf10-driven Cre recombinase mouse line reveals SAC anatomy is inconsistent with dendritic tiling	31
3.5 Arborization territories in OFF SACs limit neighboring cell proximity in MEGF10-dependent manner.....	36
3.6 Arbor Exclusion model can also be applied to development of ON SACs.....	43
3.7 MEGF10 is required for early innervation of the IPL, but acts throughout development for mosaic formation.....	51
4. Signal Transduction pathways downstream of neuronal MEGF10.....	56
4.1 Introduction.....	56
4.2 Expression pattern of MEGF10 associated signaling partners in SACs	59
4.3 Knockout of the GEF Vav3 decreases SAC regularity	66

5. Megf10 initiates cell-cell recognition events through its intracellular domain in a heterologous system	73
5.1 Introduction.....	73
5.2 MEGF10-driven cellular recognition requires ITAM signaling.....	74
5.3 Generation of Rosa26a knock-in mouse to test if MEGF10 requires ITAM signaling in SACs	85
6. Conclusions and Future Directions	89
6.1 MEGF10-driven Cre recombinase as a tool for studying development	89
6.2 Arbor exclusion model as a general cellular mechanism guiding mosaic formation	90
6.3 Neuronal MEGF10 signal transduction pathways differ from those in nonneuronal cells.....	91
6.4 Expression of MEGF10 in heterologous cells as a model for studying cell-cell recognition.....	93
References	95
Biography.....	103

List of Tables

Table 1: Key Resources Table	22
------------------------------------	----

List of Figures

Figure 1: Diagram of major retinal cell types.....	4
Figure 2: Organization of OFF SAC array at P0 requires MEGF10.....	27
Figure 3: Both control and <i>Megf10</i> knockout SACs make lateral movements in the retina plane.....	30
Figure 4: Recombination of <i>Megf10</i> driven Cre alleles label SACs early in development and removal of Neomycin cassette is required for MEGF10 protein expression.	33
Figure 5: SAC dendrites early in development grow to contact neighboring somata.....	35
Figure 6: Organization between OFF SAC arbor territories and homotypic somata requires MEGF10	41
Figure 7: Supplemental information to figure 6, Example small P0 mutant OFF SAC cell and matched/unmatched analysis on untrimmed mutant data.....	43
Figure 8: Organization of ON SAC array at P0 requires <i>Megf10</i>	45
Figure 9: Relationship between ON SAC arbor areas and homotypic somata at P0 also requires MEGF10	49
Figure 10: Supplemental information to figure 9, ON SAC arbor areas grow at P3 and match/unmatched analysis on untrimmed P0 data.	50
Figure 11: Ectopic SAC stratification patterns occur sporadically in adult MEGF10 mutants.....	52
Figure 12: Temporal requirements for MEGF10 in IPL stratification and mosaic spacing.	54
Figure 13: Schematic of MEGF10 protein with known cytoplasmic signaling motifs and engulfment pathways.....	58
Figure 14: Microarray for GULP and <i>In Situ</i> hybridization for Zap70/Syk are not abundantly expressed in SACs.	62

Figure 15: Time course of Vav3 expression by <i>In Situ</i> hybridization resembles pattern of MEGF10 expression.	63
Figure 16: ChAT labeled sections of signaling candidate knockouts reveal normal sublamination.	65
Figure 17: Regularity of OFF SAC array in Syk;Zap70 double knockout mice is indistinguishable from controls.	68
Figure 18: Regularity of OFF SAC array in Vav3 and Vav2;3 double knockout mice.	69
Figure 19: Regularity of ON SACs and HCs in Vav3 knockouts is similar to control mice.	70
Figure 20: No evidence of genetic interaction between Megf10 and Vav3 knockout mice.	71
Figure 21: Co-transfection of MEGF10 and VAV3 protein into HEK293 shows little evidence of interaction.	72
Figure 22: Transfection of MEGF10 protein into HEK293 cells appeared to mediate cell-cell recognition like event between neighbors.	74
Figure 23: Mutation of MEGF10 intracellular domain impairs formation of intercellular gaps.	77
Figure 24: Representative images of control and mutated MEGF10-GFP constructs used for quantification.	79
Figure 25: Nucleofection provides exclusive expression of single color constructs to assess intercellular borders.	80
Figure 26: Intercellular gaps between MEGF10 expressing HEK293 cells contain filopodia.	82
Figure 27: Phosphorylation of MEGF10 intracellular domain requires ITAM tyrosines.	83
Figure 28: Live imaging of HEK293 cells co-transfected with Life-Act and MEGF10 plasmids shows time course of intercellular gap formation.	84

Figure 29: Proposed model of intercellular gap formation in MEGF10 transfected HEK293 cells. 85

Figure 30: Diagram of Rosa-MEGF10 mouse and experimental design. 87

Figure 31: Rosa-MEGF10 does not appear to express enough MEGF10 protein to rescue OFF SAC mosaic phenotypes. 88

Acknowledgements

I would like to thank my Advisor, Jeremy Kay, for this mentorship, expertise and encouragement throughout graduate school. I would also like to thank my committee members, Dr. Debra Silver, Dr. Dong Yan, and Marc Caron for their guidance and feedback. Thanks to all members of the Kay Lab for their friendship and assistance with various aspects of these studies. I would also like to acknowledge the Duke Transgenic Core for their role in generating the experimental mice used here. Lastly, I would like to express my immense gratitude to my parents and family for their constant support.

1. Introduction and Background

During development, cell-cell recognition events mediate crucial steps in the formation of complex organs and tissues. These events are tightly regulated to ensure reproducible cellular morphogenesis, leading to functional tissue architecture. In the developing nervous system, cell recognition cues guide migrating neurons to appropriate terminal locations and sculpt their characteristic sizes, shapes, and connectivity (Lefebvre et al., 2015; Prigge and Kay, 2018; Yagi, 2012; Yamada and Nelson, 2007). As an extension of the central nervous system, the retina and its 100 neuronal cell types has served as an important model in understanding how neurons of the same type (homotypic) distribute themselves into regularly spaced arrays, or “mosaics”, across the retina surface (Macosko et al., 2015; Rheaume et al., 2018; Rockhill et al., 2000; Shekhar et al., 2016; Tran et al., 2019; Wassle and Riemann, 1978) This mosaic patterning ensures there is an even distribution of processing elements present across the visual field and prevents the development of ‘blind spots’ – regions unable to perform neural computations due the absence of a critical cell type. Indeed, disruption of mosaic arrangements are known to impair retinal function and visually guided behavior (Chen et al., 2013; Ray et al., 2018). Because mosaics represent a fundamental functional feature of retinal neurons, it’s important to understand the precise mechanisms that guide their formation.

A mature neuronal mosaic is defined by the presence of “exclusion zones” – areas surrounding each cell where another neuron of the same type is rarely found (Reese, 1999). This organization is not present at the time of cell cycle exit, nor is it present during radial migration, when newborn neurons traverse the outer neuroblast layer (ONBL) progenitor zone to arrive at their final laminar location within the inner neuroblast layer (INBL) (Galli-Resta et al., 1997; Hinds and Hinds, 1978). Rather, exclusion zones first become detectable soon after the completion of radial migration, when post-migratory neurons begin to elaborate their dendritic arbors (Galli-Resta et al., 1997). At this time, neurons reposition themselves laterally, dynamically adjusting their position within the tangential plane of the retina to achieve even spacing (Amini et al., 2019; Chow et al., 2015; Reese and Galli-Resta, 2002). Modeling studies have demonstrated that these short lateral movements are sufficient to transform random arrays into orderly mosaics, as long as the movements are constrained via contact-mediated repulsion (Eglen et al., 2000; Galli-Resta, 2000). It has been proposed that this repulsion occurs through a phenomenon known as dendrite tiling, whereby repulsive interactions between the growing tips of homotypic dendrites carve out non-overlapping arbor territories for neighboring cells. According to this model, cell bodies would move to match the dendritic territory established through tiling, thereby driving

intercellular mutual repulsion and imparting even cell spacing (Cook and Chalupa, 2000; Huckfeldt et al., 2009; Reese, 1999).

The tiling model of exclusion zone formation has some experimental support, but key predictions remain untested. First, most retinal neurons do not tile their dendrites at maturity, so if the model is correct, neurons must undergo a transient phase of dendrite tiling during development. While this has been observed for horizontal cells (HCs) (Huckfeldt et al., 2009), it is unclear whether transient tiling generalizes to other cell types. Second, a stringent test of this model would require investigating dendro-dendritic interactions in a system where mosaic patterning does not occur, but no such studies have been performed. We aim to test these aspects of mosaic patterning here focused on the cholinergic starburst amacrine cells (SACs), which have long served as a model for studies of mosaic formation (Galli-Resta et al., 1997; Wässle and Riemann, 1978). These cells comprise two well-defined interneuron populations: the OFF SACs of the inner nuclear layer (INL) and the ON SACs of the ganglion cell layer (GCL), which form independent mosaics (Rockhill et al., 2000; Whitney et al., 2008) (Fig 1). These cells play critical roles in controlling direction-selective selective in retinal ganglion cells (Chen et al., 2014; Duan et al., 2014; Greene et al., 2016; Kim et al., 2014). Formation of both SAC mosaics requires the transmembrane receptor MEGF10, which serves as both a receptor and ligand required for establishing SAC exclusion zones (Kay et al., 2012).

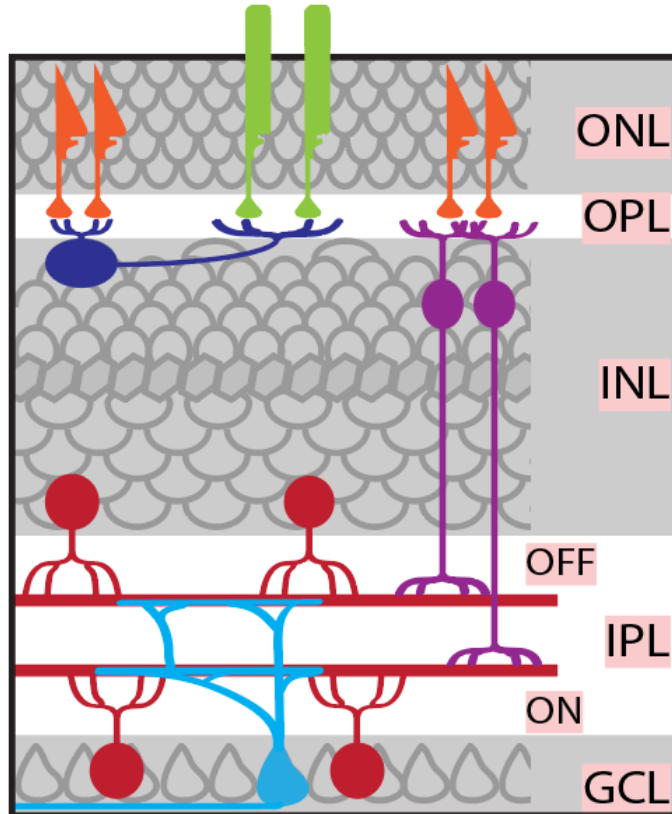


Figure 1: Diagram of major retinal cell types.

The retina is a highly organized structure consisting of three nuclear layers and two plexiform layers. Light is first detected by rod (orange) and cone (green) photoreceptors in the outer nuclear layer (ONL) before relaying this signal to bipolar cells (purple) of the inner nuclear layer (INL) and finally to retinal ganglion cells (blue), which transmit visual sensory information the brain. This light information is also modified by interneurons of the retina, horizontal cells (blue) participate in the connections between photoreceptors and bipolar cells in the outer plexiform layer (OPL), and amacrine cells (red) modify light information passing from bipolar cells to retinal ganglion cells. Here, we focus on the development of the starburst amacrine cells which represent two amacrine cell types, the OFF starbursts of the INL and the ON starbursts of the GCL (Modified from Prigge and Kay, 2018).

While it has been well established that MEGF10 is required in SACs for the formation of their mosaics, the signaling capacity of MEGF10 in neurons is completely unknown. Prior to identification of MEGF10's role in SACs, the only known manipulation to disrupt the even spacing of the SAC mosaics was intraocular injection of pharmacological agents that perturb microtubules (Galli-Resta et al., 2002). However these manipulations, performed at P0, only transiently degraded the regularity of the SAC array (Galli-Resta et al., 2002). This reversibility demonstrates that SACs contain the molecular machinery necessary to continually reorganize themselves and refine their proximity to neighboring cells. Therefore, MEGF10 must ultimately initiate a signal transduction cascade to activate the cytoskeleton, allowing the SAC to appropriately adjust its position. In non-neuronal cells, MEGF10 and its homologs have been studied as engulfment receptors, with defined signaling cascades that interact with the cytoskeleton to facilitate endocytosis (Chung et al., 2013; Scheib et al., 2012; Sullivan et al., 2014; Wu et al., 2009; Ziegenfuss et al., 2008).

Here, we aimed to examine the role of dendritic tiling in driving mutual cell repulsion to pattern the SAC mosaics and MEGF10's role in that process (Section 1). We also test if the signal transduction pathways downstream of MEGF10 in non-neuronal cells also act to shape the SACs mosaic (Section 2) and probe how MEGF10 initiates cell signaling using a heterologous cell system (Section 3). We find in both wildtype and *Megf10* knockout mice that SACs still undergo lateral movements within the retina plane, suggesting they are still capable of repositioning their somata, but are unable to appropriately refine their proximity to homotypic cells. To search for evidence that adjacent SACs determine their proximity to neighboring cells by dendritic tiling, we generated *Megf10*-driven Cre mouse lines to examine their earliest stages of development. Using this tool, we demonstrate that the morphology of SACs during the formation of their mosaics does not resemble dendritic tiling—instead SAC arbors contact neighboring homotypic cells, confining the growth of their dendritic territory. In *Megf10* mutants, SAC arbors still contact neighboring somata, but fail to exclude them from their arborization territory. Further, we find that MEGF10 must utilize distinct signal transduction pathways in neurons, as knockouts of signal transduction partner from non-neuronal cells do not affect SAC regularity. Lastly, we identify that ITAM motifs within the intracellular domain of MEGF10 are required to recapitulate a cellular recognition-like event in a heterologous cell system. These findings support a model

whereby MEGF10 signals in SACs by a distinct signal transduction mechanism to mediate dendrite-soma interactions necessary to pattern the organization of retinal neurons. This model applies to both OFF and ON populations of SACs and may serve as a general cellular patterning mechanism in other neuron types.

2. Materials and Methods

2.1 Experimental Mouse Models

2.1.1 Animals

Experiments conducted on animals were reviewed and approved by the Institutional Animal Care and Use Committee of Duke University. The animals were maintained under a 12 hour light-dark cycle with *ad lib* access to food and water.

Animals of both sexes were used in this study. Wildtype CD1 mice were purchased from Charles River Laboratories. This study was performed with the approval of the Duke University IACUC.

For these studies, the following transgenic and mutant mouse lines were used:

(1) $Megf10^{tm1b(KOMP)Jrs}$ (Kay et al., 2012) referred to as $Megf10^{-}$ or $Megf10^{LacZ}$; (2) $Chat^{tm2(cre)Lowl}$ (Rossi et al., 2011) referred to as Chat-Cre; (3) $Tg(Six3-cre)69Frty$ (Furuta et al., 2000) referred to as Six3-Cre; (4) $Vav3$ (Sauzeau et al., 2006) (5) $Vav2$ (Doody et al., 2001) (6) Syk (Saijo et al., 2003) (7) $Zap70$ (Kadlecek et al., 1998).

Two Cre reporter strains were used that express membrane-targeted green fluorescent protein (mGFP) upon Cre recombination: (1) $Gt(ROSA)26Sor^{tm4(ACTB-tdTomato,-EGFP)Lox}$, also known as mT/mG (Muzumdar et al., 2007); (2) $Rosa26^{tGFP}$ (Rawlins et al., 2009). An additional Cre reporter strain was used that expresses tdTomato fluorescent

protein upon Cre recombination: Gt(ROSA)26Sor^{tm14(CAG-tdTomato)Hze} (Madisen et al., 2010).

See Key Resources table for repository stock numbers where applicable.

To produce Megf10^{flox} mice, Megf10^{tm1a(KOMP)rs} mice (Kay et al., 2012) were crossed to germ-line Cre strain B6;SJL-Tg(ACTFLPe)9205Dym/J, thereby generating a functional allele (also known as Megf10^{tm1c}) in which exon four was flanked by loxP sites.

2.1.2 Generation of Megf10-cre mice

Production of Megf10-cre knock-in mouse lines were generated in collaboration with Duke Transgenic Core. This genomic location was targeted using homologous recombination and a modified pL253 vector (Liu et al., 2003) with mc1-driven thymidine kinase for ES cell selection. Targeted ES cell clones were validated by PCR and southern blot analysis before embryo injection. Founder mouse lines were validated by PCR. These mouse lines were engineered to modify exon 25 of Megf10, replacing the endogenous stop codon with a FLAG-epitope tag, followed by a T2A self-cleaving peptide (Liu et al., 2017) to release a Myc-epitope tagged Cre recombinase. The founder mouse line Megf10^{CreNeo}, contained an FRT flanked neomycin resistance sequence downstream of the Cre, which was removed by crossing our Megf10^{CreNeo} mice with a mouse line expressing germline FLP recombinase (ACTB:FLPe, Jackson Labs). This

generated our second mouse line, *Megf10^{Cre}*. Removal of the neomycin resistance cassette was confirmed by PCR.

2.1.3 Generation of Rosa-Megf10 mice

Production of Rosa-Megf10 mice was conducted in collaboration with Duke Transgenic Core. This Rosa26a knock-in mouse was engineered to produce Cre-dependent expression of MEGF10 and GFP. The *Megf10-T2A-GFP* sequence was also flanked by FRT sites, allowing its removal by crossing it to a germline FLP recombinase. This recombination would replace wildtype *Megf10* with a point mutated version of *Megf10* and tdtomato. The point mutated version, referred to as 4xITAM, contained tyrosine to phenylalanine mutations of both tyrosines within each ITAM motif (ITAM 1: Y1030F, Y1048F; ITAM 2: Y1099F, Y1111F). Initially the MEGF10 and 4xITAM containing sequences were cloned into pL452 and verified in HEK293T cells to give *Megf10* and GFP expression with FLP recombinase dependent expression of 4xITAM and tdtomato. Next, this plasmid was sub-cloned into the pAi9 vector to target the Rosa26a genomic location for homologous recombination and the addition of the Lox-stop-lox and neomycin resistance cassettes. Targeted ES cell clones were validated by PCR and southern blot analysis before embryo injection. Founder mouse lines were validated by PCR. After two breeding generations to make non chimeric transgenic lines, the

neomycin resistance cassette, which was flanked by attB and attP recombination sites, was removed by crossing mice with a germline phic31-recombinase mouse (Jackson Labs). Successful removal of the neomycin cassette was confirmed by PCR and this line was used for experiments, referred to as Rosa-Megf10. To generate the Rosa-4xITAM mouse line, Rosa-Megf10 was crossed to a mouse line expressing germline FLP recombinase (ACTB:FLPe, Jackson Labs) to remove the Megf10 and GFP sequences, placing 4xITAM and tdtomato in its place. Successful recombination was confirmed by PCR.

2.2 Tissue Processing and Data Collection

2.2.1 Histology and Immunohistochemistry

RETINAL CROSS SECTIONS

Mice were anesthetized by isoflurane or cryoanesthesia (neonates only) followed by decapitation. Eyes were enucleated, washed in PBS, and fixed in PBS containing 4% formaldehyde (pH 7.5) for 1.5 hours at 4°C. After fixation, eyes were washed 3X with PBS and stored in PBS containing 0.02% sodium azide at 4°C until further processing. Retinas were dissected from the eyecup, cryoprotected by equilibration in PBS containing 30% sucrose, then embedded in Tissue Freezing Medium and frozen by submersion in 2-methylbutane chilled by dry ice. Tissue sections were cut on a cryostat

to 20 mm and mounted on Superfrost Plus slides. Slides were dried on a slide warmer for 1 hr then stored at 80°C or used immediately. For antibody labeling, slides were washed for 5 min with gentle agitation in PBS to remove embedding medium and blocked for 1 hr in PBS + 0.3% Triton X-100 (PBS-Tx) containing 3% normal donkey serum. Primary antibodies were diluted in blocking buffer, added to slides, then incubated overnight at 4° C. Slides were washed with PBS 3X for 10 min followed by incubation with secondary antibodies diluted in PBS-Tx for 1–2 hr at RT. Slides were washed again with PBS 3X for 10 min then coverslipped using Fluoromount G.

RETINAL WHOLE-MOUNTS

Tissue was processed as above up to the point of dissection from the eyecup. After dissection from eyecup, retinas were washed in PBS then blocked for 3 hours with agitation at 4° C in blocking buffer (constituted as described above). Primary antibodies were diluted in blocking buffer, added to retinas, and incubated for 5–7 days with gentle agitation at 4°C. Retinas were washed 3X with PBS over the course of 2 hours with gentle agitation. Secondary antibody was diluted in PBS containing 0.3% Triton X-100 and was added to retinas followed by incubation overnight at 4° C with gentle agitation. Retinas were washed again 3X in PBS over the course of 2 hours with gentle agitation. For mounting on slides, four radial incisions separated by 90° were made centripetally,

approximately 1/3 the radius of the retina. Retinas were flattened on nitrocellulose paper photoreceptor side down and coverslipped with Fluoromount G.

2.2.3 *In situ* hybridization

Full length cDNAs for Zap70, Syk, Vav1, Vav2 and Vav3 were obtained from Thermo Fisher Scientific in vector pCMV-Sport6. Sequencing confirmed the presence of the correct insert. The plasmids were linearized at the 5' end of the insert and antisense digoxigenin-labeled RNA probes (DIG RNA labeling mix; Roche Diagnostics) were synthesized using a T7 or Sp6 site depending on the orientation of the cDNA in the vector (MAXIscript kit, Thermo Fisher Scientific). The probes were purified on a G50 spin column (GE healthcare) and hydrolyzed at 60°C in bicarbonate buffer (40mM NaHCO₃, 60mM Na₂CO₃) to appropriately 300-700bp. Retinas from P1, P6 and P18 mice were quickly dissected from the eyecup in cold Hank's balanced salt solution buffered by 10mM HEPES and fixed in 4% paraformaldehyde/1X PBS for 1.5 hours on ice, washed twice with 1X PBS, and sunk in 30% sucrose/1X PBS for 1 hour. Retinas were then embedded in TFM blocks (Triangle Biomedical Sciences) and stored at -80°C until sectioning 20 µm slices on a cryostat (Barlow Scientific). *In situ* hybridization was performed on retinal sections as previously described (Kay et al., 2011; Yamagata, 2009; Visser et al., 2015). Probe hybridization was detected with peroxidase-coupled anti-

digoxigenin followed by a Cy3-tyramide color reaction. After the color reaction, slides were washed at least 4 times over 2 hours in 1X PBS. They were then subjected to our standard retinal cross section immunohistochemistry protocol described above.

2.2.4 Microscopy and image processing

Sections and whole-mounts were imaged on a Nikon A1 or an Olympus FV300 confocal microscope. Image Z-stacks (Z-resolution 0.4–0.5 mm for whole-mount images; 0.8–1.0 mm for cross-sections) were imported to Fiji (Schindelin et al., 2012) de-noised by median-filtering (0.5–2.0 pixel radius), and projected to a single plane. The portion of the stack selected for maximum-intensity projection was determined by the Z-volume of the structure to be depicted in the final image. Except where noted, data analysis and quantification was only performed using original stacks, not Z-projections. Color channels were assembled, and minor adjustments to brightness and contrast were made, in Image J. When images were to be compared, equivalent adjustments were performed on all images in the experiment.

2.3 Cell Culture

2.3.1 HEK293T Cells

HEK293T cells were obtained from, validated by, and mycoplasma tested by ATCC. The cells were cultured in Dulbecco's Modified Eagle's Medium (DMEM) with 10% bovine growth serum, 4.5 g/L D-glucose, 2.0 mM L-glutamine, 1% Penicillin/Streptomycin in 10 cm cell culture dishes. Cells were passaged every 2–3 days to reach confluence. Before splitting, culture media were removed and Dulbecco's phosphate-buffered saline (D-PBS) was used to rinse cell layers as well as removing residual serum. Cells were detached from dish with 4 ml of 0.05% Trypsin and incubated at 37°C until cell layer is dispersed (about 5 min). Equal volume of complete culture media was added to the dish to inhibit protease activity. The suspension was centrifuged at 200 × g for 5 min. Supernatant was aspirated and the cells were suspended with appropriate amount of media and plated (1:4-1:8). Cells used for experiments were passaged no more than 10 times. Cell stocks were stored as 2 million cells per vial in complete culture media with 10% DMSO in liquid nitrogen.

2.3.2 HEK cell plasmid delivery

TRANSFECTION

HEK293T cells were grown to 80% confluency in 24 well plates (MatTek Corporation) with glass bottoms coated with poly-D-lysine (Sigma-Aldrich). Cells were then transfected using a linear polyethylenimine (PEI) transfection reagent: DNA, PEI, and Opti-MEM were mixed in a 1:3:30 ratio and incubated for 10 min at room temperature then applied to confluent cells. Cells were harvested 24 hr post-transfection.

NUCLEOFECTION

For nucleofection of HEK293T cells were cultured to 100% confluency and digested with 4 ml of 0.05% Trypsin for single cell suspensions. Cells were nucleofected with Amaxa® Cell Line Nucleofector® Kit V (Lonza) following instructions from the manufacturer. In short, 2 million cells were suspended in 100 µl of Nucleofector® Solution and 3.5 µg of plasmid DNA was added. After gentle mixing, cells were transferred to a cuvette and shocked with program S-002. Nucleofected cells were immediately mixed with 500 µl of pre-equilibrated culture medium before transferring to glass bottom dishes.

2.3.3 HEK cell immunocytochemistry

Cells were fixed 24 hours after plasmid induction with 4% PFA dissolved in PBS for 15 minutes on ice. All staining conditions were done in PBS buffer with the exception of anti-pTyr staining, which was done in TBS based buffers. After fixation, cells were washed twice with PBS and were then permeabilized and blocked with a solution

containing 0.1% Triton X-100 and 3% Normal Donkey Serum (NDS) for 10 minutes at room temperature. Cells were then incubated overnight at 4°C with primary antibody staining solutions containing the necessary primary antibodies and 3% NDS dissolved in PBS. The next day, after washing 3 times with PBS, cells were incubated with 1:1000 Donkey secondary antibodies for 1 hour at room temperature. Cells were then washed 2 times with PBS before adding 1 ml of PBS + 0.02% NaAzaide on top of the cells and sealing the chamber with parafilm.

2.3.5 HEK cell live imaging

Cells were transfected or nucleofected in 24 well glass bottom dishes and were given 6-10 hours to recover and begin expressing the plasmids. One hour before moving cells to the live imaging chamber, the cells were buffered with 1M HEPES to a final concentration of 20 mM. Cells were placed into an Okolabs imaging chamber, which maintained the temperature at 37°C and had a controlled flow of humidified carbogen gas. Imaging was performed on an inverted Nikon A1 laser scanning confocal microscope using a heated 60X objective to minimize thermal drift. Images were acquired using Nikons perfect focus system, allowing a central focal plane to be defined and took 8-17 z-stacks at a z-resolution of 0.6 μm to be taken around that point. Images were acquired every 10 minutes over 16-24 hours.

2.4 Molecular Biology

2.4.1 Plasmid cloning

The pEGFN3-MEGF10-GFP and version with removed intracellular domain have been reported previously (Kay et al., 2012; Ray et al., 2018). These plasmids were originally made from pUbC-MEGF10-GFP (Addgene #40207). To generate intracellular domain deletion (Δ 891-1025) and tyrosine to phenylalanine point mutations (NPXF, 4xITAM) we used Q5 site-directed mutagenesis kit (New England Biolabs) and followed the manufactures instructions to design primers necessary make the desired PCR products. All generated constructs were verified by Sanger sequencing (Genewiz) and diagnostic digest. Vector design and sequence alignments were done using Snapgene software.

2.4.2 Western blot

Retina lysates for western blot were replaced by dissecting quickly dissecting retinas into cold HBSS placing 2 eyes (1 pups, retina) into 100 μ l of lysis buffer (1xPBS, 1x protease inhibitor, 1% triton). Retinas were homogenized and centrifuged at Max centrifuge speed for 20 minutes at 4°C to separate soluble and insoluble fractions. The soluble fraction was placed into a new tube and stored at -80°C until ready for use. For

western blots samples were prepared in 2X laemmli sample buffer, and heated at 95°C for 10 minutes, before being loaded onto SDS-acrylamide gel (running gel: 8% acrylamide/bis Tris-HCL with 0.1% SDS, pH 8.8; stacking gel: 5% acrylamide pH 6.8; cross linked with TEMED and APS). As a molecular weight marker Precision Plus Protein Dual Color Standards (BioRad) were used. The gel was run on a BioRad minigel system with SDS-PAGE running buffer (25 mM Tris, 192mM glycine, 0.1% SDS). Electrophoresis was done at 50 V while the samples entered the stacking gel and then adjusted to 120 V until the dye reached the bottom of the gel. For transfer, BioRad Immobilon-FL PVDF membrane and Whatman filter paper were used with the BioRad mini cassette and transfer buffer (25 mM Tris, 192 mM glycine, 20% methanol) at 100V for 90 minutes at 4°C. After transfer, membrane were blocked with PBS/Odyssey blocking buffer and stained with GFP and HA antibodies diluted in Odyssey blocking buffer overnight at 4°C with shaking. Membranes were then washed with PBST four times and membranes were stained with 1:20,000 secondary antibodies for 1 hour at room temperature. The membranes were then washed four times with PBST, and then rinsed with PBS and water before imaging with LI-COR Odyssey using Image Studio Software.

2.4.3 Co-Immunoprecipitation

Plasmids encoding MEGF10-GFP, CYTO9-GFP or VAV3-HA constructs were introduced to HEK293 cells using transfection methods as described above. For Co-immunoprecipitation cells were harvested 24hrs post-transfection and were lysed with NP-40 lysis buffer (1% NP-40, 150mM NaCl, 50mM Tris-Cl, 1X proteinase inhibitor and 1X phosphatase inhibitor) by pipetting. Lysates were centrifuged at 14,000g at 4°C for 15 minutes to remove insoluble material and the soluble fractions were quantified using Bio-Rad DC assay. For immunoprecipitation, 500 μ l (1 μ g/ μ l) protein contained in lysis buffer was incubated overnight with 1.5 μ l of Anti-GFP. The next day, 10 μ l of Protein G dynabeads were added to the mixture for 1hr at 4°C while rotating. Beads were magnetically separated and flow-through was removed. Beads were washed using 500 μ l of lysis buffer (3x) while on ice and then eluted in 30 μ l of 2X Laemmli buffer containing 5% β -mercaptoethanol. These lysis buffer conditions were selected based on them being published to preserve MEGF10 protein interactions (Scheib et al., 2012).

2.5 Data Analysis

2.5.1 Mosaic Analysis

For mosaic analysis, 40x images (353.55x353.55 μ m) were taken in midperipheral retina using confocal microscopy to optically separate retinal neuron populations

stained with cell type specific markers. For developing OFF and ON SACs (P0,P5) we used anti-Sox2 to label the location of their nuclei (Whitney et al., 2014). Later in postnatal development at P19, anti-ChAT was used to label SAC populations. HC cell populations were labeled using anti-Calbindin antibodies (Kay et al., 2012). Using imageJ software, points were placed in the middle of each cell to generate X-Y coordinates. These coordinates were then used to produce Voronoi Domain Regularity Indices using Fiji software and Density Recovery Profiles using WinDRP software as previously described (Euler et al. 2003; Kay et al., 2012).

2.5.2 Analysis of SAC arbor territories

To assess if SAC arbor territories contained fewer homotypic somata than expected if they were randomly distributed, we used two channel images that contained individually labeled SAC arbors from Chat^{Cre}; mGFP reporter mice which were co-labeled with anti-sox2 to label the entire SAC populations. Arbor territories were drawn in ImageJ by lines connecting arbor tips to generate a series of ROIs representing each SAC's arbor territory. Next, looking at the sox2 channel which matched our reference SAC, we counted the number of homotypic somata completely contained within those territories including the somata belonging to the reference cell. These arbor territory ROIs were transposed onto unmatched arrays of SACs and the number of cells counted

again. Then, the average number of SACs found across the unmatched samples was averaged and compared to the matched averages. We further compared these averages using frequency distributions plots. To do this, we made frequency distribution plots for the number of unmatched somatas contained within each individual arbor. The average of these plots provides a measure of how frequent one would expect to observe a given number of cells within a SAC territory. These expected frequencies were then compared using chi-squared tests to determine the probability that the observed matched distribution had occurred by chance alone.

2.5.3 Statistical analysis

Error bars are reported at mean +/- standard deviation unless otherwise noted. Students t-tests performed are unpaired, two-tailed t-tests. Parameters of statistics (i.e. sample size, tests conducted and statistical significance) can be found within figures or figure legends. All analyses were performed in JMP 12 (SAS Institute) or GraphPad Prism 8.1.1.

2.6 Key Resources

Table 1: Key Resources Table

Reagent or Resource	Source	Identifier
Primary Antibodies		
ChAT: goat, 1:400	Millipore	AB144P
GFP: rabbit 1:1000	Millipore	AB3080P
GFP: chicken 1:1000	Life Technologies	A10262
Calbindin: rabbit 1:10,000	Swant	CB-38

Vglut3: guinea pig 1:2500	Chemicon	AB5421
Megf10: rabbit 1:600	Millipore	Abc10
Sox9: rabbit 1:4000	Millipore	AB5535
Sox9:goat 1:2000	R&D Systems	AF3075
Sox2: rabbit 1:500	Abcam	AB97959
Sox2: goat 1:500	Santa Cruz	SC-17320
mCherry: rabbit 1:3000	Kerafast	AMU106
Bgal: rabbit 1:4000	Sanes lab	N/A
RFP: rat 1:1000	ChromoTek	5f8-20
Experimental Mouse Lines		
Mouse: CD-1	Charles River	022
Mouse: C57bl16/J	Jackson Labs	000664
Mouse: Megf10 ^{LacZ} or Megf10 ⁻	(Kay et al., 2012)	Megf10 ^{tm1b(KOMP)Jrs}
Mouse: Megf10 ^{Flox} or Megf10 ^F	(Ray et al., 2018)	Megf10 ^{tm1c}
Mouse: Chat-Cre	Jackson Labs	006410
Mouse: Six3-Cre	Jackson Labs	019755
Mouse: Isl1-Cre	Jackson Labs	024242
Mouse: Vav3		
Mouse: Vav2		
Mouse: Syk ^{Flox} (Syk ^{tm1.2Tara})	Jackson Labs	017309
Mouse: Zap70 ^{tm1Weis}	Jackson Labs	004225
Mouse: Pax2-Cre	Jackson Labs	
Mouse: Rosa26 ^{Ai14} (Gt(ROSA)26Sor ^{tm14(CAG-tdTomato)Hze1/J})	Jackson Labs	007914
Mouse: Rosa26 ^{mtmg} Gt(ROSA)26Sor ^{tm4(ACTB-tdTomato-EGFP)Luo}	Jackson Labs	007676
Mouse: Rosa26 ^{fGFP}	(Rawlins et al., 2009)	Gt(ROSA)26Sor ^{tm1(CAG-EGFP)blh}
Mouse: ACTB:FLPe	Jackson Labs	003800
Mouse: Megf10 ^{CreNeo}	See methods	
Mouse: Megf10 ^{Cre}	See methods	
Mouse: Rosa26-Megf10	See methods	
Mouse: Rosa26-4xITAM	See methods	
Mouse: Phic31 recombinase	Jackson Labs	007743
Plasmids		
CMV-M10-GFP	(Kay et al., 2012)	
CMV-M10-mCherry	(Kay et al., 2012)	

Syk cDNA		
Zap70 cDNA		
Vav1 cDNA		
Vav2 cDNA		
Vav3 cDNA		
Software		
Fiji/ImageJ	(Schindelin et al., 2012)	
GraphPad Prism 7.0	GraphPad	RRID:SCR_002798
Image Studio™	LI-COR Biosciences	
Illustrator	Adobe	
WinDRP v1.6.4	T.Euler (Tubingen)	
Olympus CellSens	Olympus Lifescience	
NIS-Elements	Nikon	
JMP 12	SAS Institute	
Other		
HEK293T	ATCC	293T (ATCC CRL-3216)

3. Determining cellular mechanism of MEGFG10-mediated mosaic formation in SACs

3.1 Introduction

To identify the cellular mechanisms underlying cell-cell repulsion and exclusion zone formation, we conducted a detailed examination of the spatial relationships between SAC arbors and neighboring homotypic cells during the formation of their mosaic. While the dendrites of adult SACs are well known to highly overlap with each other, it has been hypothesized that early in development their dendrites might transiently tile, providing spatial information on their proximity to neighboring cells allowing them to form exclusion zones (Cook and Chalupa, 2000; Huckfeldt et al., 2009). Further, ACs early in development have been observed in live imaging studies to dynamically reposition themselves in lateral plane of the retina. (Barrasso et al., 2018; Chow et al., 2015). The cellular defect underlying the *Megf10* phenotype could therefore be due to either due to defects in dendritic tiling during development, or an inability to reposition themselves – leaving them randomly distributed. Indeed, modeling studies have shown that short lateral movements are sufficient to transform random arrays into regular arrays resembling the SAC mosaics (Eglen et al., 2000; Galli-Resta, 2000). Studies of newborn SAC morphology following their radial migration found that SACs extend projections that contact neighboring SAC somata (Ray et al., 2018). This study raises

questions about the feasibility of dendritic tiling in sculpting exclusion zones necessary for mosaic formation.

3.2 Emergence of OFF SAC regularity requires *Megf10* at P0

Focusing first on the OFF SAC array, we identify that exclusion zones grow postnatally; however, their orderly positioning is established on the first postnatal day. This was done by labeling the OFF SAC population at P0, P5, and P17, with age appropriate markers and taking images from mid-peripheral retinas (Fig. 2A) (Whitney et al., 2014) We found no difference in cell density between wildtype and *megf10* knockout retinas at any age (Fig. 2B) and the density decreased similarly between genotypes, while the retina expanded in area (Fig. 2C). We assessed the regularity of the array using the Voronoi domain regularity index (VDRI), which quantifies the variation in areas nearest to a reference cell (Keeley et al., 2007; Raven et al., 2003). As a comparison, we generated a simulated dataset of random distributions, matching cell density and SAC diameter for each age. This allowed us to assess if our observed spatial statistics were achievable by chance when the only limitation on cell spacing was the physical presence of another cell body. We find that wildtype SACs are indeed more regular than chance at all ages measured, and a small improvement in regularity occurs from P0 to P19 (Tukey's HSD, $p=0.0047$) (Fig. 2D). To visualize cell exclusion zones over development, we generated density recovery profiles (DRPs), which is a plot of the

estimated cell density as a function of distance from each reference SAC (Rodieck, 1991). We can see in these plots that as wildtype retinas expand and cell density decreases the DRP shifts rightward, scaling with retina growth (Fig. 2F). By contrast, the VDRI of OFF SACs in *Megf10* knockout retinas were indistinguishable from chance at all ages (Fig. 2D) and the DRPs overlap while the retina expands (Fig. 2G). Since mutant OFF SACs are already disordered at P0, MEGF10 protein must be required at this time to pattern them into regular distributions.

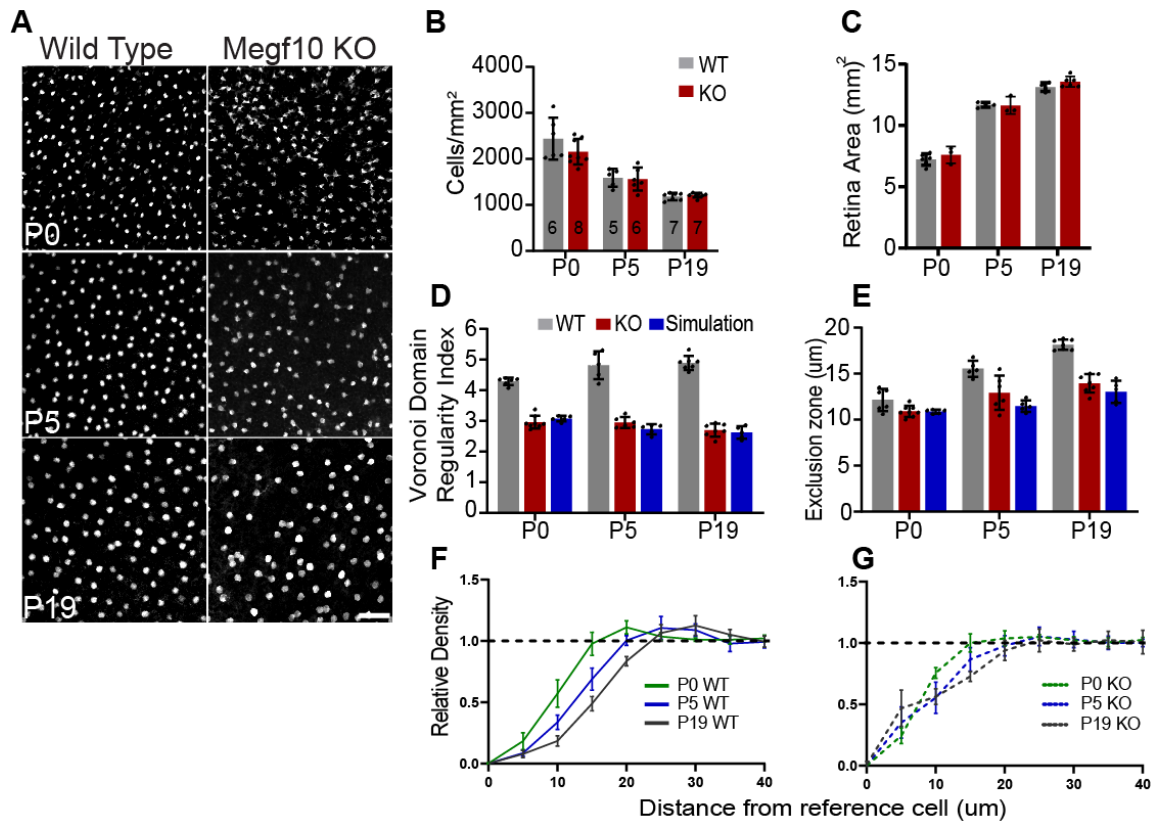


Figure 2: Organization of OFF SAC array at P0 requires MEGF10

(A) Labeling of OFF SAC array in control and *Megf10* knockout retinas imaged using age-appropriate markers (Anti-Sox2; P0, P5) (Anti-ChAT; P19) (Anti-Bgal; P0 MEGF10 KO). (B) Density of SACs is similar between control and *Megf10* knockouts at all ages. Number of mice analyzed for each each/genotype is indicated. Data from all mice is averaged from 3 mid-peripheral images. (C) No difference in *Megf10* knockout retina areas compared to controls at any age. (D) Regularity of control OFF SAC array assessed by VDRI is significantly higher than in *Megf10* knockout retinas, while knockouts and cell density matched simulations were indistinguishable (E) Exclusion zones only differ from simulations for control retinas after P0. (F) Density recovery profiles for control retinas shift rightward with development while (G) mutant profiles do not scale as the retina expands. Scale bar: 50 μm –all images. Standard deviation shown on all graphs.

3.3 Tangential dispersion occurs in SACs lacking MEGF10

To understand why *Megf10* mutant mosaics are disordered at P0, we next examined the cellular mechanisms that become impaired in these mutants. Retina cell types that organize themselves into mosaic patterns are known to move laterally within the plane the retina following their radial migration from the ONBL (Reese and Galli-Resta, 2002). If *Megf10* is required for SAC tangential movements, this could explain the failure to arrange into mosaics. To test this possibility, we took advantage of a Pax2-Cre BAC transgenic line crossed to Cre-conditional tdTomato reporter mouse, which drives reporter expression in a small subset of multipotent progenitor cells and their clonally labeled progeny. In control P2 retinas, this labeling revealed densely packed radial columns as well as laterally displaced cells (Fig. 3A). Co-labeling with Anti-Sox2 to mark SACs, we found that about half of all SACs were located outside of clones (Fig. 3B).

These observations are consistent with previous studies examining SACs in other paradigms labeling retina progenitors (Reese and Galli-Resta, 2002; Reese et al., 1995). If the intercellular repulsion mediated by MEGF10 is required to drive lateral cell movements, then in *megf10* mutants all SACs labeled by *tdtomato* will not tangentially disperse from their clones of origin. Instead, we find no difference between dispersion rates between mutant and control retinas ($p=0.0914$, $n=163$, $N=3$ mutants and $n=196$, $N=3$ controls) (Fig. 3A, B). Further, there was no difference in the average displacement distance for SACs located outside of clones (Fig. 3C, D). These results demonstrate that although SACs in *Megf10* knockout retinas are randomly distributed, they are still subject to tangential dispersion. We conclude that SACs lacking MEGF10 are still capable of making the lateral movements thought to be necessary to distance themselves from each other, but lack the ability to recognize when they are not positioned appropriately relative to another homotypic cell.

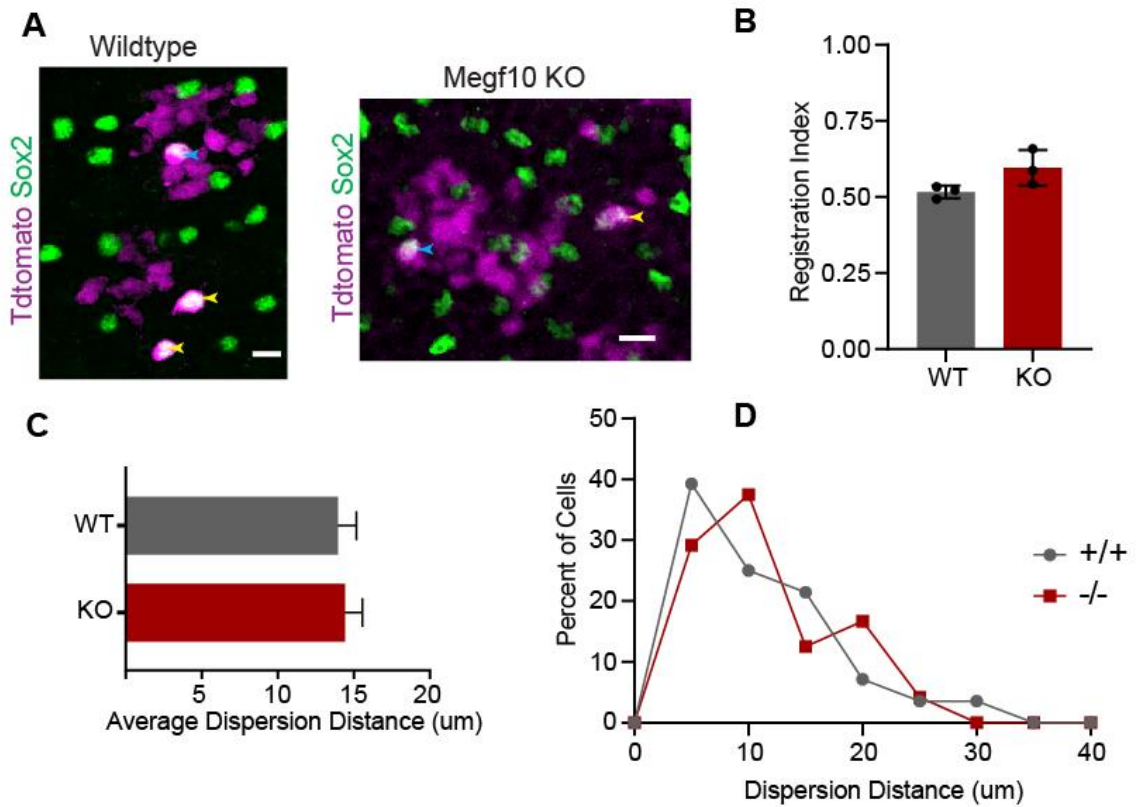


Figure 3: Both control and *Megf10* knockout SACs make lateral movements in the retina plane

(A) Pax2-cre driven expression of tdtomato labels columns of cell derived from the same progenitor cell. This method reveals SACs (labeled by anti-sox2) can be found outside of these patches due to lateral movements. SACs within columns labeled by blue arrowheads, SACs that moved outside of columns labeled by yellow arrowheads (B) Registration index determined by dividing the number of tdtomato labeled cells residing in columns by total tdtomato labeled cells. N=3 per genotype, n~60 cells per animal, two-tailed t-test, p=0.09 (C) Average distance SACs displaced from edge of nearest column is the same in control and knockouts (control n=24, knockout n=28; two-tailed t-test p=0.78) (D) Plots for the fraction of cells at given distance from column overlap. Scale bar: 10um

3.4 Megf10-driven Cre recombinase mouse line reveals SAC anatomy is inconsistent with dendritic tiling

Megf10cre mouse line enables labeling of SACs during early development

To test the possibility that defects in cell-cell recognition underlie the Megf10 mutant phenotype, we set out to document the anatomical nature of SAC-SAC contacts in developing retinas. A previously utilized genetic strategy to specifically label SACs during development was a Chat-driven cre mouse line crossed with a membrane-targeted GFP reporter (Ray et al., 2018). This mouse line labeled individual starbursts starting at birth; however, it did not label SACs during the earliest stages of development when SACs first contact each other. Expression of MEGF10 is known to begin in SACs following their radial migration down from the outer neuroblast layer (ONBL) as they begin to innervate what will become the inner plexiform layer (IPL) (Kay et al., 2012). Therefore, we generated a transgenic knock-in mouse with Cre downstream from exon 25 of Megf10, to reveal SAC morphologies at their earliest stages of development (Fig. 4A). Two iterations were generated: one that contained an FRT flanked neomycin cassette used to select the transgenic ES cells and a second iteration, made by breeding this line to an embryonic FLP to remove the neomycin cassette. To validate these mouse lines, Megf10CreNeo and Megf10Cre were crossed to a Cre-dependent membrane-targeted GFP (mGFP) reporter. At P3, both SAC populations and horizontal cells were labeled and in the second postnatal week, these lines showed

mGFP expression in muller glia, consistent with Bgal immunolabeling performed on the previously generated Megf10 knockout allele (Fig. 4B) (Kay et al., 2012). These Cre alleles were crossed with the knockout allele of megf10, as well as the mGFP reporter to examine MEGF10 protein expression at P3. Immunohistochemistry with anti-Megf10 demonstrates that MEGF10 protein was only produced if the neomycin cassette had been removed (Fig. 4C). The morphology of SACs lacking MEGF10 protein had disruptions in IPL innervation as previously described (Ray et al., 2018). Further, the mature OFF SAC array in Megf10CreNeo^{-/-} was found to phenocopy the irregular distribution of complete megf10 knockouts (Fig. 4D). No difference in VDRI was found for homozygous Megf10Cre (Fig. 4D). These results demonstrate that our megf10 driven Cre lines serve as a reliable marker of SACs and the expression and function of MEGF10 protein is dependent on removal of the neomycin cassette.

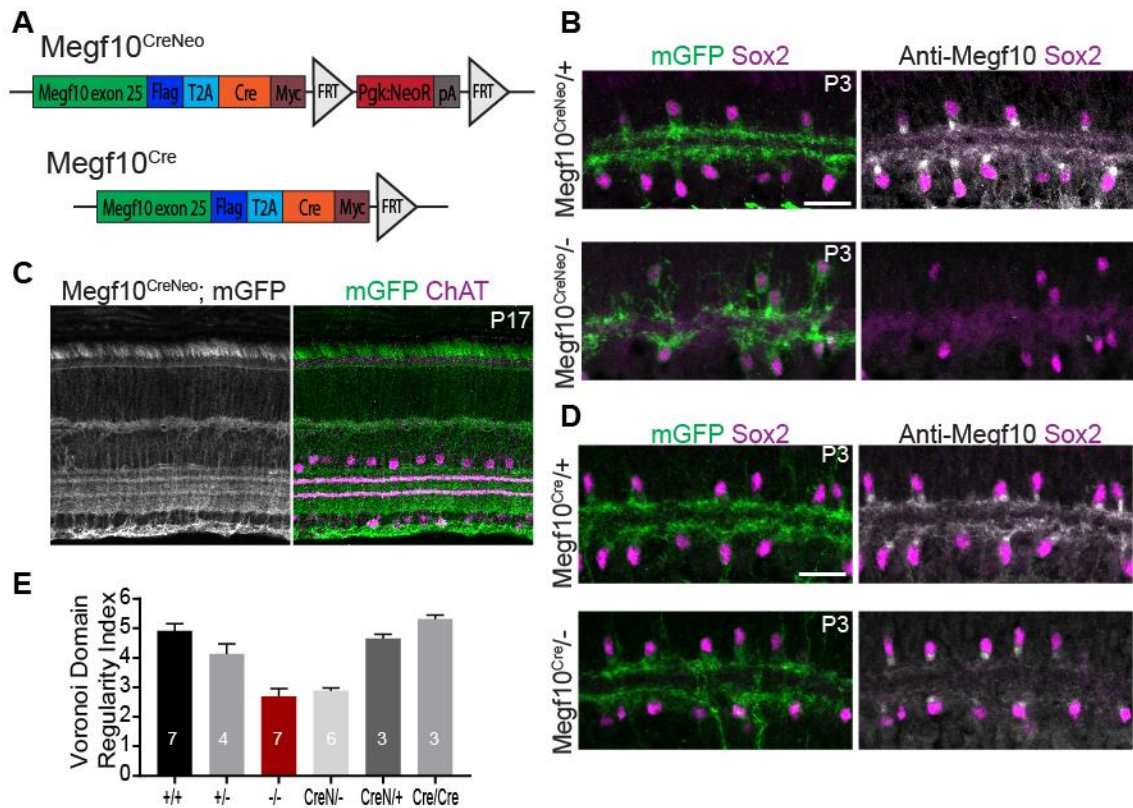


Figure 4: Recombination of *Megf10* driven Cre alleles label SACs early in development and removal of Neomycin cassette is required for MEGF10 protein expression.

(A) Schematic of *Megf10* alleles. Removal of neomycin cassette by breeding with FLP-recombinase mouse generates second mouse line. (B) *Megf10*^{CreNeo} allele drives expression of mGFP in starbursts at P3. Mice containing *Megf10*^{CreNeo} allele and *Megf10* knockout allele (-) do not express MEGF10 protein and show innervation defects previously observed in *Megf10* knockouts. (C) Recombination pattern of *Megf10*^{CreNeo} at P17 shows labeling across whole retina due to expression in Muller Glia. (D) After removal of Neomycin *Megf10*^{Cre} drives expression of mGFP reporter in SACs and is capable of producing MEGF10 protein, preserving their innervation of the IPL (E) Regularity of OFF SAC array in MEGF10^{CreNeo} serves as a knockout allele resulting in similar mosaic phenotypes while MEGF10^{Cre} allele does not disrupt mosaic formation. Standard deviation shown. Scale bars = 25µm.

Morphogenesis of embryonic SAC arbors is not consistent with dendrite-dendrite tiling

If SACs position themselves using dendritic tiling to assess their proximity to adjacent homotypic cells, we should be able to visualize dendrite-dendrite tiling at some developmental stage. Adult SACs are well known to have large dendritic trees and to highly overlap (Fig. 5A), so this dendritic tiling event must occur during a transient developmental phase. Using our *Megf10^{CreNeo}* mouse line to drive expression of our mGFP reporter, we examined the morphology of E16 SACs as they complete their radial migration to the nascent IPL. We observed that SAC arbors often contacted neighboring cell somata, even as they first begin to innervate the IPL (Fig. 5C). By P0, SACs extended a network of arbors within both the IPL and INL as previously reported (Fig. 5D) (Ray et al., 2018). In *megf10* knockout mice, we found that the morphology of E16 SAC arbors also readily overlapped, appearing similar to control mice (Fig. 5E) Assessing quantitative measures of mosaic regularity in flat mounted embryonic retinas was not possible as OFF and ON SACs could not be clearly resolved in a single plane. Clear differences between the genotypes appeared by P0, when SACs lacking MEGF10 could be seen to under innervate the IPL, while the INL network appeared more elaborate

(Fig. 5F). In conclusion, we found that SAC arbors in the earliest stages in development extend to at least the next adjacent soma, providing no support to the hypothesis that dendritic tiling drives the refinement of their mosaic. This suggests that another mechanism must be used by SACs to determine their proximity to adjacent homotypic cells.

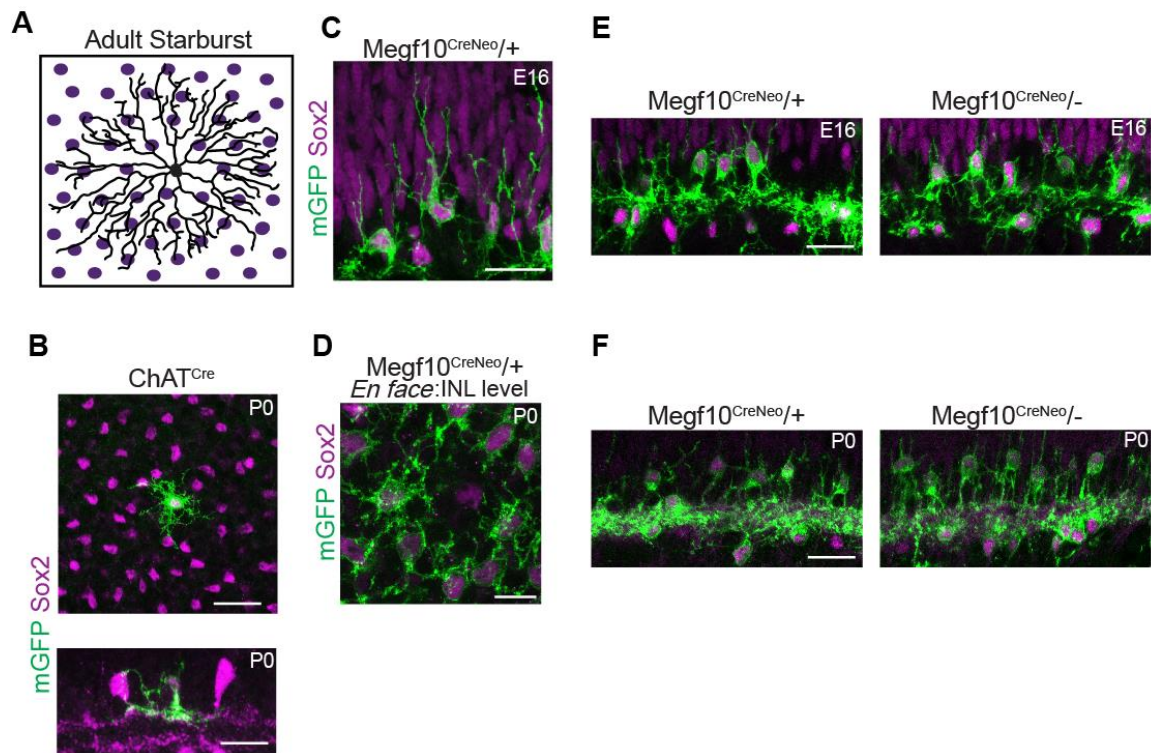


Figure 5: SAC dendrites early in development grow to contact neighboring somata

(A) Schematic adult SAC dendrites highly overlap with making it unclear how they might determine their proximity to neighboring cells. (B) *Chat^{Cre}* driving mGFP reporter allows labeling of individual SACs before the whole population begins expressing it.

Sections (bottom) and *en face* (top) views show that cells tend to grow to contact neighboring cells. (C) Shows embryonic SACs as they complete their migration to IPL extend processes to neighboring cells. (D) Network of SAC arbors in the INL can be seen growing to SAC not yet expressing mGFP. (E) Arbors from E16 SACs in both control and knockout retinas overlap with each other. (F) Control and mutant SACs extend network of arbors in INL. Mutant SACs under innervate IPL as previously reported. Scale bars: 10 μ m (D) 25 μ m (others).

3.5 Arborization territories in OFF SACs limit neighboring cell proximity in MEGF10-dependent manner

If SAC dendrites do not tile as previously hypothesized, how do developing SACs detect where their soma is positioned relative to homotypic cells? Since we could not find evidence that developing SACs exhibit transient dendrite-dendrite tiling, we wondered if another patterning mechanism could be used sculpt their exclusion zones. Our observations of OFF SACs extending arbors to neighboring somata during embryonic ages, and the expansion of this network at P0 when SACs are beginning to show signs of regularity, led us to wonder about the relationship between SAC arborization territories and neighboring somata. If SAC arbors could recognize they had contacted another homotypic cell body, it would provide them with spatial information about their proximity to neighbors and allow them to reposition themselves.

To test this hypothesized relationship between P0 SAC arbor areas and the positioning of adjacent cells, we measured how frequently SACs were located within another's cell's dendritic territory. To measure this, we drew areas from the tips of

individually labeled reference Off SAC arbors and counted the number of other SACs completely enclosed within their reference cell's arbor territory. In order to determine if fewer cells were found within an arbors territory than expected by chance, we also took these reference Off SAC arbor territories and randomly placed them on Off SAC array images from unmatched data (Off SAC array is unmatched from the reference cell). We found that on average fewer cells were contained within the reference cells arbor territory when the SAC array was matched to the reference cell (Fig. 6A). Plotting the frequency distribution of this data we found that the majority of Off SAC arbors (~60%) contained only the SAC cell body belonging to the reference cell. The unmatched data plot shows the frequency that you would find a given number of cells within an arbor territory at random. Comparing these frequencies we determined that the distribution we observed is highly unlikely to have occurred by chance (chi-squared, $p=0.005$, $df=6$) (Fig. 6C). To validate this method, we next tested this dendrite-soma relationship at a P3 when the mosaic was more refined. At this age, SACs have on average have grown larger (Fig. 6D) and past adjacent set homotypic cells. Here, we find no difference in the average number of SACs enclosed by a reference cell when varying matched and unmatched SAC arrays. Further, there is no difference in the frequency distribution plots (chi-squared, $p=0.34$, $df=6$) (Fig. 6F). These results demonstrate that Off SAC arbors

at P0 exhibit a transient relationship between the size of their arbors and their proximity to adjacent cells.

We next wanted to examine what the relationship between *Megf10* mutant arbors and their adjacent OFF SAC neighbors. If the arborization territories in *Megf10* mutants are still bounded by neighboring cells, then we will continue to detect few cells within their arbor territory. This would suggest their ability to recognize homotypic cells remains intact, but instead the lack of MEGF10 prevents them from growing uniformly. Alternatively, if MEGF10 is required for cell-cell recognition between homotypic cells, then their arborization territories would grow irrespective of neighboring cells (Fig. 6G). Using our Chat-Cre; mGFP reporter mouse line, we labeled individual ON SACs in *Megf10* mutant retinas and counted the number of cells within their arbor territory compared to transposition of unmatched mutant arrays (Fig. 6H, 7B). We found that the average number of cells within an arbor territory approached being significantly lower in unmatched arrays while the frequency distribution curves overlapped (Fig. 7C, D). This result is likely due to the arbor areas in *Megf10* mutant retinas being smaller than those in wildtype; these small arbor areas when transposed onto unmatched arrays could often report no cells present within a territory and skewing average measures lower (Fig. 6H). One possible outcome from our models predicts that there would be greater variation in cell arbor size if their growth was constrained by neighboring cell

proximity (which is more irregular in mutants). Although mutant arbors areas can be smaller, no difference in overall variability was found (Levene's variance test, f -ratio=0.45, $p=0.51$). To make fair comparisons between our mutant and wildtype arbors, we controlled for cell size by only using reference cell arbors that were within 1 standard deviation of wildtype arbors. Applying this standardization, we found that the average number of cells located within a mutant OFF SAC arbor territory was greater than in controls. Using our matched/unmatched analysis, we again found that in control OFF SACs the average number of cells within a given territory was greater in our unmatched data set, while in mutant OFF SACs, no difference was found between matched and unmatched arrays (Fig. 6J). Further, the frequency distribution plot for matched mutant arbors transposed with unmatched mutant OFF SAC arrays overlap (chi-squared, $p=0.46$, $df=6$), suggesting that the observed arrangement of OFF SAC arborization territories relative to neighboring cells could have occurred by chance alone (Fig. 6K). As a control, wildtype OFF SAC mosaic arrays were transposed onto mutant arbor territories, which resulted in frequency distribution plots similar to those found in unmatched mutant arrays, demonstrating the regularity of the OFF SAC mosaic did not dramatically influence the number of cells that by chance end up within the reference cells territory. (Fig. 6K). Together, these results establish that at P0, wildtype OFF SAC arborization territories enclose fewer neighbors than expected by chance and this

relationship is lost in *Megf10* knockouts where arbors grow irrespective of homotypic cell positioning.

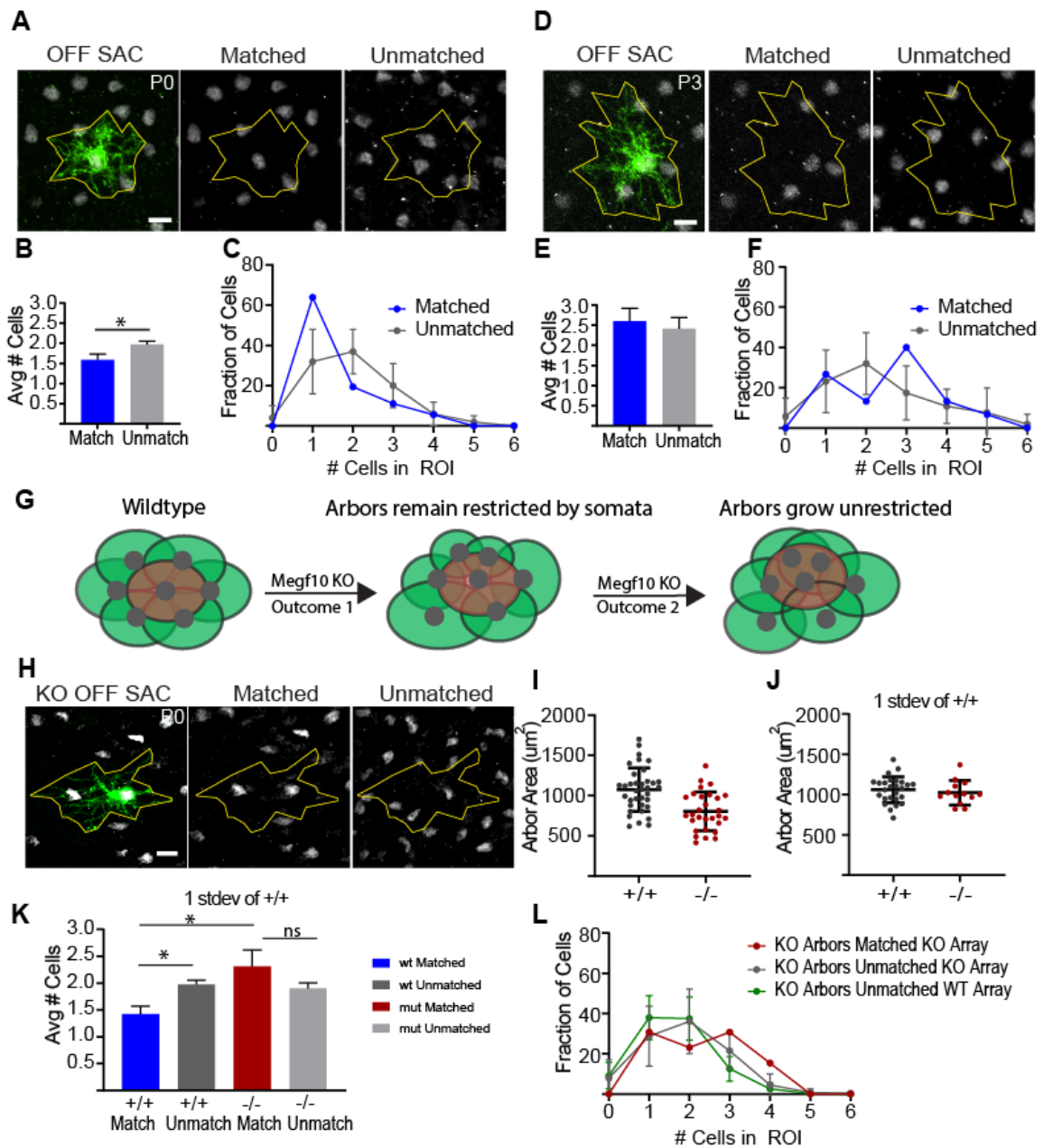


Figure 6: Organization between OFF SAC arbor territories and homotypic somata requires MEGF10

(A) *Chat^{cre}*; mGFP labels individual OFF SACs at P0 and P3 (D) to draw territories from arbor tips. Using these territories, the number of anti-sox2 labeled OFF SACs from the

image matching the arbor are counted. To assess if fewer cells occupy the dendrites territory than expected by chance, OFF SAC arrays from other images are transposed at random. (P0; n=36 arbors, 36 unmatched territories, P3; n=15 arbors, 22 unmatched territories) (B) Fewer OFF SACs are found at P0 within matched territories (two-tailed t-test; $p < 0.05$) and the (C) frequency distribution of the data differs from chance. (chi-squared, $p = 0.0005$, $df = 6$) (E) While at P3 there is no difference in the average number of cells in matched vs unmatched territories or their (F) frequency distribution. (chi-squared, 0.34 , $df = 6$) (G) Wildtype OFF SAC are patterned to have fewer than expected SACs within their dendritic territories. This relationship can either be conserved in *Megf10* mutants, with arbors remaining restricted by neighboring or somata (Outcome 1), or arbors might grow irrespective of their neighbors (Outcome 2). (H) Chat^{cre}; mGFP labeling of P0 OFF SACs matched and unmatched field example images. (I) Arbor areas in mutant P0 OFF SACs are smaller than controls. (control; n=36, mutant; n=31: two tailed t-test: $p < 0.0001$) (J) Arbors of comparable size selected for matched/unmatched analysis based on falling into 1 standard deviation of wildtype. (K) Average number of cells in arbor territory for Matched/unmatched analysis of OFF SACs with comparable arbor sizes (1 stdev) (control; n=26, knockout; n=13). (L) Frequency distributions plots for number of cells contained within mutant arbors are indistinguishable from those with unmatched mutant and control arrays. (mutant matched vs mutant unmatched: chi-squared, $p = 0.46$, $df = 6$) (mutant matched vs control unmatched: chi-squared, $p = 0.33$, $df = 6$) S.E.M shown on graphs. Scale bars: 10 μ m.

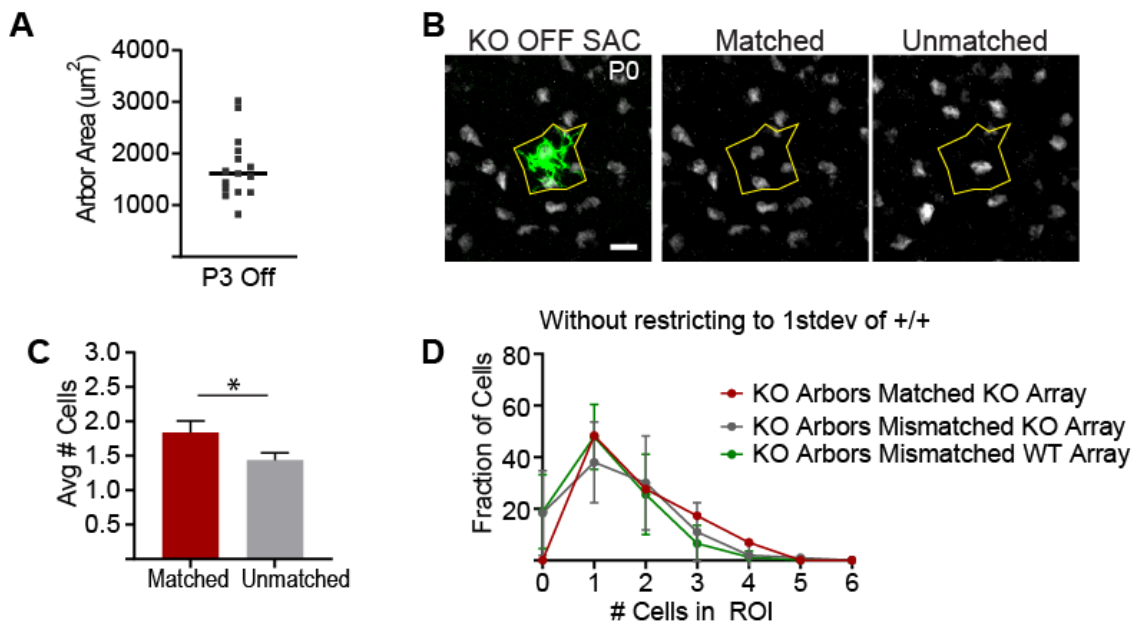


Figure 7: Supplemental information to figure 6, Example small P0 mutant OFF SAC cell and matched/unmatched analysis on untrimmed mutant data.

(A) Control P3 OFF SAC arbors are larger on average than P0 OFF SACs (two tailed t-test: $p < 0.01$) (B) Example image of matched/unmatched OFF SAC array analysis for small P0 cell. (C) Small difference in average number of cells for arbor areas for untrimmed mutant P0 OFF SACs ($n=31$; two tailed t-test: $p < 0.05$) (D) Small arbor sizes skewed frequency distributions leftwards for untrimmed data since random transposition often resulted in no somata contained within the arbor territory. S.E.M shown. Scale bar: $10\mu\text{m}$.

3.6 Arbor Exclusion model can also be applied to development of ON SACs

MEGF10 is required at P0 to form the ON SAC mosaic

Next, we wanted to determine if the developmental time course we observed for the OFF SAC mosaic also applied to the ON SAC population. Again, using age

appropriate markers and taking images from mid-peripheral retina, we labeled the ON SAC array at P0, P5, and P19 (Fig. 8A). Similar to the OFF SACs, we found no difference in the density of ON SACs compared to controls (Fig. 8B). Although, we noted that at P0, imaging the ON SACs in *Megf10* mutant retinas required thicker z-projections to capture the full cell population as they did not yet occupy a monolayer. In examining the distribution of ON SACs across development, we again found that the DRPs of controls rose gradually and shifted rightward at later ages (Fig. 8E). At P0, the exclusion zone of control ON SACs was slightly larger compared to our density matched random simulations, a difference which increased later in development (Fig. 8D). Additionally, the regularity of the ON SAC array, as measured by VDRI, was also greater than expected for a random distribution at all ages, demonstrating that the cellular events patterning the ON SAC array occurs at or just before P0 (Fig. 8C). Examining the ON SAC arrays in *Megf10* knockouts, we found DRPs increased rapidly and did not show any shift as the cell density decreased/retina expanded (Fig. 8E). Further, the exclusion zones and VDRI measured for mutant ON SAC arrays were smaller than the values we determined our random simulations (Fig. 8C, D). This finding is likely due to their delay in occupying a monolayer, allowing cells to be closer in proximity within the plane of the retina since their cell bodies reside at slightly different depths. We conclude that

similar to the OFF SACs, the orderly positioning of the ON SACs must be established before or at P0 and that MEGF10 protein is again required for their orderly arrangement.

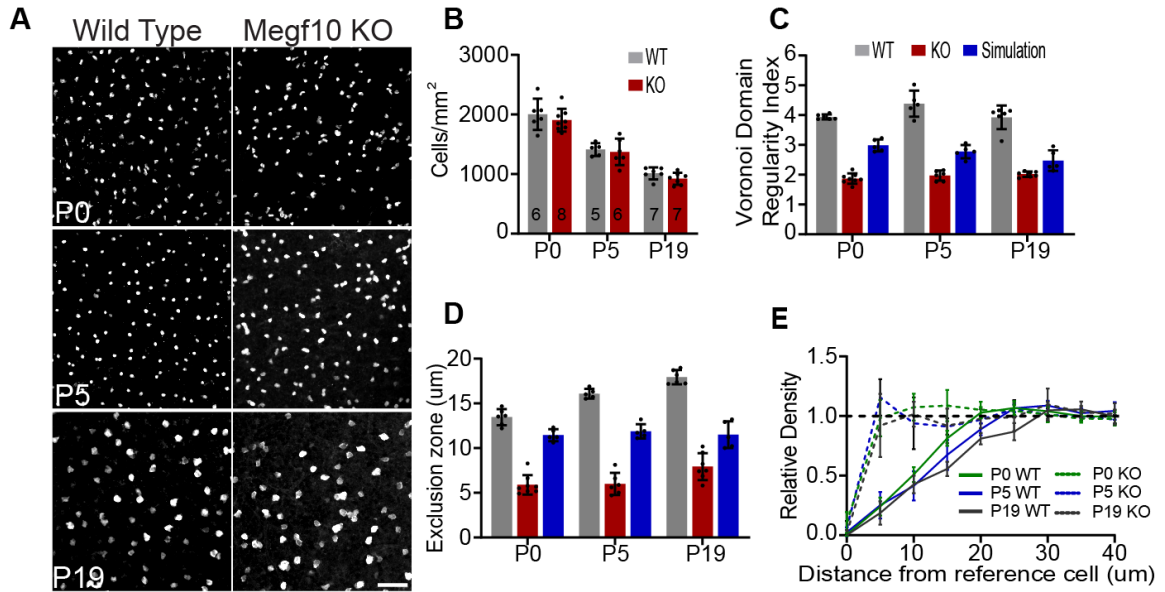


Figure 8: Organization of ON SAC array at P0 requires Megf10.

(A) Labeling of ON SAC array with anti-sox2 (P0, P5) or anti-ChAT (P17) (B) Density of ON SACs is similar at all ages for control and *Megf10* knockouts. Same sizes indicated apply to other analyses as well. (C) VDRI in controls is higher than simulated and knockout data at all ages (one-way ANOVA: $p < 0.001$ at all ages followed by Tukeys HSD: $p < 0.001$). *Megf10* knockout VDRI is lower than cell density matched simulations except at P19 (Tukeys HSD: $p < 0.001$) (D) Exclusion zone was also higher than simulated and knock data at all ages (one-way ANOVA: $p < 0.001$) (P0 WT vs simulation Tukeys HSD: $p = 0.008$) and *Megf10* knockout exclusion zones were significantly lower than simulated data at all ages (Tukeys HSD: $p < 0.001$) (E) Density recovery profiles for control ON SAC arrays shift rightwards with age while *Megf10* knockouts are strongly shifted to the left. Standard deviation shown on all graphs. Scale bar: $50\mu\text{m}$ – all images.

P0 ON SACs arborization territories also require *Megf10* to restrict proximity of homotypic cells

Our experiments focusing on the formation of the OFF SAC mosaic found that their dendrites did not appear to exhibit dendritic tiling at any age; instead, we found that P0 cells tended to arborize without growing past adjacent cell bodies, and this relationship between arbor territories and somata was lost in *Megf10* mutants. We next wanted to investigate if this relationship was also true for the development of the ON SAC mosaic. Similar to the OFF SACs, the ON SACs migrate down from the ONBL to the nascent IPL and being arborizing, however, they must also simultaneously transition through the IPL to the GCL (Chow et al., 2015). We observed this process during embryonic development, which prevented us from conducting mosaic analysis at ages earlier than P0, as cells could not be optically isolated into distinct ON and OFF populations. After the ON SACs completed their migration into the GCL, we previously observed that they also extended lateral arbors in the GCL between neighboring cell bodies in a similar but less extensive manner than the network formed in the INL by the OFF SACs (Fig. 5E, F) (Ray et al., 2018). These projection patterns are inconsistent with what might be expected for dendritic tiling, so we again used our Chat-Cre driven mGFP reporter mice to label individual ON SACs at P0 and P3 to determine if fewer homotypic cells were contained within an arbor area than expected by chance. At P0, we

found that fewer homotypic cells were found inside a reference cells arbor territory compared to unmatched transposition of random ON SAC arrays (Fig. 9A, B). Plotting the frequency distribution for the number of cells within an arbors territory, we again found that ~60% of ON SACs contained only the cell body belonging to the reference cell, a distribution unlikely to have occurred by chance (chi-squared: $p < 0.001$, $df = 6$) (Fig. 9C). By P3, most ON SACs had grown past their first neighboring cell, thus the average number of cells found within an arbor territory, and their frequency distributions, were indistinguishable what might occur by chance in unmatched arrays (Fig. 9D, E, F, Fig. 10A). We conclude that, similar to the OFF SACs, the ON SACs go through a transient developmental phase at P0 such that their arborization territories limit neighboring cell proximity.

Examining this relationship between arbor territories and homotypic cells in P0 ON SACs lacking MEGF10, we find that their arbor territories grow irrespective of neighboring cells. Similar to the OFF SACs, ON SACs at P0 were also smaller than controls (Fig. 9H). Again, we found no difference in the overall variation of arbor sizes (Levenes test, $f\text{-ratio} = 2.24$, $p = 0.15$), which would be expected if the arbor size scaled to match the more varied distribution of adjacent cells. To repeat our matched/unmatched array analysis, we again selected arbors of comparable sizes (Fig. 9I). Despite this normalization, fewer cells on average were found within matched control dendrite

territories compared to array matched mutants (Fisher's LSD: $p < 0.001$) (Fig. 9J, 10B). However, the matched/unmatched array analysis for both wildtype and mutant arbor territories significantly differed (Fisher's LSD: $p < 0.05$) (Fig. 9J). This was also true for the frequency distribution plots for matched vs unmatched transposition of mutant arrays, (Chi-squared: $p = 0.007$, $df = 6$) as well as transposition of unmatched wildtype arrays (Chi-squared: $p = 0.008$, $df = 6$) (Fig. 9K, 10C). These results demonstrate that the organization of ON SACs relative to an individual cell within is not random; instead, they tend to be closer. A result also backed up by our analysis of VDRI and exclusion zones comparing ON SAC arrays in *Megf10* knockouts to randomly simulated arrays (Fig. 6C,D). Therefore, the defect in both populations of SACs when MEGF10 knocked out is an inability to restrict the growth of their arbors with respect to surrounding homotypic cells.

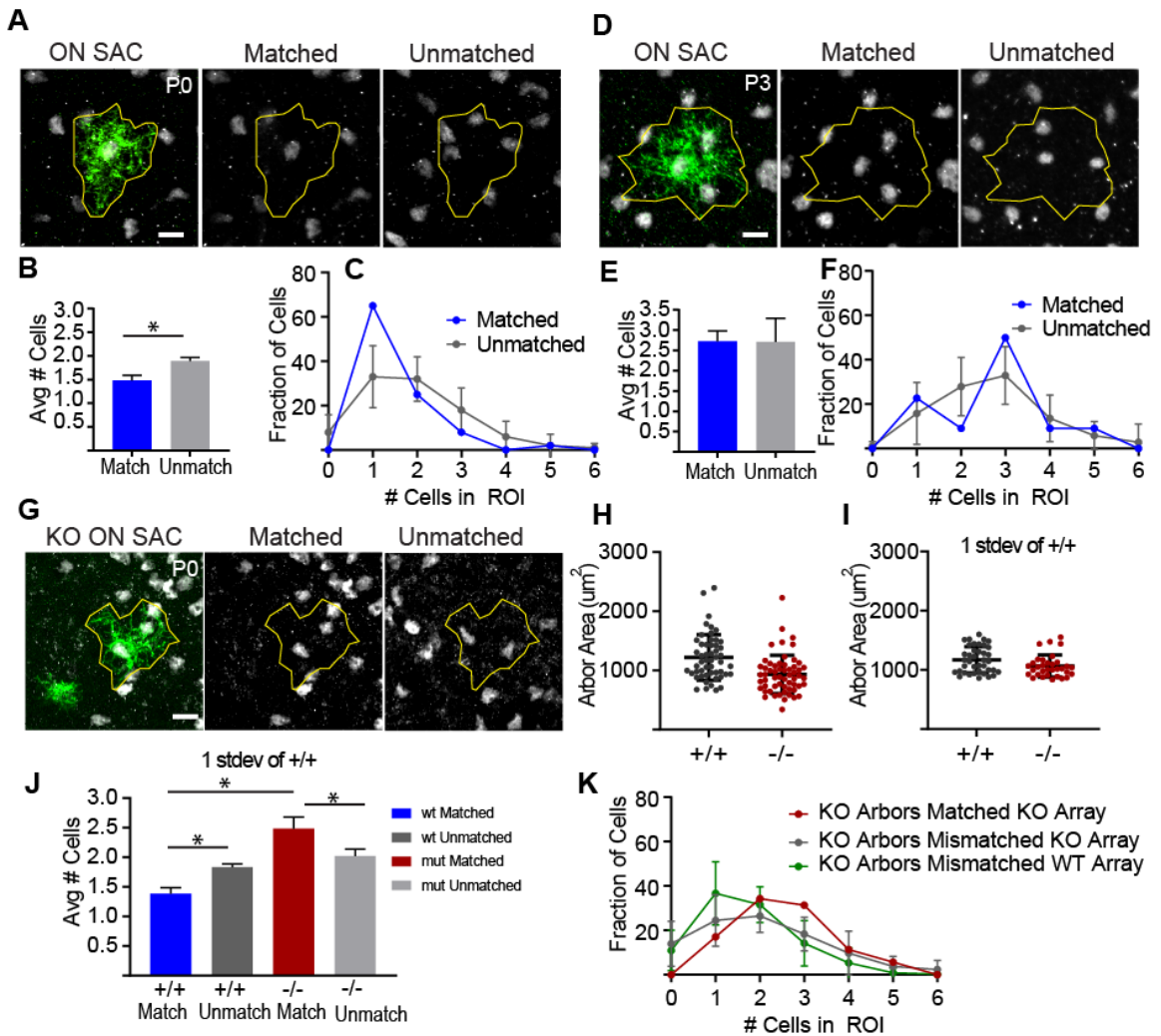


Figure 9: Relationship between ON SAC arbor areas and homotypic somata at P0 also requires MEGF10

(A) Individual ON SAC arbors labeled at P0 and P3 (D) with ChAT^{Cre}; mGFP mice used to again count the number of cells within an arbor territory for image matched and unmatched arrays of ON SACs. (B) Fewer cells on average are found within ON SAC arbor territories at P0 (two tailed t-test: $p < 0.01$) and (C) frequency distribution plots show this arrangement is unlikely to have occurred by chance. (Chi-squared: $p < 0.001$, $df = 6$) (E) At P3 no difference is found in the average number of cells within an arbor territory compared to unmatched arrays or (F) in frequency distribution plots (Chi-squared: $p = 0.32$, $df = 6$). (G) Individually labeled dendrite territory for ON SACs in

Megf10 mutant mice used for matched/unmatched analysis. (H) Average arbor size is smaller in *Megf10* mutant mice (control; n=52, mutant; n=58: two tailed t-test: $p < 0.0001$) (I) Arbors of comparable size selected for match/unmatched analysis based on falling into 1 standard deviation of wildtype. (J) Average number of cells in arbor territory for Matched/unmatched analysis of ON SACs with comparable arbor sizes (1 stdev). Results for two tailed t-test shown $p < 0.05$. (control; n=39, knockout; n=33). (K) Frequency distributions plots for number of cells contained within mutant arbors are distinguishable from what would be expected by chance for unmatched transposition of mutant arrays (mutant matched vs mutant unmatched; Chi-squared: $p = 0.007$, $df = 6$) and from unmatched transposition of control arrays. (mutant matched vs control unmatched: Chi-squared, $p = 0.008$, $df = 6$) S.E.M shown on graphs. Scale bars: $10\mu\text{m}$.

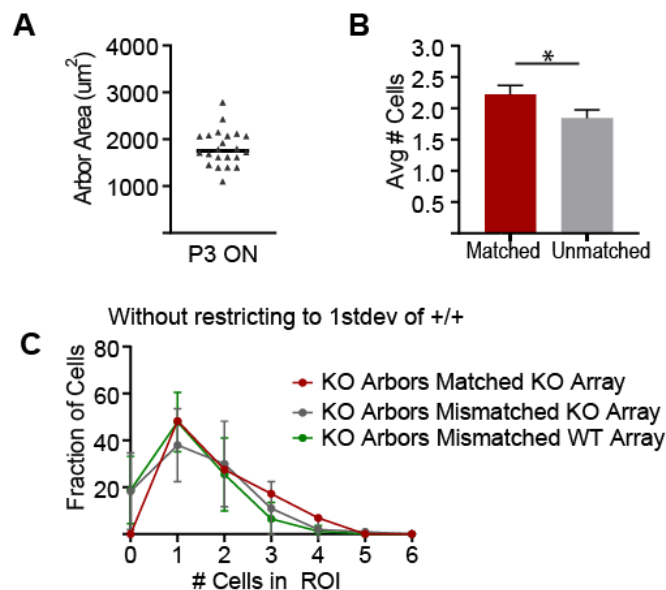


Figure 10: Supplemental information to figure 9, ON SAC arbor areas grow at P3 and match/unmatched analysis on untrimmed P0 data.

(A) Average arbor areas for ON SACs increase from P0 to P3 (two tailed t-test: $p < 0.001$) (B) Average number of cells within untrimmed P0 ON SAC arbor territories is higher in matched arrays (two tailed t-test: $p < 0.05$) (C) Frequency distribution plots for mutant matched and unmatched arrays as well as control ON SAC arrays all overlap due to small arbors still contained in data.

3.7 MEGF10 is required for early innervation of the IPL, but acts throughout development for mosaic formation

In adult *Megf10* knockout mice, the SAC phenotype is not limited to the disruption of their mosaic spacing. The SACs of wild type mice normally display two distinct continuous sublayers containing the dendrites of the OFF or ON populations. However, in *Megf10* knockout mice, sporadic disruptions in their sublayers can be observed at seemingly arbitrary locations (Ray et al., 2018) (Fig. 11A, B). These discontinuities suggest that SACs are never able to fully recover from their initial IPL innervation deficit early in development (Fig. 5F). Additionally, ectopic SAC sublayers can also form, which are thought to be derived from elaboration of their soma-layer projections (Ray et al., 2018). These ectopic layers have been found to be sufficient to recruit projections from presynaptic bipolar cells and postsynaptic direction selective ganglion cells (Ray et al., 2018). Together, these results demonstrate that SAC laminar formation is imperfect in the absence of MEGF10, with other mechanisms capable of partially compensating.

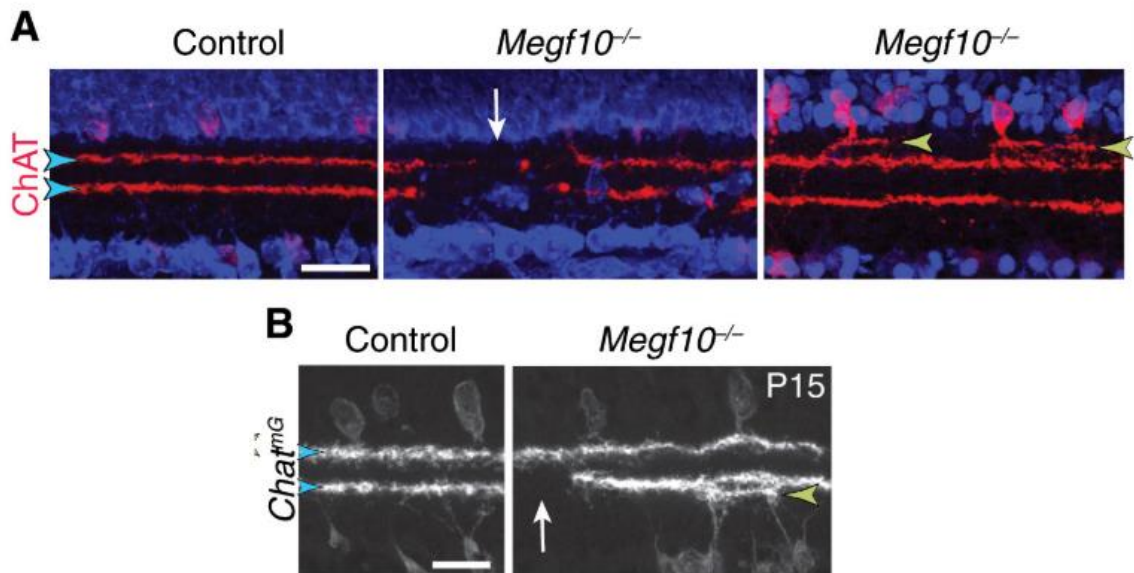


Figure 11: Ectopic SAC stratification patterns occur sporadically in adult MEGF10 mutants

(A) SAC IPL labeled by anti-ChAT (blue arrowheads) in control retinas show two continuous laminar sublayers. In *Megf10* knockouts, occasional laminar errors can be observed in addition to their mosaic phenotype, such as sublayer gaps (white arrow) and the formation of ectopic lamina (yellow arrowheads). (B) These errors can occur for both OFF and ON SAC populations. Scale bars: 25 μ m. Figure adapted from (Ray et al., 2018).

To examine the relationship between these laminar errors and the formation of SAC mosaics. We used a Cre-conditional *Megf10* knockout allele (*Megf10^{Flox}*) in combination with mice that drive Cre recombinase expression at different time points in development. To remove MEGF10 protein early in development we used *Six3-Cre* to drive expression of Cre expression in the embryonic retina (~E7) (Furuta et al., 2000).

Using this early deletion strategy, we were able to fully copy the ectopic sublayer and a mosaic phenotype indistinguishable from the constitutive *Megf10* knockout mice (Fig. 12A, B). Further, these results also verify functional removal of MEGF10 protein using the Cre-conditional *Megf10^{Flox}* allele. Next, we used *Chat^{Cre}* (Xu et al., 2016) to remove MEGF10 protein from SACs during postnatal development. This knockout strategy has been demonstrated to remove detectable MEGF10 protein between P3 and P5 (Ray et al., 2018). If MEGF10 is only required in SACs for early IPL innervation then defects in sublayers should be longer be present; alternatively, MEGF10 expression could be required throughout postnatal development to keep dendrites confined into their respective lamina. Two outcomes are also possible for the regularity of the SACs. Since MEGF10 protein would be present throughout embryonic development and at P0, when dendrite territories appear to exclude homotypic somata, then the regularity of OFF SACs could be normal. However, if MEGF10 is required throughout postnatal development to refine the mosaics then cells might still be irregular. We found that late deletion of MEGF10 with *Chat^{Cre}* resulted in largely normal SAC sublayers with exceedingly rare ectopic projections and sublayer discontinuities (Fig. 12A). While the OFF SAC array remained irregular in its distribution of cells (Fig. 12B). These experiments demonstrate that MEGF10 protein has two functions which occur at partially overlapping time points in development. First, MEGF10 is required early in

development to promote SACs to innervate the IPL. Second, MEGF10 is required throughout development to refine the regular spacing of SACs to promote normal mosaic formation.

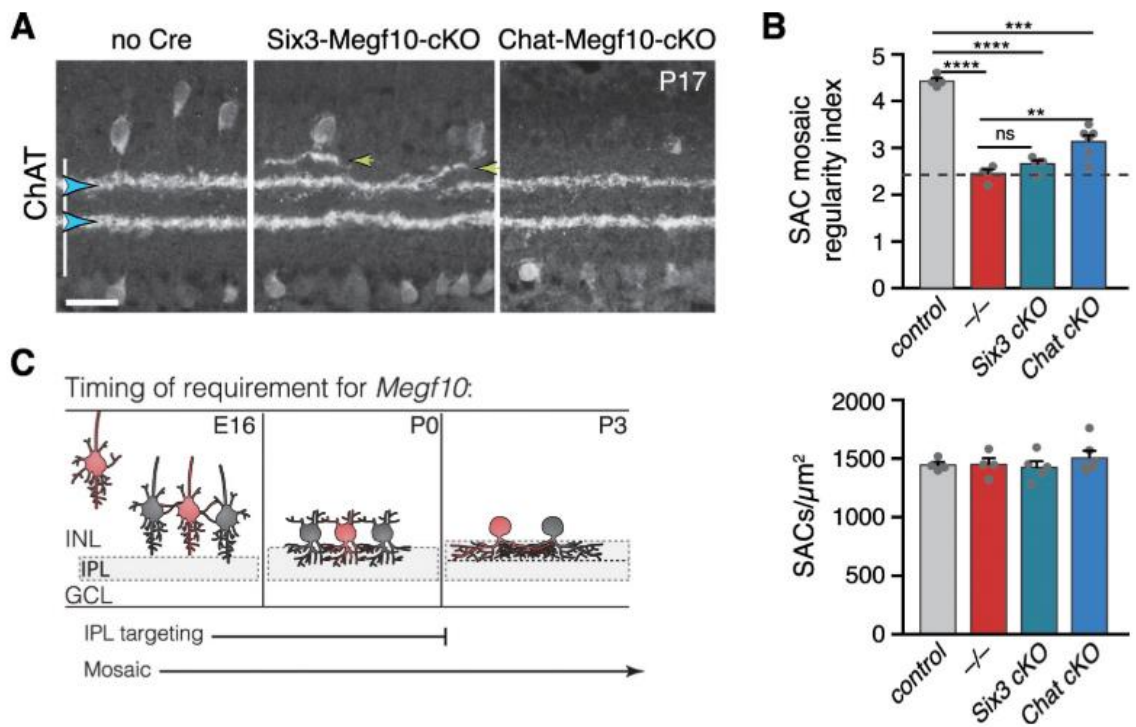


Figure 12: Temporal requirements for MEGF10 in IPL stratification and mosaic spacing.

(A) SAC IPL errors (yellow arrowheads) induced by early deletion of Megf10 in Six3-Megf10-cKO mice, but not deletion between P3-5 in Chat-Megf10-cKO mice. Blue arrowheads, SAC sublayers. (B) Mosaic spacing phenotype measured at P17 using Voronoi domain regularity index (top graph). Dashed line, index for simulated random SAC arrays. In both Six3 and Chat conditional mutants, SAC positioning is less regular than in controls (ChatCre; Megf10^{flox/+}). Megf10^{-/-} and simulation data from (Kay et

al., 2012). ns; $p=0.6438$; ** $p=0.0023$; *** $p=2.1 \times 10^{-6}$; **** $p < 1.0 \times 10^{-6}$ (one-way ANOVA/Tukey's post-hoc test). Bottom graph, regularity effects are not due to changes in SAC cell density across genotypes. One-way ANOVA, $F(3, 15)=0.6063$; $p=0.6210$. (C) Summary of results from all conditional *Megf10* mutant studies. Loss of MEGF10 while soma-layer arbors are present (i.e. prior to P3) disrupts both SAC mosaic patterning and IPL laminar targeting. When MEGF10 is lost after P3, as is the case for most *Chat-Megf10-cKO* SACs (Ray et al., 2018), only mosaic is disrupted. Thus, MEGF10 acts at distinct, albeit partially overlapping times, to influence IPL innervation and mosaic spacing. Figure adapted from (Ray et al., 2018).

4. Signal Transduction pathways downstream of neuronal MEGF10

4.1 Introduction

During the development of the retinal mosaics, it is thought that homotypic neighbors contact and recognize each other, leading to the activation of short-range repulsive signals in order to evenly space cells (Eglen, 2006; Galli-Resta, 2000; Galli-Resta et al., 1997; Reese and Galli-Resta, 2002). The precise mediator of this cell type-specific recognition event in SACs appears to be to activation of MEGF10 (Kay et al., 2012; Ray et al., 2018), leading to the initiation of repulsive signaling events. In addition to patterning the SAC mosaics, MEGF10 also works in combination with MEGF11 to pattern the mosaics for horizontal cells (HCs) in the outer plexiform layer (OPL). The signaling capacity of MEGF10 in neurons is unknown; however, in non-neuronal cells evolutionarily conserved signaling pathways have been identified downstream of MEGF10 and its homologs (Scheib et al., 2012; Sullivan et al., 2014; Wu et al., 2009; Ziegenfuss et al., 2008). We hypothesized that some of these signaling pathways would be active following MEGF10 homotypic recognition and be required for repulsive signaling in SACs. To test this hypothesis, we used *in situ* hybridization to detect if these signaling proteins are expressed in SACs during development, as well as knock-out mouse models to remove these signaling components, and quantitatively assess how this impacts SAC mosaic development.

Megf10 belongs to a family of genes known to play key roles in the phagocytic clearance of cellular debris. Its invertebrate homologs include the classical *Caenorhabditis elegans* engulfment receptor, CED-1, and *Drosophila* Draper, as well as two closely related vertebrate homologs: MEGF11, which has not been tested for a role in engulfment, and MEGF12 (also known as PEAR1 or JEDI-1), a well-defined engulfment receptor (Scheib et al., 2012; Sullivan et al., 2014; Wu et al., 2009; Zhou et al., 2001). These receptors have been found to initiate signal transduction events through their intracellular domains to activate the cellular machinery needed for engulfment. Two evolutionarily conserved signaling pathways have been found to be necessary for this activity. Both of these pathways are activated by ligand-dependent phosphorylation of conserved tyrosines within the intracellular domain (Fig. 13). The first signaling pathway is initiated by the adaptor protein GULP1 (CED-6 in *C.elegans*) (Sullivan et al., 2014). Recruitment and activity of GULP1 is mediated by binding of its phosphotyrosine binding (PTB) domain to an NPXY motif in the engulfment receptor. This recruitment is required to facilitate engulfment (Sullivan et al., 2014). The second pathway is initiated by phosphorylation of immunoreceptor tyrosine activation motifs (ITAMs) to recruit Syk-family kinases (Logan et al., 2012; Scheib et al., 2012; Thomas and Brugge, 1997). This recruitment activates Syk to phosphorylate downstream substrates, enabling the necessary cytoskeletal reorganizations needed for engulfment (Chu et al., 1998). One route by which Syk

phosphorylation affects cytoskeletal changes is by phosphorylating Vav-family guanine exchange factors (GEF) (Aghazadeh et al., 2000). Phosphorylation of Vav relieves its autoinhibitory interactions, allowing it to then activate Rho-family small GTPases, such as Rac1, to drive cytoskeletal rearrangements (Hall et al., 2006). These signaling pathways, initiated by PTB or ITAM domains, could all potentially result in activation of the cytoskeleton and facilitate MEGF10-mediated repulsion/recognition programs for mosaic formation. This work provides the first steps in uncovering the molecular basis for how cell-cell recognition cues initiate patterning of neuronal mosaics.

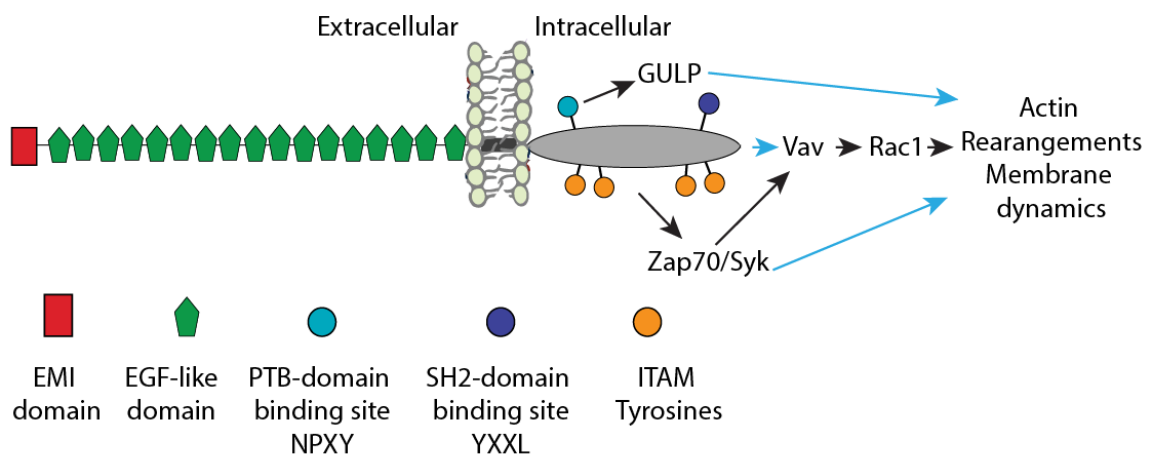


Figure 13: Schematic of MEGF10 protein with known cytoplasmic signaling motifs and engulfment pathways.

Megf10 contains an extracellular domain with one EMI, 17 EGF-like repeats, and a single transmembrane domain. The intracellular domain contains tyrosine phosphorylation sites that trigger either ITAM or NPXY pathways. Each ITAM comprises a pair of tyrosines that can serve as SH2-domain binding sites for the kinases Syk/Zap70, which

can then activate the guanine exchange factor Vav. Vav facilitates the activation of Rho-family small GTPases such as Rac1, which stimulate actin dynamics. The NPXY motif can act to bind the PTB domain in the adaptor protein GULP which can then activate the cytoskeleton. Black arrows show known direct activation; blue arrows show possible alternative routes.

4.2 Expression pattern of MEGF10 associated signaling partners in SACs

To test the hypothesis that the major signal transduction pathways known to act downstream of MEGF10 in the context of engulfment also function in SACs, we first aimed to assess if they were expressed in SACs during retinal development. As a first pass, we looked for evidence of these components being expressed in SACs within the a previously published cell type specific microarray data set (Kay et al., 2012). For the adaptor protein GULP, it appeared to be more highly expressed in other amacrine cell types than SACs (Fig. 14C) while the expression pattern of Syk and Zap70 was less clear (data not shown). The microarray data also provided evidence that Vav2 and Vav3 could be enriched in SACs (data not shown). Next, we aimed to verify if Vav2 and Vav3 were expressed in SACs and determine the expression pattern of Syk and Zap70 in the developing retina using *in situ* hybridization. Expression in SACs was assessed by colocalization between calbindin and our anti-sense digoxigenin-labeled RNA probes designed to cDNAs for our genes of interest (Fig. 14). For Zap70 probes, little signal could be detected at P0 and P2 whereas by P6 and P18 it appeared to be expressed most

strongly in an amacrine cell type other than SACs (Fig. 14A). By contrast, Syk probes revealed an odd expression pattern, with high signal in the ONL and INL with low expression in the GCL (Fig. 14C). Results for Vav3 probes showed expression in SACs and HCs throughout development, a pattern similar to the time course of MEGF10 expression (Fig. 15A, C).

Syk and Zap70 expression patterns made it difficult to conclude that they were unequivocally not expressed in SACs (Fig. 14A, B). For this reason, we acquired mice with Zap70 or Syk knocked out to examine if formation of the SAC array was affected. Constitutive Zap70 knockout mice were available; however, knockout of Syk required use of a floxed knockout allele. To drive the knockout of Syk, we crossed our Cre-conditional knockout mice to Six3-cre to remove Syk during embryonic retina development. This Six3-Cre strategy should provide appropriate timing to generate MEGF10 related phenotypes, as we already knew it was sufficient to knockout MEGF10 (Fig. 12B). When assessing the regularity of the OFF SAC array by VDRI and SAC sublamination in these knockouts, we found no differences compared to litter mate controls (data not shown). While Syk and Zap70 are best known for mediating B and T cell receptor signaling respectively, they have been known to partially compensate for each other during development (Mócsai et al., 2010; Palacios and Weiss, 2007). For this reason, we bred double knockouts (dKO) of Zap70 and Syk and found no differences in

the sublamination of SACs (Fig. 16A), or in the regularity of the OFF SAC mosaic (Fig. 17).

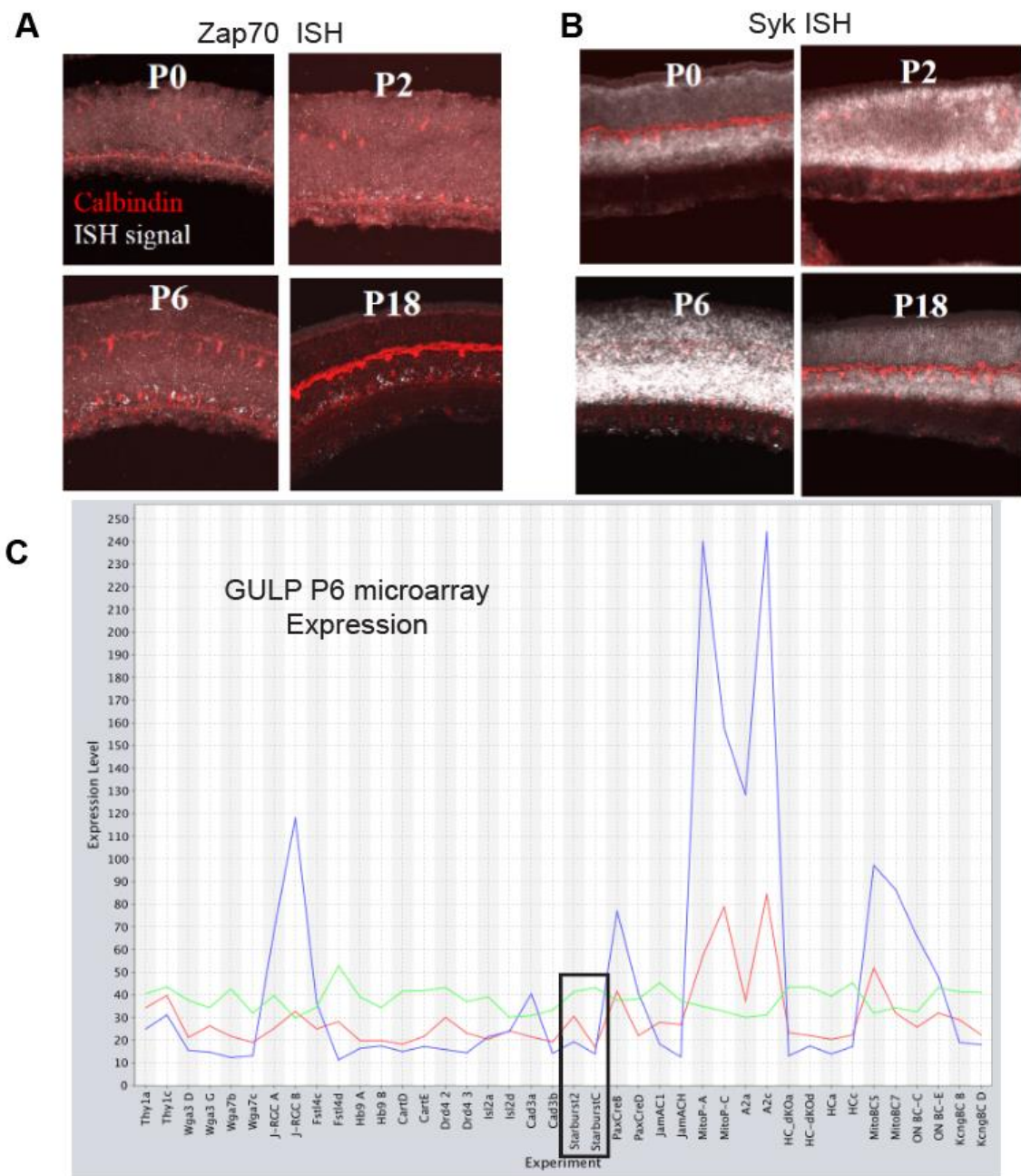


Figure 14: Microarray for GULP and *In Situ* hybridization for Zap70/Syk are not abundantly expressed in SACs.

(A) Time course of *In situ* hybridization with anti-sense digoxigenin-labeled RNA probes for Zap70 does not appear to show colocalization with SACs but possibility another amacrine cell type. (B) *In situ* hybridization time course for Syk shows strong signal in ONL and INL but little signal in the GCL. (C) Microarray data (Kay et al., 2012) for GULP at P6 shows little evidence it is expressed in SACs, while it is highly expressed in other amacrine cell types. Box highlights expression in duplicate SAC populations. Different color lines represent different microarray probes for GULP with blue only showing strong signal in cells that are not starbursts while the green probe shows a flat signal suggesting it did not work.

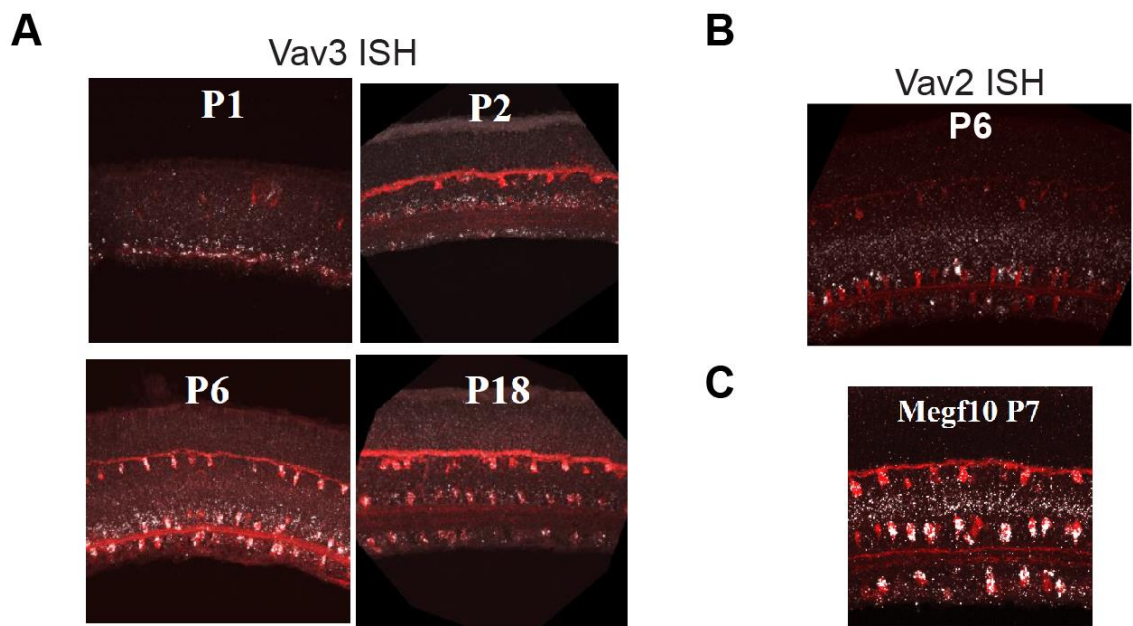


Figure 15: Time course of Vav3 expression by *In Situ* hybridization resembles pattern of MEGF10 expression.

Time course of Vav3 expression by *in situ* hybridization with anti-sense digoxigenin-labeled RNA probes. (A) Vav3 appears to be expressed in SACs and HCs (red-calbindin) resembling expression pattern of Megf10 (C) (Kay et al., 2012) (B) Expression pattern of Vav2 suggests it is not highly expressed in SACs.

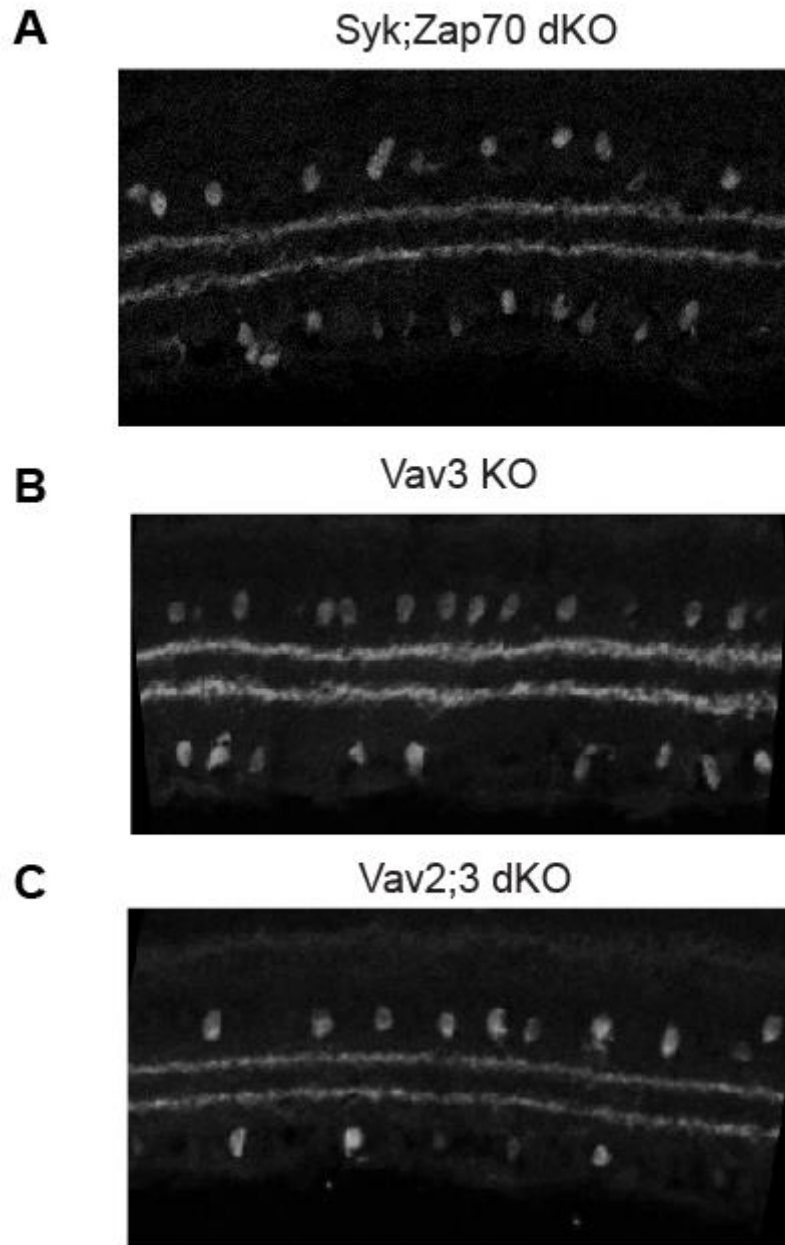


Figure 16: ChAT labeled sections of signaling candidate knockouts reveal normal sublamination.

Lamination of ChAT sublayers examined at P17 in knockouts of multiple signaling candidates (A) Six3-cre driven knockout of Syk bred with Zap70 constitutive knockouts, (B) Vav3 knockout and (C) Vav3;Vav2 double knockouts reveal normal sublamination.

4.3 Knockout of the GEF Vav3 decreases SAC regularity

Because the *in situ* signal for Vav3 probes demonstrated that it was expressed in SACs and HCs in a time course similar to Megf10 (Fig. 15), we next assessed the development of the OFF SAC array in Vav3 knockouts. Additionally, since it was difficult to rule out the expression of Vav2 in SACs and these GEFs are known to have overlapping functions, we also generated double knockout (dKO) mice. (Fig. 15B) (Fujikawa et al., 2003; Pearce et al., 2004). We found that in both Vav2;3 dKO and Vav3 KO mice that at P17 the SAC sublayers appeared similar to littermate controls (Fig. 16B, C). Examining the OFF SAC array by VDRI, we found a small but significant decrease in their regularity and no change in the total density of cells or exclusion zone (Fig. 18). This decrease in VDRI was borderline significant for the Vav2;3 dKO (Tukeys Posthoc: $p=0.08$) (Fig. 18D). If Vav3 acts as a signaling partner downstream of MEGF10 then one would expect that Vav3 knockouts would also impair the regularity of ON SACs and HCs, since it is expressed in both of those cells types (Fig. 15A) and they are known to utilize MEGF10. However, we find VDRI in both ON SACs and HCs is indistinguishable from controls (Fig. 19). Next, we wanted to see if we could amplify the irregularity phenotype of Vav3 knockout mice by breeding them to Megf10 knockouts. Because heterozygous Megf10 knockout leads to a mild phenotype, we could use this sensitized

background to generate a stronger Vav3 phenotype (Kay et al., 2012). Measuring the regularity of OFF SACs again by VDRI in these mice, we find no enhancement of the OFF SAC Vav3 phenotype beyond what would be expected for heterozygous Megf10 mutation (Fig. 20) (Kay et al., 2012). Lastly, we investigated if MEGF10 and VAV3 proteins interact. Other receptors such as EphA4 have been found to directly interact with Vav3 to drive repulsive signaling in axon guidance (Cowan et al., 2005). To do this, we conducted co-immunoprecipitation experiments with MEGF10-GFP and an HA-tagged VAV3 to see if they formed a complex using detergent conditions previously found to preserve MEGF10 intracellular domain interactions (Scheib et al., 2012); however, we did not observe any HA signal after immunoprecipitation for MEGF10-GFP (Fig. 21B). Together, these results provide little evidence that MEGF10 signals through Vav3.

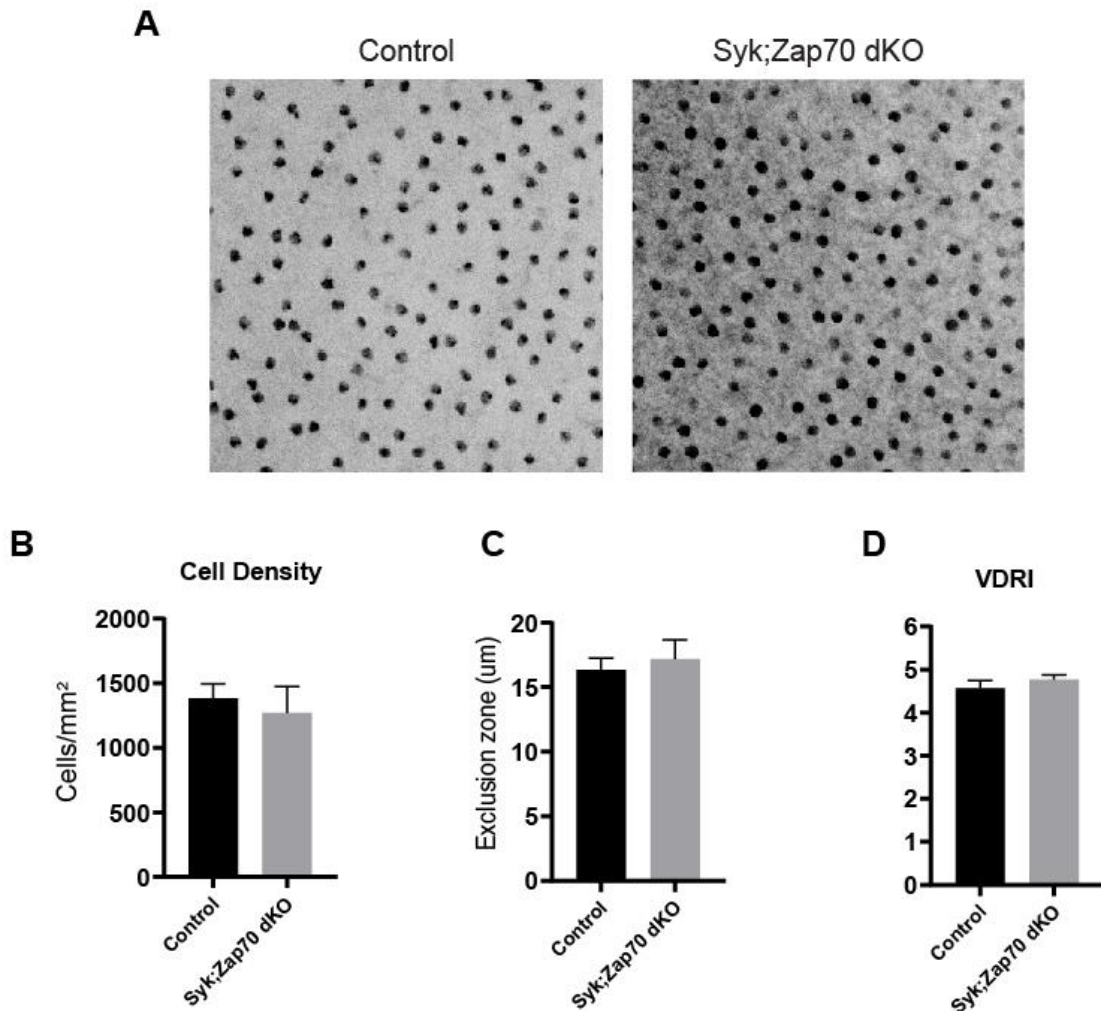


Figure 17: Regularity of OFF SAC array in Syk;Zap70 double knockout mice is indistinguishable from controls.

(A) Representative images of P17 anti-ChAT labeled OFF SACs in Syk;Zap70 double knockout (dKO) mice. (B) No difference in OFF SAC density is observed (t-test: $p=0.44$) Further, both exclusion zone (t-test: $p=0.45$) (C) and VDRI (t-test: $p=0.17$) are indistinguishable from littermate controls. N=3 retinas/genotype: n=3 images/mouse.

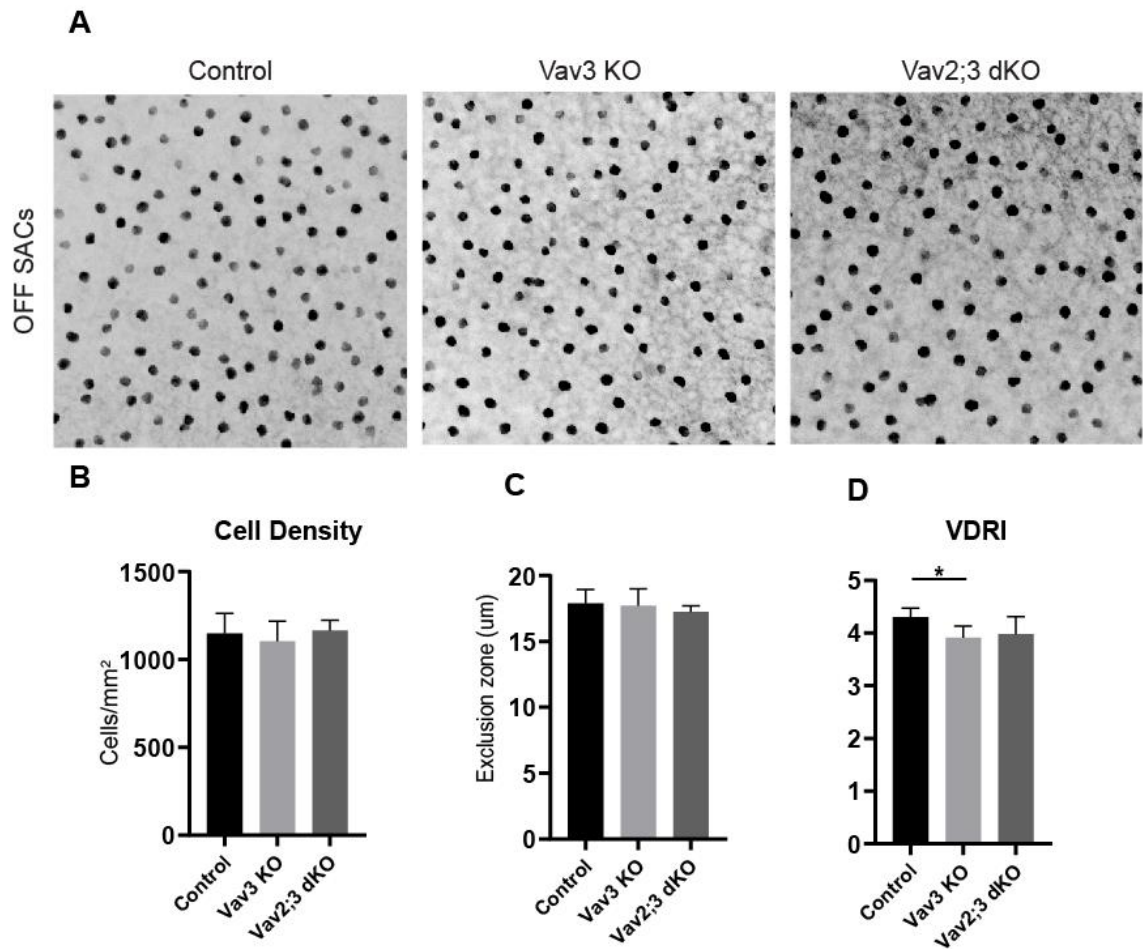


Figure 18: Regularity of OFF SAC array in Vav3 and Vav2;3 double knockout mice.

(A) Representative images of P17 anti-ChAT labeled OFF SACs for Vav3 and Vav2;Vav3 double knockout mice compared to controls. No difference in cell density (B) (One-way ANOVA: $F=0.47$, $p=0.64$) or exclusion zone (C) (One-way ANOVA: $F=0.35$, $p=0.71$) is observed. For assessment VDRI finds a difference in cell regularity (One-way ANOVA: $F=5.8$, $p=0.01$). Tukeys post hoc test; $*p=0.01$. $N=7$ for control and Vav3 retinas/genotype with $N=4$ for Vav2;3dKO: $n=3$ images/mouse.

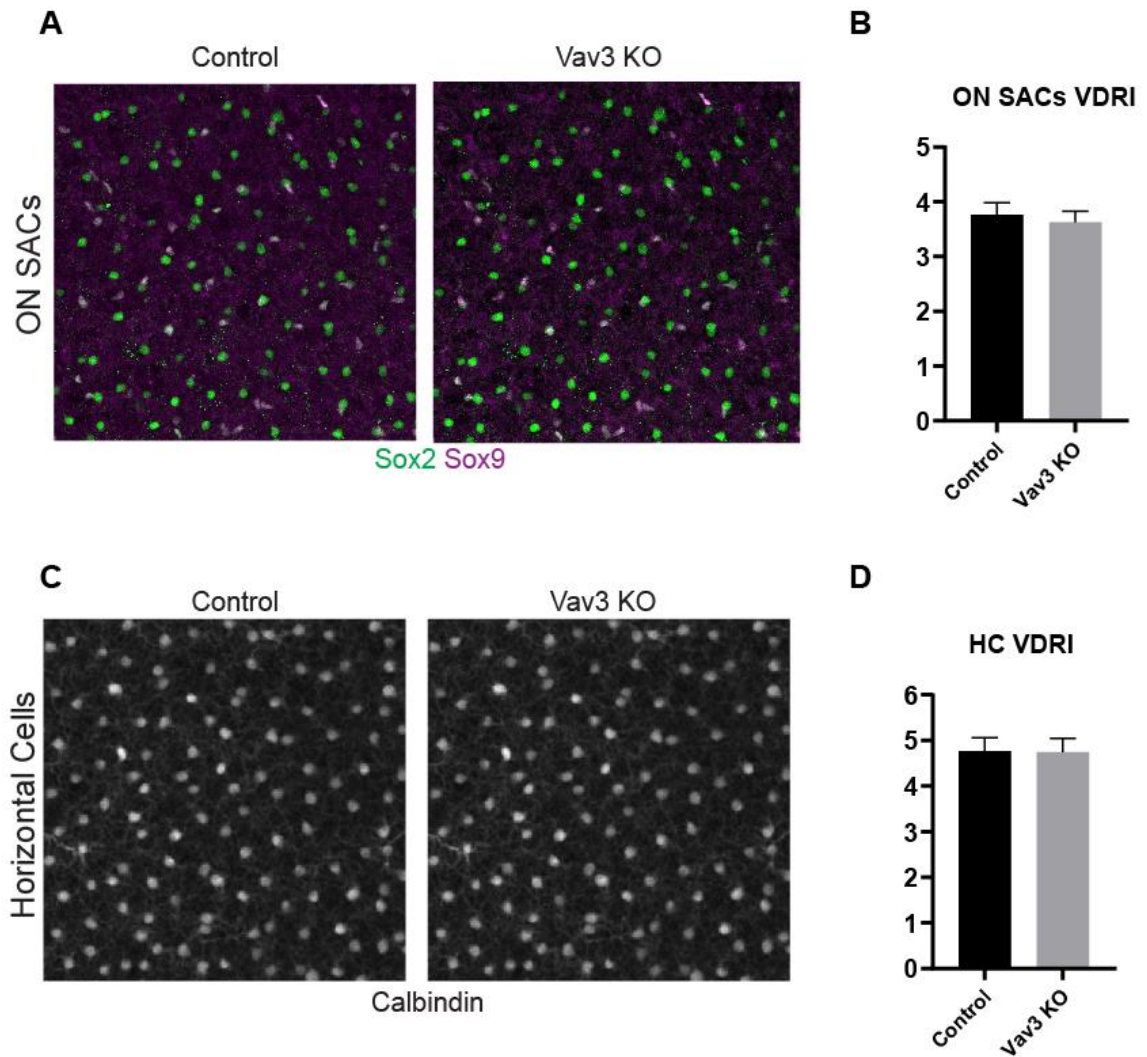


Figure 19: Regularity of ON SACs and HCs in Vav3 knockouts is similar to control mice.

(A) Representative images of P17 ON SACs whose positions were determined by anti-Sox2 positive, anti-Sox9 negative immunohistochemistry. (B) No difference cell regularity was found between littermate control and Vav3 knockout mice (t-test: $p=0.24$) $N=8$ for control, $N=6$ for Vav3 knockout. $n=3$ image/mouse. (C) Representative images of P17 HCs labeled by calbindin. (D) No difference in HCs regularity as measured by VDRI (t-test: $p=0.91$) $N=4$ for control and Vav3 knockout. $n=3$ images/mouse.

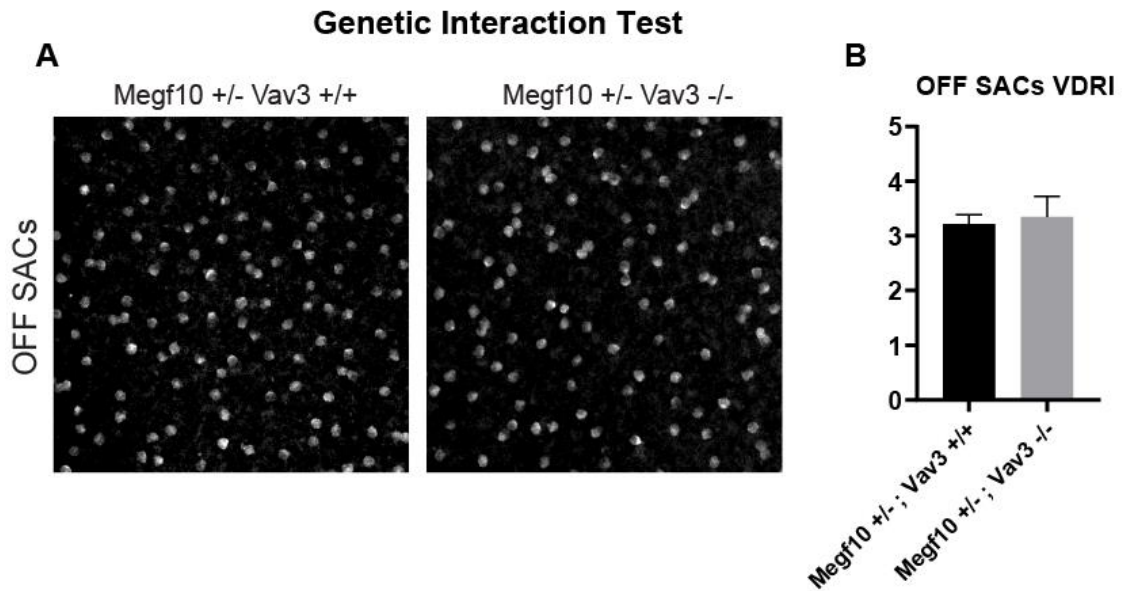


Figure 20: No evidence of genetic interaction between Megf10 and Vav3 knockout mice.

(A) Representative images of P17 anti-ChAT labeled OFF SACs in Megf10 heterozygous mice compared to those on Vav3 knockout backgrounds. (B) No difference is found in the regularity of their array by VDRI (t-test: $p=0.55$). Heterozygous Megf10 VDRI phenotype is comparable to previous results (Kay et al., 2012). $N=4$ for both genotypes. $n=3$ images/mouse.

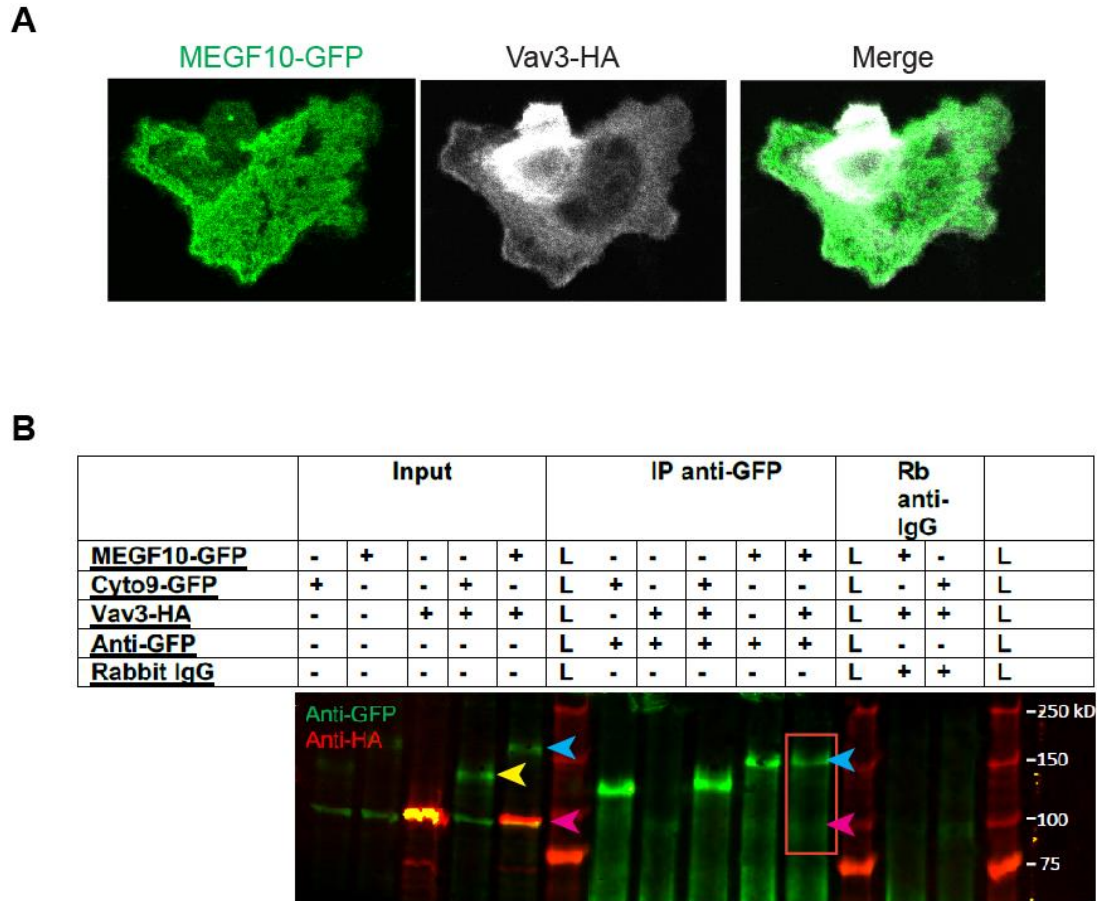


Figure 21: Co-transfection of MEGF10 and VAV3 protein into HEK293 shows little evidence of interaction.

(A) Representative HEK293 cell transfected with indicated plasmids and visualized with anti-GFP and anti-HA. (B) Immunoprecipitation of HEK cells cotransfected with Vav3-HA or full length MEGF10-GFP or a truncated MEGF10 lacking an intracellular domain (Cyto9-GFP). Immunoprecipitation was done with Anti-GFP and CO-IP was probed for using anti-HA to detect VAV3. Pink arrowhead – VAV3-HA, Yellow arrowhead – Cyto9-GFP, Blue arrowhead – MEGF10-GFP. Box indicated CO-IP lane with no HA signal where it would be expected if MEGF10 and Vav3 bound in a complex.

5. Megf10 initiates cell-cell recognition events through its intracellular domain in a heterologous system

5.1 Introduction

Cell-cell recognition through homotypic receptors represent the first step in the process that leads to repulsion and mosaic formation. For these outcomes to occur, recognition of neighbors must trigger signaling events within the cell. MEGF10-triggered signaling events in the context of engulfment are mediated by phosphorylation of ITAM and PTB motifs followed by subsequent activation of conserved signaling proteins (Fig. 12) (Scheib et al., 2012; Sullivan et al., 2014; Wu et al., 2009; Ziegenfuss et al., 2008). To elucidate how MEGF10 initiates cell-cell recognition/repulsion we devised an *in vitro* assay using heterologous cells. Neighboring HEK293 cells will normally contact and overlap (Fig. 22A); however, if these cells express MEGF10, they display a flattened interdigitating pattern separated by a 1-2 μ m gap (Fig. 22B). This morphology does not occur at the borders between MEGF10 and non-MEGF10 expressing cells suggesting that the observed pattern between two MEGF10 expressing cells is due to cell-cell recognition (Fig. 22C) (Kay et al., 2012). While it has been shown that MEGF10 requires its intracellular domain to form this pattern, the precise domain required for this cell recognition-like event is unknown. We identify ITAM phosphotyrosines as critical, and make a mouse to express ITAM point mutated MEGF10 in SACs to see if it is also required to mediate cell-cell in SACs.

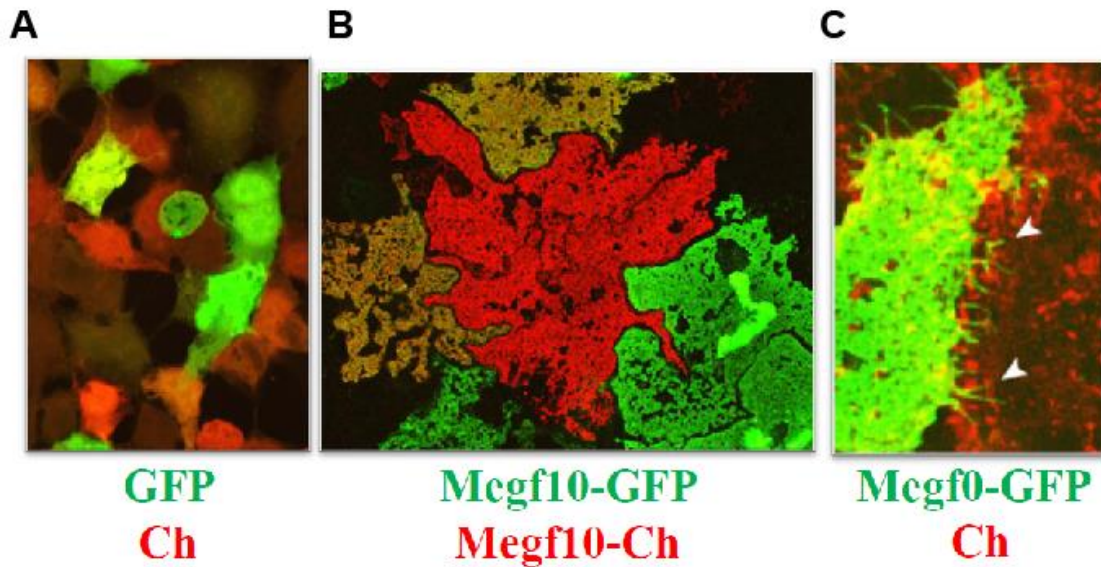


Figure 22: Transfection of MEGF10 protein into HEK293 cells appeared to mediate cell-cell recognition like event between neighbors.

(A) Transfection of HEK293 cells with constructs for cytosolic GFP or Cherry shows that cells often overlap with each other. (B) When HEK cells are transfected with MEGF10-GFP or Megf10-Cherry constructs they appear to flatten in the plane of the coverslip and form an interdigitating pattern with a 1-2 μ m gap separating them from adjacent cells. (C) Cells transfected with MEGF10-GFP do not form this pattern when next to a cell not expressing MEGF10. Adapted from (Kay et al., 2012).

5.2 MEGF10-driven cellular recognition requires ITAM signaling

To determine which protein domain in MEGF10 induces the formation of intercellular gaps in HEK293 cells, we generated a series of truncations, deletions, and point mutations to map the required region of the intracellular domain (Fig. 23A). Two major divisions were made, effectively cutting the intracellular domain in half. In

addition, point mutations were generated to phosphotyrosines known to be used to initiate engulfment signal transduction pathways (Fig. 13). To quantify how frequently intercellular gaps were observed, we co-transfected our MEGF10 mutated constructs with a plasmid encoding a histone-tagged cherry protein so we could be sure we were assessing fields with similar numbers of cells (H2B-cherry). For each construct, the number of intercellular gaps observed that were greater than $>10\mu\text{m}$ were counted and normalized to the number of H2B-Cherry cells observed in field. No differences were found in the average number of H2B-Cherry cells across different constructs tested, but the tiling frequencies varied (Fig. 23B, C; Fig. 24 for representative images). Wildtype MEGF10-GFP constructs were more successful than all other mutations at inducing the formation of intercellular gaps, with the pTB binding domain having the smallest impact (Fig. 23C). Mutation of all four tyrosines belonging to MEGF10s two ITAM domains (4xITAM) provided the strongest phenotype for the precise change to the intracellular domain. To examine the how mutation of MEGF10 ITAM domains influence cell-cell interactions, we used a nucleofection assay to exclusively express constructs with different fluorophore fusions, allowing us to carefully examine cell borders (Fig. 25). We found that while pairs of adjacent MEGF10 expressing HEK cells often formed gaps, the borders of 4xITAM expressing pairs often overlapped or were tightly apposed to each other (Fig. 25F).

If ITAM tyrosines of MEGF10 are required to mediate cell-cell interactions in HEK293 cells, then we would expect to see that they are phosphorylated. Using a general phosphotyrosine antibody, we probed for phosphorylation in MEGF10 mutant transfected HEK293 cells (Fig. 27). We found that phosphotyrosine (pTyr) signal in MEGF10 expressing cells was localized to cell borders surrounding intercellular gaps (Fig. 27A). While pTyr signal in 4xITAM point mutants was comparable to a MEGF10 construct that contained almost no intracellular domain (Fig. 27B, C). Curiously, deleting half of the intracellular domain and leaving behind the portion that still contains the ITAM tyrosines resulted in high pTyr signal despite it not inducing higher levels of intercellular tiling than the other constructs (Fig. 23C).

Lastly, we wanted to examine the time course of how the intercellular gaps form in MEGF10 expressing HEK293 cells. Co-transfection of MEGF10-GFP and Life-Act (to label filamentous actin) demonstrates that gaps at these cell borders could often contain filopodia with low MEGF10 protein signal (Fig. 26A). While Life-Act signal in 4xITAM-GFP point mutations appeared to co-localize (Fig. 26B). To visualize the dynamics of the actin cytoskeleton we conducted live imaging of transfected HEK293 cells. We observed that the intercellular gaps between MEGF10-GFP expressing HEK cells contained dynamic F-actin rich structures that resembled lamellipodia (Fig. 28A). Whereas in

4xITAM point mutant constructs, no obvious organization was observed during the imaging session (Fig. 28B).

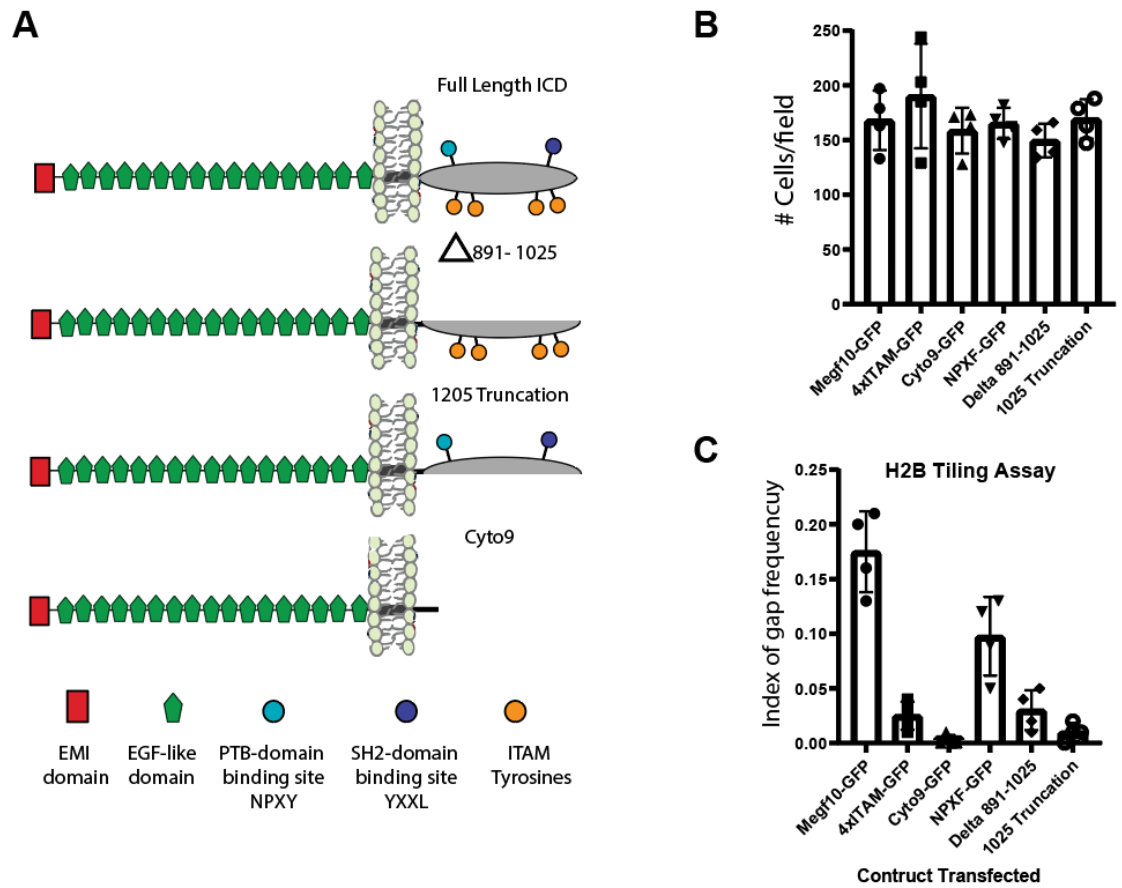


Figure 23: Mutation of MEGF10 intracellular domain impairs formation of intercellular gaps.

(A) Multiple mutations were made to MEGF10-GFP constructs to either remove large portions of the intracellular domain (ICD) or introduce tyrosines to phenylalanine point mutations. HEK293 cells were transfected with the indicated version of MEGF10-GFP as

well as a plasmid encoding an H2B-cherry to label nuclei (See Figure 24 for images). (B) Quantifies the number of H2B-cherry cells in a given field as measure of how densely the cells are transfected. There is no difference in the total number of cells/field (One-way ANOVA: $F=1.1$, $p=0.42$). (C) Number of intercellular gaps longer than $10\mu\text{m}$ divided by the number of H2B-cherry cells within a field provides an index of how frequency intercellular gaps form. (One-way ANOVA: $F=33.2$, $p<0.001$) Tukeys post hoc: MEGF10-GFP differs from all other $*p<0.001$. NPXF-GFP vs 4xITAM $*p=0.003$. No differences between 4xITAM-GFP, Cyto9-GFP, Δ 891-1025-GFP and 1025-GFP. $N=4$ fields examined/construct. See Materials and Methods for more details on quantification.

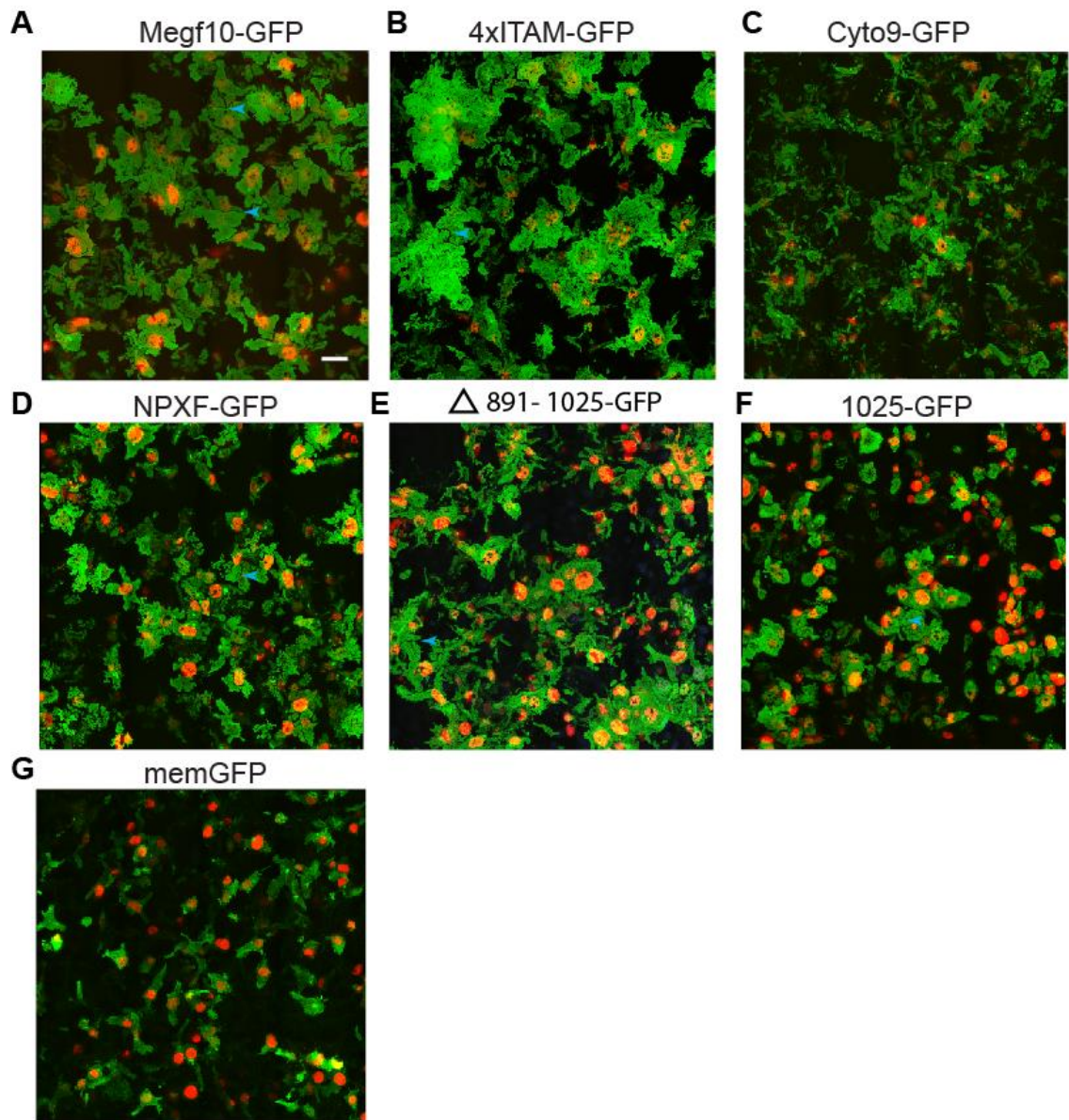


Figure 24: Representative images of control and mutated MEGF10-GFP constructs used for quantification.

Images used for quantification scheme described in Figure 22. Panels are labeled with indicated variation of MEGF10 intracellular domain used for co-transfection with H2B-Cherry. (A,B,C,D,E,F). (G) Shows morphology for normal HEK293 cells transfected with

a membrane target GFP. Blue arrowheads indicate examples of GAPs $>10\mu\text{m}$ were counted for Figure 23. Scale bar $20\mu\text{m}$.

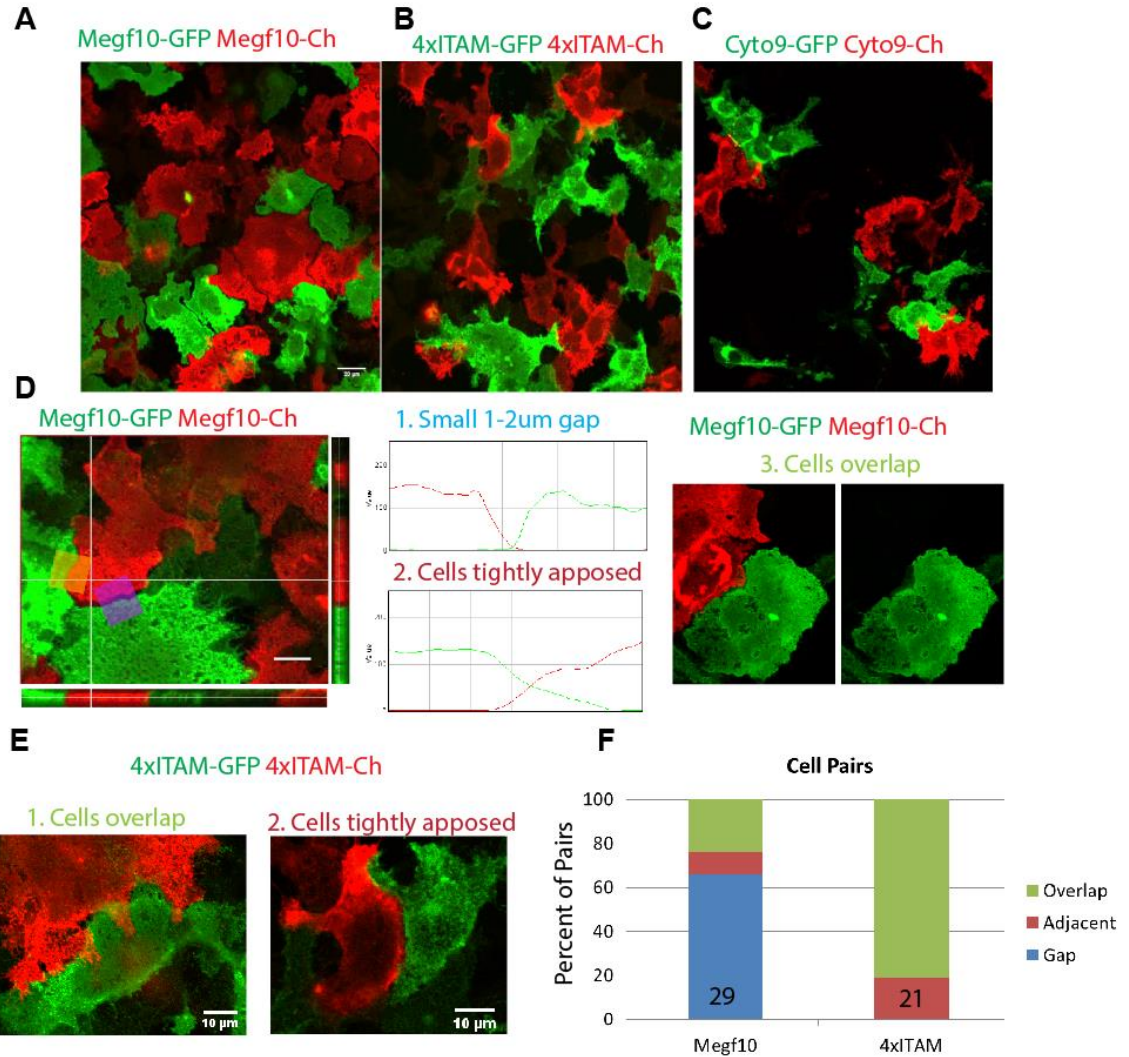


Figure 25: Nucleofection provides exclusive expression of single color constructs to assess intercellular borders.

HEK293 were nucleofected with each of the individual constructs first before cell mixing to provide cell exclusive expression. (A) MEGF10 expressing cells show expected puzzle pattern-like morphology with intercellular gaps while 4xITAM (B) and Cyto9 (C) do not

show this type of organization. (D) Three outcomes were observed at the borders of adjacent MEGF10 cells: cells could either form 1-2 μ m gaps, be tightly apposed (fully adjacent) or overlap. (E) Borders of adjacent 4xITAM fell into two categories, overlapping or apposed. (F) Quantification of percentage of cell pairs with indicated relationship. Scale bars: 20 μ m (A,B,C) 10 μ m (D,E).

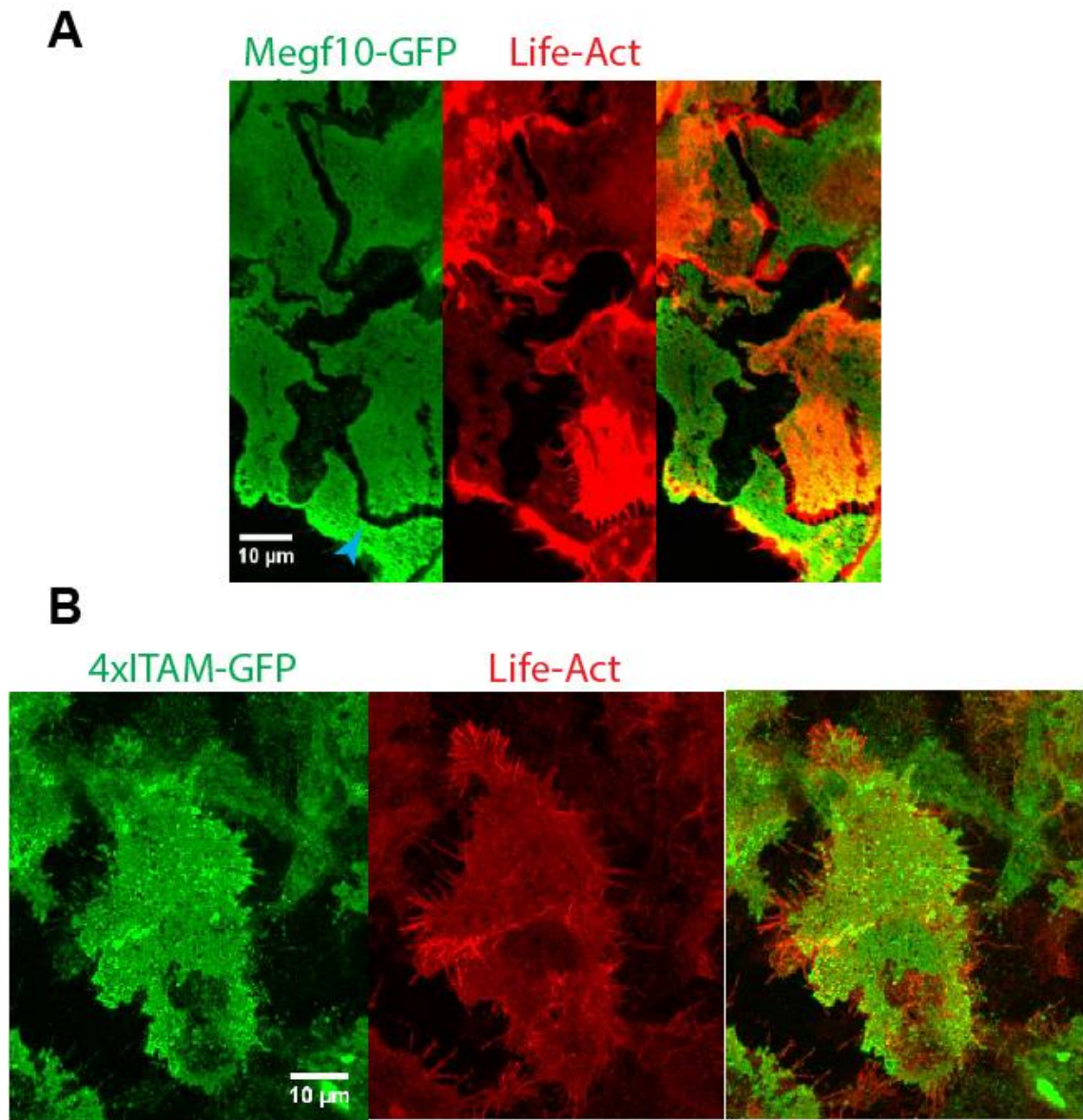


Figure 26: Intercellular gaps between MEGF10 expressing HEK293 cells contain filopodia.

(A) HEK293 cells co-transfected with MEGF10-GFP and Life-Act to label filamentous actin. Intercellular gaps between MEGF10-GFP expressing cells can be observed and

have filopodia projecting into them while other areas do not. (B) This organization is not seen with co-transfection of 4xITAM-GFP. Scale bars: 10 μ m.

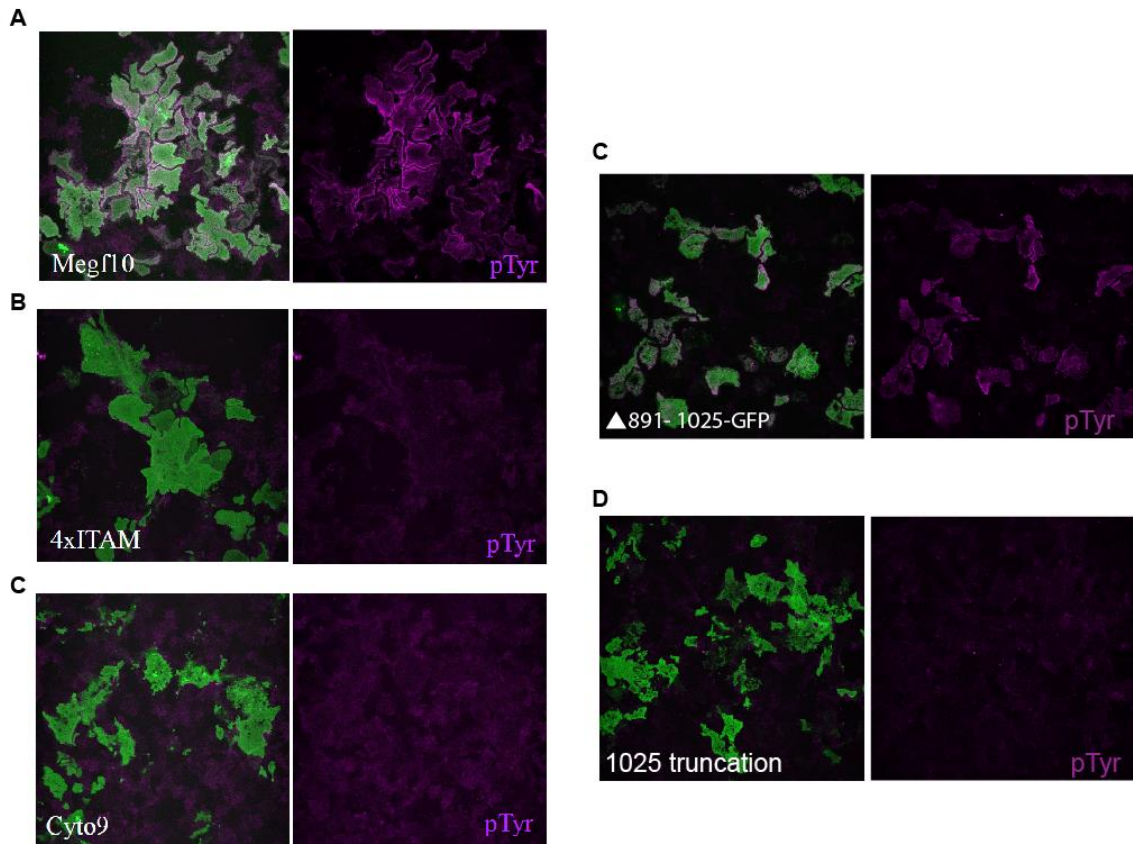


Figure 27: Phosphorylation of MEGF10 intracellular domain requires ITAM tyrosines.

HEK293 cells transfected with indicated plasmids and stained for anti-phosphotyrosine (pTyr). (A) MEGF10-GFP expressing cells show pTyr signal on their cell borders while no clear localization is present in 4xITAM (B), Cyto9 (C) or 1025 truncation (D). Some pTyr signal remains for Δ 891-1025-GFP, which retains the ITAM domains. See figure 23.

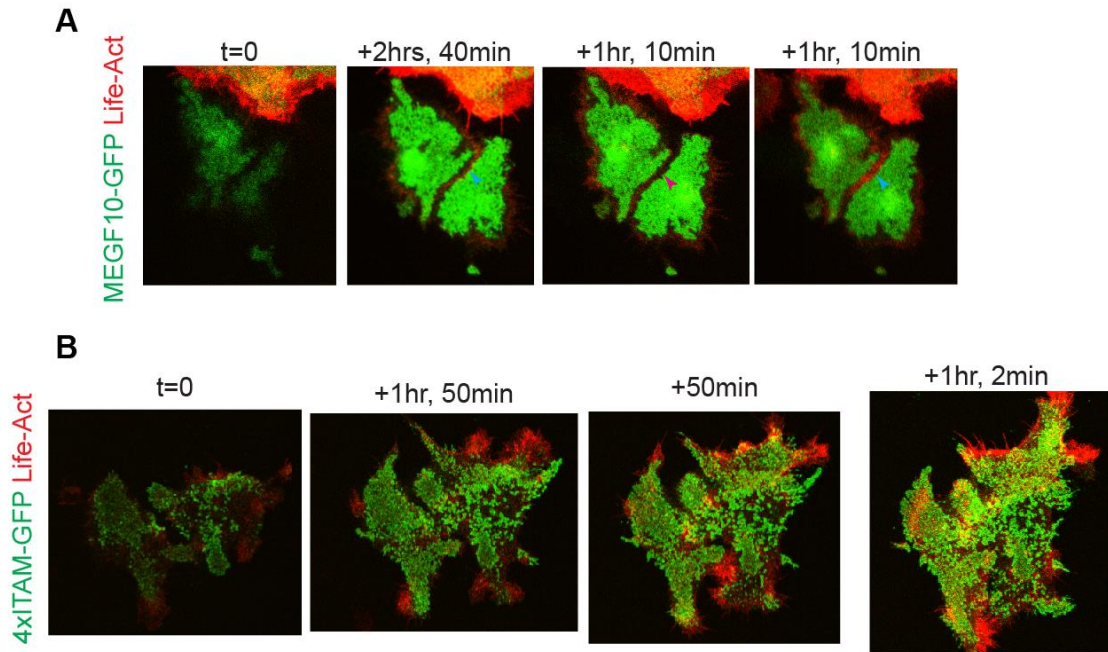


Figure 28: Live imaging of HEK293 cells co-transfected with Life-Act and MEGF10 plasmids shows time course of intercellular gap formation.

Live imaging of HEK293 cells co-transfected with Life-Act/memCh and MEGF10-GFP plasmids and imaged at 10minute intervals. (A) Two MEGF10-GFP expressing cells grow to form intercellular gap which is dynamically filled with high (blue arrowhead) or low (pink arrowhead) actin signal. (B) Cells expressing 4xITAM-GFP show no such organization. Times above image indicate duration since previous still-image was taken.

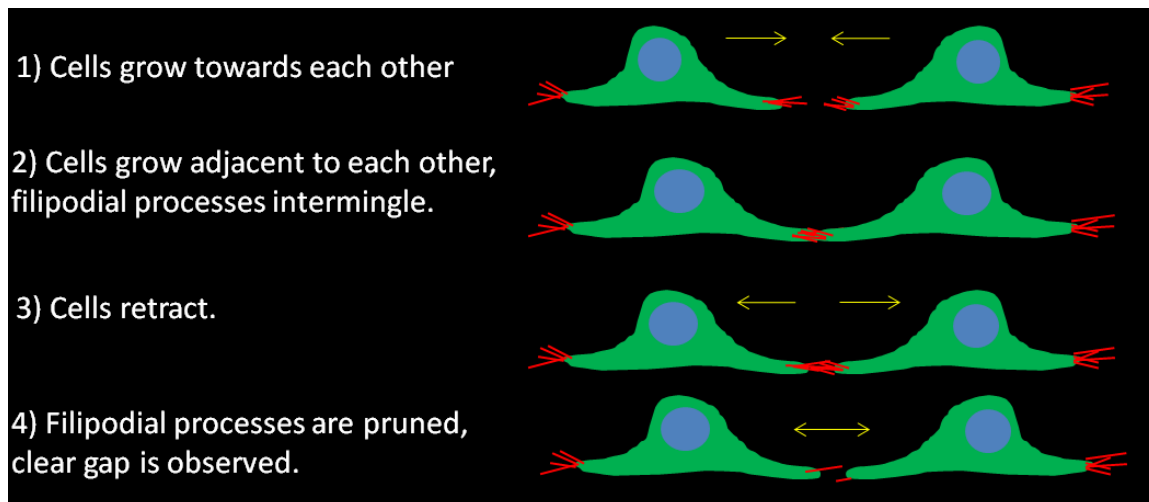


Figure 29: Proposed model of intercellular gap formation in MEGF10 transfected HEK293 cells.

HEK293 cells expressing MEGF10 protein show an affinity for the coverslip and interdigitate at their cell borders, forming a gap in between individual cells. These gaps form as neighboring cells grow to contact each other. MEGF10 expressing HEK293 cells also display complex actin protrusions on their cell borders where we propose MEGF10-mediated homophilic interactions occur. At the onset of these interactions, MEGF10 intracellular domain is phosphorylated and trafficked out of these processes.

5.3 Generation of Rosa26a knock-in mouse to test if MEGF10 requires ITAM signaling in SACs

Because we identified that MEGF10 induced cellular recognition patterns in HEK293 cells relied on ITAM tyrosines, we investigated whether these same domains were also required to initiate MEGF10 repulsive signaling in SACs. To do this, we generated a Rosa26a knock-in mouse to express either wildtype or the tyrosine point mutated (4xITAM) MEGF10 protein (Fig. 30). We hypothesized that using our

Megf10^{CreNeo} knockout strategy to remove endogenous MEGF10 protein (Fig. 4), we could then rescue the SAC mosaic phenotype with exogenous MEGF10 expressed from the Rosa-MEGF10 allele (Fig. 30B). We observed in P2 retinal sections that little exogenous MEGF10 or GFP was produced in SACs even in mice homozygous for the Rosa-MEGF10 allele (Fig. 31A,B). To test if this small amount of MEGF10 expression was abundant enough to function in organizing the SAC mosaic, we measured the regularity of the OFF SAC array. We found that the OFF SACs from our rescue experiment mice remained indistinguishable in their regularity from MEGF10 knockouts (Fig. 31C), suggesting that insufficient protein was produced from Rosa-MEGF10 allele. Lastly, we also tested if expression of our 4xITAM point mutant (Rosa-4xITAM) could influence the regularity of the OFF SAC array. Again, little protein expression was found during development (data not shown) and it did not appear to influence the VDRI of the OFF SAC array.

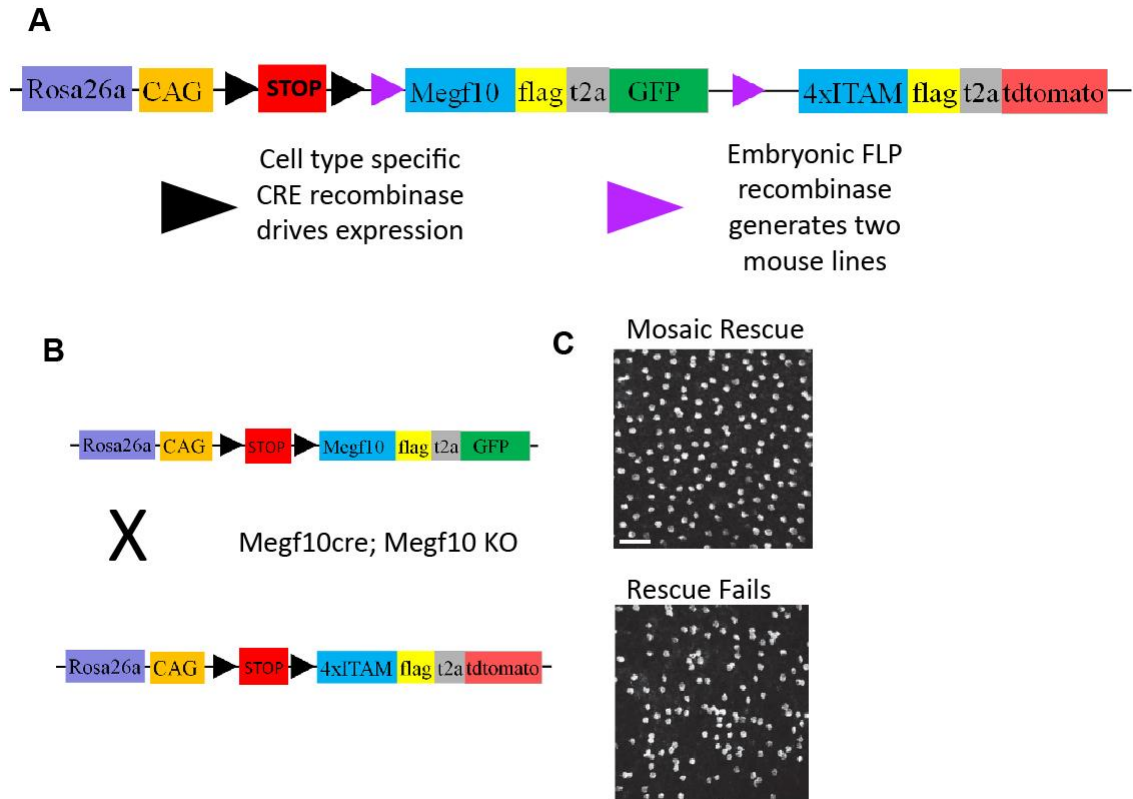


Figure 30: Diagram of Rosa-MEGF10 mouse and experimental design.

(A) Schematic of Rosa26a knock-in allele. Allele contains CAG-driven followed by lox-stop-lox sequence for Cre-conditional expression of MEGF10 protein and GFP. A second mouse line was generated by crossing embryonic FLP recombinase mice to replace MEGF10-GFP coding sequence with point mutated (4xITAM-tdtomato). Sequences of t2a self-cleaving peptides (Liu et al., 2017) are placed in between MEGF10 and fluorescent proteins to separate protein products. (B) These mouse lines were crossed into MEGF10 knockout backgrounds and expression of MEGF10 protein was driven by MEGF10^{Cre} mice. (C) We predicted that expression of exogenous MEGF10 protein would rescue the SAC mosaic phenotype while expression of 4xITAM would fail to restore the regularity of the SAC array if it is required to initiate signal transduction signals necessary for mosaic formation.

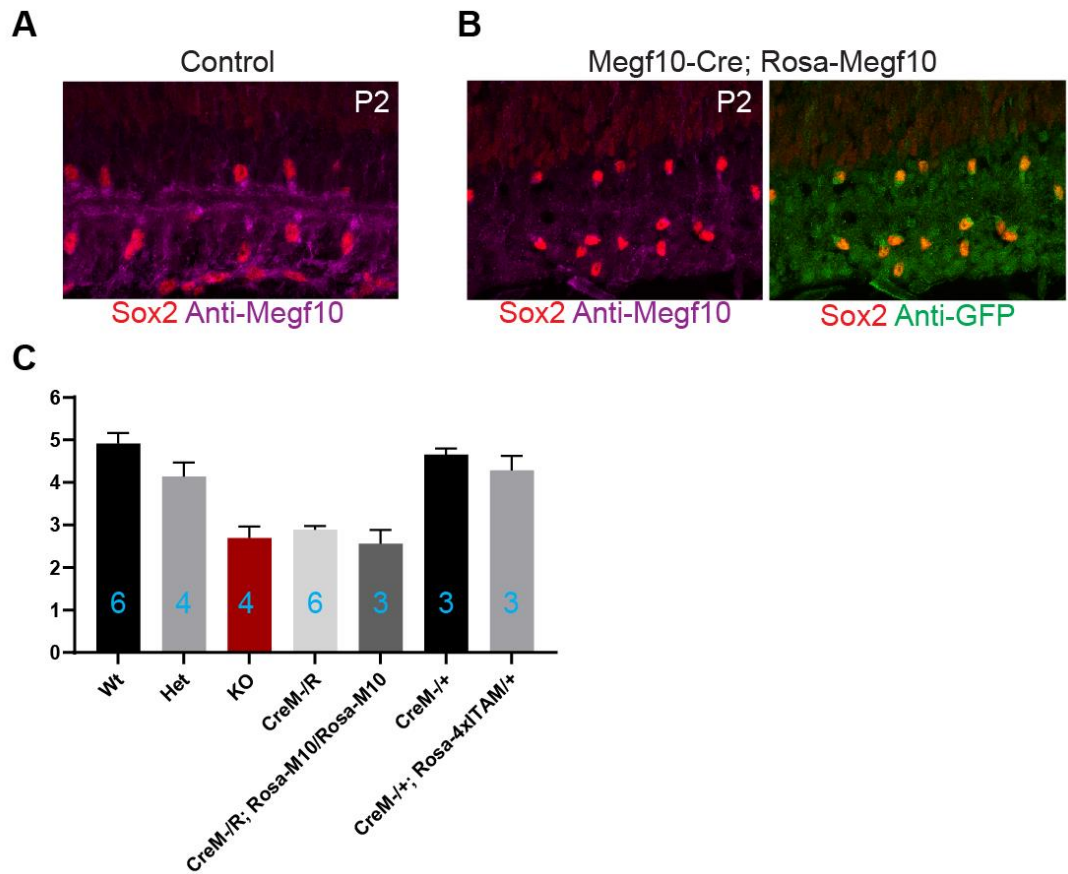


Figure 31: Rosa-MEGF10 does not appear to express enough MEGF10 protein to rescue OFF SAC mosaic phenotypes.

(A) Labeling of Anti-MEGF10 on P2 control mice shows expression in SACs as expected (Ray et al., 2018). (B) While Anti-MEGF10 staining on MEGF10-Cre mice driving homozygous Rosa-MEGF10 shows little exogenous MEGF10 expression and Anti-GFP signal is correspondingly low. (C) Regularity of P17 OFF SAC arrays assessed by VDRI shows no improvement in organization in rescue mice (Tukeys Post hoc: $p=0.57$). Further, overexpression of point mutant 4xITAM does not degrade cell regularity (Tukeys Post hoc: $p=0.56$). Number of mice assessed indicated on graph. 3 images/mouse.

6. Conclusions and Future Directions

6.1 *MEGF10-driven Cre recombinase as a tool for studying development*

In these studies, we generated two mouse lines to drive expression of Cre in SACs during embryonic development. The first MEGF10^{CreNeo} appeared to serve as a MEGF10 knockout allele and second MEGF10^{Cre} produced MEGF10 protein and had no functional impact on the development of the OFF SAC mosaic (Fig. 4). It remains unclear why removal of the neomycin cassette restored expression of MEGF10 protein, one possibility is that *Megf10* mRNA relies on its proximity to its 3'UTR for mRNA stability and high levels of translation (Mayr, 2018). Regardless, both mouse lines were capable driving fluorescent reporters in SACs and HCs with only occasional recombination in progenitor cells prior expression in Muller Glia, consistent previously reported MEGF10 expression (Kay et al., 2012; Ray et al., 2018). Because SAC array development in MEGF10^{Cre} mice proceeds without disrupting MEGF10 function (Fig. 4), this mouse line could be used in future studies to examine and manipulate early interactions between SACs and their synaptic partners in the direction selective circuit.

6.2 Arbor exclusion model as a general cellular mechanism guiding mosaic formation

Retinal mosaics are defined by their evenly spaced arrangements of homotypic somata; here we aimed to understand how this organization emerges by focusing on how the dendrites of these cells are organized with respect to neighboring homotypic somata. While the dendrites of some retinal neuron types exhibit non-overlapping dendritic territories which impart cell spacing, many mosaic forming populations display overlapping dendrites, making it unclear how they determine their proximity to neighboring cells (Reese and Keeley, 2015; Wassle and Riemann, 1978). For example, the dendrites of parasol cells in the primate retinas overlap, however, the size of their dendritic fields correspondingly increase as parasol density decreases with retinal eccentricity (Dacey and Brace, 1992). This has also been observed for adult horizontal cell (HC) dendrites which also inversely scale their dendritic size with cell density (Wassle et al., 1978). This relationship remains conserved if genetic manipulations are used to half the number of HCs resulting in a corresponding doubling in HC dendritic size (Poché et al., 2008). Although these studies provide correlational evidence linking dendritic size and homotypic cells, we demonstrate here that this type of scaling can be impaired by manipulation of cell-cell recognition molecules relied upon for detection of neighboring cells. Our observations suggest that this detection of neighboring cells occurs between dendrite-somata contacts early in postnatal development, (Fig. 5) but

how MEGF10 specifically distinguishes somata from dendrites is unclear. One possibility is that MEGF10 or another interacting protein is expressed in a gradient on SACs, with the highest receptor density subcellularly localized to somata, in a manner similar to neurofascin localization to purkinje cell axon hillocks (Sanes and Yamagata, 2009). Since MEGF10 and MEGF11 are both known to be required for HC mosaic formation, it remains to be determined if they specifically influence transient dendritic tiling or dendrite-somata interactions (Huckfeldt et al., 2009).

6.3 Neuronal MEGF10 signal transduction pathways differ from those in nonneuronal cells

Although signal transduction pathways for MEGF10 and its homologs have been found to be evolutionarily conserved in the context of engulfment, we found little evidence that they act downstream of MEGF10 to promote SAC mosaic formation. The only candidate signaling molecule that appeared to influence SAC array regularity was the guanine exchange factor (GEF) Vav3. We found that *in situ* hybridization for Vav3 showed it was expressed in SACs and HCs, similar to MEGF10 (Fig. 15). However, phenotypes in Vav3 knockouts were only found for the OFF SAC array, while the ON SAC and HC arrays were indistinguishable from wildtype (Fig. 18). Further, we also found that the mild Vav3 phenotype was not due to compensation by Vav2 (Fig. 18). To assess if Megf10 and Vav3 acted together in the same pathway, we examined Vav3 knockout mice on a heterozygous Megf10 background, but did not find any further

deficit in SAC regularity suggesting they do not act in the same pathway (Fig. 20).

Because Vav3 acts as a GEF to activate Rho-family small GTPases, one possible future direction is to examine knockouts of small GTPases directly to determine if they are required to mediate cellular movements necessary for mosaic formation.

Recent studies in *Drosophila* have identified TNF *receptor associated 4* (TRAF4) as binding the intracellular domain of Draper, MEGF10's *Drosophila* homolog, and this interaction is required to activate c-Jun N-terminal kinase (JNK) signaling in glia after axon injury (Lu et al., 2017). In our lab, we identified TRAF4 as binding to MEGF10 in an unbiased immunoprecipitation experiments from cerebellum lysates (Wang, 2019).

However, it remains unknown if this was due to an interaction that took place in neurons or glia of the cerebellum, therefore future studies will have to first examine the expression of TRAF4 in the SACs during and then derive a knockout strategy to test if it is required for mosaic development. Together, these results demonstrate that MEGF10's function as a cell-cell recognition molecule mediating mosaic formation represents a curious case of evolution utilizing a receptor for distinct functions in different cell types. Alternatively, further studies on MEGF10 protein in astrocytes and neurons could uncover molecular similarities and unify its function across cell types.

6.4 Expression of MEGF10 in heterologous cells as a model for studying cell-cell recognition

We find that expression of MEGF10 in HEK293 cells induces a cellular recognition event that requires ITAM tyrosines of MEGF10's intracellular domain. Mutation of these tyrosines to phenylalanine reduced the ability of MEGF10 to induce the formation of intercellular gaps to levels similar to full deletion of the intracellular domain (Fig. 23-27). While we found that wildtype MEGF10 transfected into HEK293 cells was highly phosphorylated at the borders of cells, this signal was completely eliminated in 4xITAM mutants suggesting that homophilic MEGF10 interactions might induce phosphorylation (Fig. 27). This homophilic interaction has been shown by co-immunoprecipitation and it appears to act as its own receptor/ligand in the retina, therefore the formation of these gaps must be preceded by cell-cell contact and subsequently retraction (Kay et al., 2012; Ray et al., 2018) (Fig. 29). We find that these intercellular gaps often contain filopodia or lamellipodia-like structures rich with filamentous actin (F-actin) where MEGF10 protein could come into contact with neighboring cells (Fig. 26A). Live imaging reveals that these actin structures in MEGF10 transfected cells are dynamic and extend in between adjacent cells to form the observed gaps (Fig. 28). While cells transfected with 4xITAM-GFP do not appear to impart any organization on adjacent cells (Fig. 28). We propose a model whereby MEGF10 in HEK293 cells is initially present in these F-actin structures where it could homophilically

interact with other MEGF10 expressing cells. Upon homophilic binding, it is phosphorylated and trafficked to the base of the structure resulting in high pTyr signal surrounding the borders of MEGF10 expressing HEK cells. One important test of this model would be the use of a stripe assay, coating coverslips with MEGF10 protein and seeing if MEGF10 expressing HEK cells still respond to its ligand. While it appeared that the ITAM tyrosines were the primary targets of phosphorylation, mutation of its PTB-binding domain impaired the intercellular gap formation, although to a smaller extent. This could be due to some utilization of the GULP pathway. Alternatively, the intracellular domain of Draper was found to bind TRAF4 which required a 60aa region that also contains its PTB domain. This homologous region also exists in MEGF10's intracellular domain and would be removed in the Δ 891-1025 deletion mutation used here and could be why it was not sufficient to maintain intercellular gap formation (because Δ 891-1025 still contains the ITAMs, which are phosphorylated). It remains unknown if these ITAM tyrosines are utilized to initiate repulsive MEGF10 signaling in SACs to drive the formation of their mosaic. However, this heterologous system provides a platform where candidate signaling molecules, such as TRAF4, could be screened for functions in MEGF10 cellular recognition before testing for *in vivo* function in neurons.

References

- Aghazadeh, B., Lowry, W. E., Huang, X. Y. and Rosen, M. K. (2000). Structural basis for relief of autoinhibition of the Dbl homology domain of proto-oncogene Vav by tyrosine phosphorylation. *Cell* 102, 625–633.
- Amini, R., Labudina, A. A. and Norden, C. (2019). Stochastic single cell migration leads to robust horizontal cell layer formation in the vertebrate retina. *Development* 146, dev173450.
- Barrasso, A. P., Wang, S., Tong, X., Christiansen, A. E., Larina, I. V. and Poché, R. A. (2018). Live imaging of developing mouse retinal slices. *Neural Dev.* 13, 1–14.
- Chen, S.-K., Chew, K. S., McNeill, D. S., Keeley, P. W., Ecker, J. L., Mao, B. Q., Pahlberg, J., Kim, B., Lee, S. C. S., Fox, M. A., et al. (2013). Apoptosis Regulates ipRGC Spacing Necessary for Rods and Cones to Drive Circadian Photoentrainment. *Neuron* 77, 503–515.
- Chen, M., Lee, S., Park, S. J. H., Looger, L. L. and Zhou, Z. J. (2014). Receptive field properties of bipolar cell axon terminals in direction-selective sublaminae of the mouse retina. *J. Neurophysiol.* 112, 1950–1962.
- Chow, R. W., Almeida, A. D., Randlett, O., Norden, C. and Harris, W. A. (2015). Inhibitory neuron migration and IPL formation in the developing zebrafish retina. *Development* 142, 2665–2677.
- Chu, D. H., Morita, C. T. and Weiss, A. (1998). The Syk family of protein tyrosine kinases in T-cell activation and development. *Immunol. Rev.* 165, 167–180.
- Chung, W.-S., Clarke, L. E., Wang, G. X., Stafford, B. K., Sher, A., Chakraborty, C., Joung, J., Foo, L. C., Thompson, A., Chen, C., et al. (2013). Astrocytes mediate synapse elimination through MEGF10 and MERTK pathways. *Nature* 504, 394–400.
- Cook, J. E. and Chalupa, L. M. (2000). Retinal mosaics: New insights into an old concept. *Trends Neurosci.* 23, 26–34.

- Cowan, C. W., Shao, Y. R., Sahin, M., Shamah, S. M., Lin, M. Z., Greer, P. L., Gao, S., Griffith, E. C., Brugge, J. S. and Greenberg, M. E. (2005). Vav family GEFs link activated Ephs to endocytosis and axon guidance. *Neuron* 46, 205–217.
- Dacey, D. M. and Brace, S. (1992). A coupled network for parasol but not midget ganglion cells in the primate retina. *Vis. Neurosci.* 9, 279–290.
- Doody, G. M., Bell, S. E., Vigorito, E., Clayton, E., McAdam, S., Tooze, R., Fernandez, C., Lee, I. J. and Turner, M. (2001). Signal transduction through Vav-2 participates in humoral immune responses and B cell maturation. *Nat. Immunol.* 2, 542–547.
- Duan, X., Krishnaswamy, A., De La Huerta, I. and Sanes, J. R. (2014). Type II cadherins guide assembly of a direction-selective retinal circuit. *Cell* 158, 793–807.
- Eglen, S. J. (2006). Development of regular cellular spacing in the retina: Theoretical models. *Math. Med. Biol.* 23, 79–99.
- Eglen, S. J., Van Ooyen, A. and Willshaw, D. J. (2000). Lateral cell movement driven by dendritic interactions is sufficient to form retinal mosaics. *Netw. Comput. Neural Syst.* 11, 103–118.
- Fujikawa, K., Miletic, A. V., Alt, F. W., Faccio, R., Brown, T., Hoog, J., Fredericks, J., Nishi, S., Mildiner, S., Moores, S. L., et al. (2003). Vav1/2/3-null Mice Define an Essential Role for Vav Family Proteins in Lymphocyte Development and Activation but a Differential Requirement in MAPK Signaling in T and B Cells. *J. Exp. Med.* 198, 1595–1608.
- Furuta, Y., Lagutin, O., Hogan, B. L. M. and Oliver, G. C. (2000). Retina- and ventral forebrain-specific Cre recombinase activity in transgenic mice. *Genesis* 26, 130–132.
- Galli-Resta, L. (2000). Local, possibly contact-mediated signalling restricted to homotypic neurons controls the regular spacing of cells within the cholinergic arrays in the developing rodent retina. *Development* 127, 1509–1516.
- Galli-Resta, L., Resta, G., Tan, S.-S. and Reese, B. E. (1997). Mosaics of Islet-1-Expressing Amacrine Cells Assembled by Short-Range Cellular Interactions. *J. Neurosci.* 17, 7831–7838.

- Galli-Resta, L., Novelli, E. and Viegi, A. (2002). Dynamic microtubule-dependent interactions position homotypic neurones in regular monolayered arrays during retinal development. *Development* 129, 3803–14.
- Greene, M. J., Kim, J. S. and Seung, H. S. (2016). Analogous Convergence of Sustained and Transient Inputs in Parallel On and Off Pathways for Retinal Motion Computation. *Cell Rep.* 14, 1892–1900.
- Hall, A. B., Gakidis, M. A. M., Glogauer, M., Wilsbacher, J. L., Gao, S., Swat, W. and Brugge, J. S. (2006). Requirements for Vav guanine nucleotide exchange factors and Rho GTPases in Fc γ R- and complement-mediated phagocytosis. *Immunity* 24, 305–316.
- Hinds, J. W. and Hinds, P. L. (1978). Early development of amacrine cells in the mouse retina: An electron microscopic, serial section analysis. *J. Comp. Neurol.* 179, 277–300.
- Huckfeldt, R. M., Schubert, T., Morgan, J. L., Godinho, L., Di Cristo, G., Huang, Z. J. and Wong, R. O. L. (2009). Transient neurites of retinal horizontal cells exhibit columnar tiling via homotypic interactions. *Nat. Neurosci.* 12, 35–43.
- Kadlecek, T. A., van Oers, N. S., Lefrancois, L., Olson, S., Finlay, D., Chu, D. H., Connolly, K., Killeen, N. and Weiss, A. (1998). Differential requirements for ZAP-70 in TCR signaling and T cell development. *J. Immunol.* 161, 4688–94.
- Kay, J. N., de la Huerta, I., Kim, I. J., Zhang, Y., Yamagata, M., Chu, M. W., Meister, M. and Sanes, J. R. (2011). Retinal ganglion cells with distinct directional preferences differ in molecular identity, structure, and central projections. *J. Neurosci.* 31, 7753–7762.
- Kay, J. N., Chu, M. W. and Sanes, J. R. (2012). MEGF10 and MEGF11 mediate homotypic interactions required for mosaic spacing of retinal neurons. *Nature* 483, 465–469.
- Keeley, P. W., Whitney, I. E., Raven, M. A. and Reese, B. E. (2007). Dendritic spread and functional coverage of starburst amacrine cells. *J. Comp. Neurol.* 505, 539–546.

- Kim, J. S., Greene, M. J., Zlateski, A., Lee, K., Richardson, M., Turaga, S. C., Purcaro, M., Balkam, M., Robinson, A., Behabadi, B. F., et al. (2014). Space-time wiring specificity supports direction selectivity in the retina. *Nature* 509, 331–336.
- Lefebvre, J. L., Sanes, J. R. and Kay, J. N. (2015). Development of Dendritic Form and Function. *Annu. Rev. Cell Dev. Biol.* 31, 741–777.
- Liu, P., Jenkins, N. A. and Copeland, N. G. (2003). A highly efficient recombineering-based method for generating conditional knockout mutations. *Genome Res.* 13, 476–484.
- Liu, Z., Chen, O., Wall, J. B. J., Zheng, M., Zhou, Y., Wang, L., Ruth Vaseghi, H., Qian, L. and Liu, J. (2017). Systematic comparison of 2A peptides for cloning multi-genes in a polycistronic vector. *Sci. Rep.* 7, 1–9.
- Logan, M. A., Hackett, R., Doherty, J., Sheehan, A., Speese, S. D. and Freeman, M. R. (2012). Negative regulation of glial engulfment activity by Draper terminates glial responses to axon injury. *Nat. Neurosci.* 15, 722–730.
- Lu, T. Y., MacDonald, J. M., Neukomm, L. J., Sheehan, A. E., Bradshaw, R., Logan, M. A. and Freeman, M. R. (2017). Axon degeneration induces glial responses through Draper-TRAF4-JNK signalling. *Nat. Commun.* 8, 1–9.
- Macosko, E. Z., Basu, A., Satija, R., Nemes, J., Shekhar, K., Goldman, M., Tirosh, I., Bialas, A. R., Kamitaki, N., Martersteck, E. M., et al. (2015). Highly parallel genome-wide expression profiling of individual cells using nanoliter droplets. *Cell* 161, 1202–1214.
- Madisen, L., Zwingman, T. A., Sunkin, S. M., Oh, S. W., Zariwala, H. A., Gu, H., Ng, L. L., Palmiter, R. D., Hawrylycz, M. J., Jones, A. R., et al. (2010). A robust and high-throughput Cre reporting and characterization system for the whole mouse brain. *Nat. Neurosci.* 13, 133–140.
- Mayr, C. (2018). What Are 3' UTRs Doing? *Cold Spring Harb. Perspect. Biol.* a034728.
- MD, M., B, T., K, M., L, L. and L, L. (2006). A Global Double-Fluorescent Cre Reporter Mouse. *Genesis* 224, 219–224.

- Mócsai, A., Ruland, J. and Tybulewicz, V. L. J. (2010). The SYK tyrosine kinase: A crucial player in diverse biological functions. *Nat. Rev. Immunol.* 10, 387–402.
- Palacios, E. H. and Weiss, A. (2007). Distinct roles for Syk and ZAP-70 during early thymocyte development. *J. Exp. Med.* 204, 1703–1715.
- Pearce, A. C., Senis, Y. A., Billadeau, D. D., Turner, M., Watson, S. P. and Vigorito, E. (2004). Vav1 and Vav3 have critical but redundant roles in mediating platelet activation by collagen. *J. Biol. Chem.* 279, 53955–53962.
- Poché, R. A., Raven, M. A., Kwan, K. M., Furuta, Y., Behringer, R. R. and Reese, B. E. (2008). Somal positioning and dendritic growth of horizontal cells are regulated by interactions with homotypic neighbors. *Eur. J. Neurosci.* 27, 1607–1614.
- Prigge, C. L. and Kay, J. N. (2018). Dendrite morphogenesis from birth to adulthood. *Curr. Opin. Neurobiol.* 53, 139–145.
- Raven, M. A., Eglen, S. J., Ohab, J. J. and Reese, B. E. (2003). Determinants of the exclusion zone in dopaminergic amacrine cell mosaics. *J. Comp. Neurol.* 461, 123–136.
- Rawlins, E. L., Okubo, T., Xue, Y., Brass, D. M., Auten, R. L., Hasegawa, H., Wang, F. and Hogan, B. L. M. (2009). The Role of Scgb1a1+ Clara Cells in the Long-Term Maintenance and Repair of Lung Airway, but Not Alveolar, Epithelium. *Cell Stem Cell* 4, 525–534.
- Ray, T. A., Roy, S., Kozlowski, C., Wang, J., Cafaro, J., Hulbert, S. W., Wright, C. V., Field, G. D. and Kay, J. N. (2018). Formation of retinal direction-selective circuitry initiated by starburst amacrine cell homotypic contact. *Elife* 7,.
- Reese, B. E. (1999). Modelling the mosaic organization of rod and cone photoreceptors with a minimal-spacing rule. *Eur. J. Neurosci.* 11, 1461–1469.
- Reese, B. E. and Galli-Resta, L. (2002). The role of tangential dispersion in retinal mosaic formation. *Prog. Retin. Eye Res.* 21, 153–168.
- Reese, B. E. and Keeley, P. W. (2015). Design principles and developmental mechanisms underlying retinal mosaics. *Biol. Rev.* 90, 854–876.

- Reese, B. E., Harvey, A. R. and Tan, S. S. (1995). Radial and tangential dispersion patterns in the mouse retina are cell- class specific. *Proc. Natl. Acad. Sci. U. S. A.* 92, 2494–2498.
- Rheaume, B. A., Jereen, A., Bolisetty, M., Sajid, M. S., Yang, Y., Renna, K., Sun, L., Robson, P. and Trakhtenberg, E. F. (2018). Single cell transcriptome profiling of retinal ganglion cells identifies cellular subtypes. *Nat. Commun.* 9,.
- Rockhill, R. L., Euler, T. and Masland, R. H. (2000). Spatial order within but not between types of retinal neurons. *Proc. Natl. Acad. Sci.* 97, 2303–2307.
- Rodieck, R. W. (1991). The density recovery profile: A method for the analysis of points in the plane applicable to retinal studies. *Vis. Neurosci.* 6, 95–111.
- Rossi, J., Balthasar, N., Olson, D., Scott, M., Berglund, E., Lee, C. E., Choi, M. J., Lauzon, D., Lowell, B. B. and Elmquist, J. K. (2011). Melanocortin-4 receptors expressed by cholinergic neurons regulate energy balance and glucose homeostasis. *Cell Metab.* 13, 195–204.
- Saijo, K., Schmedt, C., Su, I. hsin, Karasuyama, H., Lowell, C. A., Reth, M., Adachi, T., Patke, A., Santana, A. and Tarakhovsky, A. (2003). Essential role of Src-family protein tyrosine kinases in NF- κ B activation during B cell development. *Nat. Immunol.* 4, 274–279.
- Sanes, J. R. and Yamagata, M. (2009). Many Paths to Synaptic Specificity. *Annu. Rev. Cell Dev. Biol.* 25, 161–195.
- Sauzeau, V., Sevilla, M. A., Rivas-Elena, J. V., De Álava, E., Montero, M. J., López-Nova, J. M. and Bustelo, X. R. (2006). Vav3 proto-oncogene deficiency leads to sympathetic hyperactivity and cardiovascular dysfunction. *Nat. Med.* 12, 841–845.
- Scheib, J. L., Sullivan, C. S. and Carter, B. D. (2012). Jedi-1 and MEGF10 signal engulfment of apoptotic neurons through the tyrosine kinase syk. *J. Neurosci.* 32, 13022–13031.

- Schindelin, J., Arganda-Carreras, I., Frise, E., Kaynig, V., Longair, M., Pietzsch, T., Preibisch, S., Rueden, C., Saalfeld, S., Schmid, B., et al. (2012). Fiji: An open-source platform for biological-image analysis. *Nat. Methods* 9, 676–682.
- Shekhar, K., Lapan, S. W., Whitney, I. E., Tran, N. M., Macosko, E. Z., Kowalczyk, M., Adiconis, X., Levin, J. Z., Nemesh, J., Goldman, M., et al. (2016). Comprehensive Classification of Retinal Bipolar Neurons by Single-Cell Transcriptomics. *Cell* 166, 1308-1323.e30.
- Sullivan, C. S., Scheib, J. L., Ma, Z., Dang, R. P., Schafer, J. M., Hickman, F. E., Brodsky, F. M., Ravichandran, K. S. and Carter, B. D. (2014). The adaptor protein GULP promotes Jedi-1-mediated phagocytosis through a clathrin-dependent mechanism. *Mol. Biol. Cell* 25, 1925–1936.
- Thomas, S. M. and Brugge, J. S. (1997). Cellular Functions Regulated By Src Family Kinases. *Annu. Rev. Cell Dev. Biol.* 13, 513–609.
- Tran, Nicholas M. Shekar, Karthik. Whitney, Irene. E. Jacobi, Anne. Benhar, Inbal. Hong, Guosong. Yan, Wenjun. Adiconis, Xian. Arnold, Mckinzie. E. Lee, Jung. Min. Levin, Joshua. Z. Lin, Dingchang. Wang, Chen. Lieber, Charles. M. Regev, Aviv. He, Zhigang., J. R. (2019). Single-cell profiles of retinal neurons differing in resilience to injury reveal neuroprotective genes. *bioRxiv*.
- Visser, J. J., Cheng, Y., Perry, S. C., Chastain, A. B., Parsa, B., Masri, S. S., Ray, T. A., Kay, J. N. and Wojtowicz, W. M. (2015). An extracellular biochemical screen reveals that FLRTs and Unc5s mediate neuronal subtype recognition in the retina. *Elife* 4, 1–27.
- Wassle, H. and Riemann, H. J. (1978). The mosaic of nerve cells in the mammalian retina. *Proc. R. Soc. London - Biol. Sci.* 200, 441–461.
- Wassle, H., Peichl, L. and Boycott, B. B. (1978). Topography of horizontal cells in the retina of the domestic cat. *Proc. R. Soc. London - Biol. Sci.* 203, 269–291.
- Whitney, I. E., Keeley, P. W., Raven, M. A. and Reese, B. E. (2008). Spatial patterning of cholinergic amacrine cells in the mouse retina. *J. Comp. Neurol.* 508, 1–12.

- Whitney, I. E., Keeley, P. W., John, A. J. S., Kautzman, A. G., Kay, J. N. and Reese, B. E. (2014). Sox2 regulates cholinergic amacrine cell positioning and dendritic stratification in the retina. *J. Neurosci.* 34, 10109–10121.
- Wu, H. H., Bellmunt, E., Scheib, J. L., Venegas, V., Burkert, C., Reichardt, L. F., Zhou, Z., Farías, I. and Carter, B. D. (2009). Glial precursors clear sensory neuron corpses during development via Jedi-1, an engulfment receptor. *Nat. Neurosci.* 12, 1534–1541.
- Xu, H. P., Burbridge, T. J., Ye, M., Chen, M., Ge, X., Zhou, Z. J. and Crair, M. C. (2016). Retinal wave patterns are governed by mutual excitation among starburst amacrine cells and drive the refinement and maintenance of visual circuits. *J. Neurosci.* 36, 3871–3886.
- Yagi, T. (2012). Molecular codes for neuronal individuality and cell assembly in the brain. *Front. Mol. Neurosci.* 5, 1–31.
- Yamada, S. and Nelson, W. J. (2007). Synapses: Sites of Cell Recognition, Adhesion, and Functional Specification. *Annu. Rev. Biochem.* 76, 267–294.
- Zhou, Z., Hartwig, E. and Horvitz, H. R. (2001). CED-1 is a transmembrane receptor that mediates cell corpse engulfment in *C. elegans*. *Cell* 104, 43–56.
- Ziegenfuss, J. S., Biswas, R., Avery, M. A., Hong, K., Sheehan, A. E., Yeung, Y. G., Stanley, E. R. and Freeman, M. R. (2008). Draper-dependent glial phagocytic activity is mediated by Src and Syk family kinase signalling. *Nature* 453, 935–939.

Biography

Christopher Kozlowski completed his undergraduate B.S. degree in Biochemistry and Molecular Biology at The Pennsylvania State University. Here he was recognized by phi-kappa-phi honors society for academic achievement and worked in the lab of Dr. Melissa Rolls. In August 2013, he began his Ph.D studies at Duke University in the Program Cell and Molecular Biology (CMB) and received an Honorable Mention from the National Science Foundation for his proposal written during his rotation with Dr. Dan Tracey. In the summer of 2014 he joined the lab of Dr. Jeremy Kay and affiliated with the Department of Neurobiology. During graduate school his work was presented at Society for Neuroscience and FASEB conferences as well as at Duke Neurobiology Department Retreats. He is expected to complete his Ph.D in Neurobiology in Fall 2019.

Published Work

Ray, T.A., Roy, S., **Kozlowski, C.**, Wang, J., Cafaro, J., Hulbert, S.W., Wright, C.V., Field, G.D., and Kay, J.N., Formation of retinal direction-selective circuitry initiated by starburst amacrine cell homotypic contact. *Elife*. Apr3;7 (2018) doi: 10.7554/eLife.34241.

Submitted Work

Ray, T.A., Cochran, K.N., **Kozlowski, C.**, Wang, J., Alexander, G., Cady, M., Spencer, W.J., Ruzycski, P.A., Clark, B.S., Laermans, A., He, M., Wang, X., Park, E., Iannaccone, A., Hu, G., Fedrigo, O., Skiba, N.P., Arshavsky, V.Y., Kay, J.N., 2019, "Hidden mRNA isoforms diversify the cell-surface proteome in neural development and disease"